

Electronic Supplementary Information

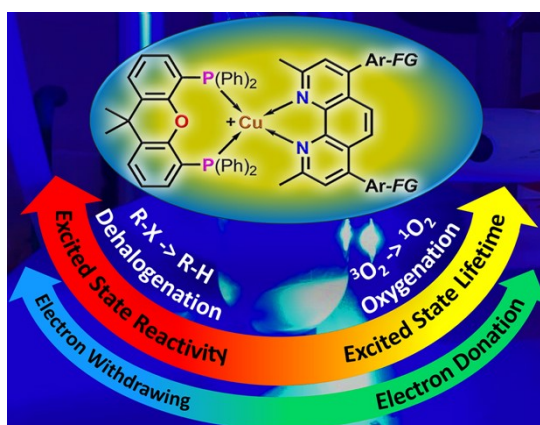
Rich or Poor: The Impact of Electron Donation and Withdrawal on the Photophysical and Photocatalytic Properties of Phenanthroline-Based Copper(I) Complexes

Florian Doettinger¹, Christian Kleeberg², Clémence Queffélec³, Stefanie Tschierlei¹, Yann Pellegrin^{3,*} and Michael Karnahl^{1,*}

¹ Department of Energy Conversion, Institute of Physical and Theoretical Chemistry, Technische Universität Braunschweig, Rebenring 31, 38106 Braunschweig, Germany.

² Institute of Inorganic and Analytical Chemistry, Technische Universität Braunschweig, Hagenring 30, 38106 Braunschweig, Germany.

³ Nantes Université, CNRS, CEISAM, UMR 6230, F-44000 Nantes, France



Electronic Supplementary Information - Table of Contents

1	Experimental Details	page	S2
2	Synthetic Details	page	S4
3	NMR spectra	page	S9
4	MS spectra	page	S21
5	Crystallographic Data	page	S26
6	Calculated Ground State Structures	page	S27
7	Electrochemical Data	page	S34
8	Time-resolved Spectroscopy	page	S37
9	Radiative and Non-Radiative Constants	page	S39
10	Excited State Reduction Potentials	page	S40
11	Singlet Oxygen Generation and Catalytic Oxygenation	page	S41
12	Photocatalytic Dehalogenation	page	S52
	References	page	S58

1 Experimental Details

NMR spectroscopy. Nuclear magnetic resonance (NMR) spectra were acquired by the analytical service of the Institute of Inorganic and Analytical Chemistry at the Technische Universität Braunschweig. A Bruker Avance III HD 500 spectrometer operating at frequencies of 500 MHz (^1H), 126 MHz (^{13}C) and 203 MHz (^{31}P) was used. The measuring temperature was 298 K, if not stated otherwise. The spectra were processed using the TopSpin software (version 4.1.1). All spectra were referenced against the residual solvent peak of the respective deuterated solvent. Coupling constants J are represented in Hz. Characterization of the NMR signal splitting is noted *via* the following abbreviations: *s* = singlet, *d* = doublet, *t* = triplet, *dd* = doublet of doublets, *td* = triplet of doublets and *m* = multiplet. Quintet splitting is described as *quintet*.

Mass spectrometry. Mass spectrometric (MS) measurements were performed by the analytical service of the Institute of Organic Chemistry at the Technische Universität Braunschweig. High resolution mass spectra were obtained applying electrospray ionization (ESI) on an LTQ-Orbitrap Velos orbitrap mass analyser by ThermoFisher Scientific. Samples were dissolved in methanol (0.1 mg/mL tetradecyltrimethylammonium bromide). MS values are given as *m/z*.

X-ray analysis. Single crystals of suitable quality for X-ray crystallography were mounted on a Hampton loop and placed in a cold stream of nitrogen gas on the diffractometer ($T = 100\text{ K}$). The diffraction intensities were collected on a *Rigaku Oxford Diffraction Synergy-S* instrument using mirror-focused $\text{CuK}\alpha$ radiation (*Rigaku PhotonJet* microfocus sources). The reflections were indexed, integrated and absorption corrections were applied as implemented in the CrysAlisPro software package (CrysAlisPro 1.171.41.105a, Rigaku Oxford Diffraction, **2021**).¹ The structures were solved employing the program SHELXT and refined anisotropically for all non-hydrogen atoms by full-matrix least squares on all F^2 using SHELXL software.² During refinement and analysis of the crystallographic data the programs Mercury, PLATON and OLEX² were used.³ For further details see the available supplementary crystallographic data.

CCDC 2237581 ($[(\text{xant})\text{Cu}(\text{MeCN})_2][\text{PF}_6](\text{CH}_2\text{Cl}_2)_2(\text{C}_6\text{H}_{14})_{1/2}$) and CCDC 2237580 (**CuOMe**) contain the supplementary crystallographic data for this publication. These data can be obtained free of charge by the Cambridge Crystallographic Data Centre via www.ccdc.cam.ac.uk/data_request/cif or by emailing data_request@ccdc.cam.ac.uk or by contacting The Cambridge Crystallographic Data Centre, 12 Union Road, Cambridge CB2 1EZ, UK.

Cyclic voltammetry. Cyclic voltammograms were measured in acetonitrile solution using 0.1 M Bu_4NPF_6 as the supporting electrolyte. An Autolab potentiostat PGSTAT204 from Metrohm was used with a three-electrode configuration. The working electrode was a glassy carbon disc with a 3 mm diameter stick, while a Pt wire served as the counter electrode. The reference electrode was a non-aqueous Ag/Ag^+ electrode (0.01 M AgNO_3 in acetonitrile or Ag/AgCl in 2M LiCl in ethanol) with the ferrocene/ferricenium (Fc/Fc^+) couple as external reference, which was added to the solution after each measurement. All potentials are reported *versus* the Fc/Fc^+ couple. All scan rates are 0.1 V/s unless otherwise noted.

Steady-state absorption and emission spectroscopy in solution. Steady-state UV/vis absorption spectra were recorded at a JASCO V-770 spectrophotometer. Emission and excitation spectra were acquired using a Horiba Jobin-Yvon FluoroMax Plus-C automated benchtop fluorescence spectrometer. Measurements under ambient conditions were conducted in ROTISOLV® (UV/IR) grade acetonitrile from Carl Roth and/or dichloromethane (HPLC grade) from Fischer Chemical.

Emission lifetime. Emission lifetime measurements were conducted using a Q-switched pulsed Nd:YAG laser from Quantel (Q-smart, 450 mJ) with pulse durations of approx. 6 ns at a repetition rate of 10 Hz. As excitation pulses the Nd:YAG output at 1064 nm was sum-frequency tripled to 355 nm using beta barium borate (β -BaB₂O₄, BBO). The excitation light was passed through a laser line filter (CWL = 355 \pm 2 nm, FWHM = 10 \pm 2 nm) to exclude light of longer wavelength remaining from harmonic generation. The power of the pump beam was about 1.0 mJ per pulse at the sample. The sample had an optical density (OD) of approximately 0.1 at the excitation wavelength. The emission lifetime was measured at the respective emission maximum of the sample. The emission was recorded using a photo multiplier tube (Hamamatsu R928P) of an LP980 spectrometer from Edinburgh Instruments.

Singlet oxygen measurement. For the determination of the singlet oxygen quantum yields ϕ_{1O_2} , the luminescence of ¹O₂ at approximately 1276 nm was detected with a Horiba Jobin-Yvon FluoroMax Plus-C automated benchtop spectrofluorometer. The fluorometer is equipped with a 150 W Xe arc excitation lamp, a R13456 photomultiplier tube detector (190-930 nm), a liquid-nitrogen cooled DSS-IGA020L InGaAs photodiode detector (800- 1550 nm) and Czerny-Turner monochromators with NIR grating blazed at 1000 nm. Absorption spectroscopy was conducted at a JASCO Spectrometer V-770, before and after each singlet oxygen measurement to ensure stability of the solutions.

For each sample, emission spectra were recorded upon excitation at 390 nm. As a reference, the procedure was repeated for the known standard phenalenone in exactly the same way using the same parameters. The detected singlet oxygen emissions were baseline corrected at 1327 nm and the area below the signals were integrated. The respective singlet oxygen quantum yield ϕ_{1O_2} was calculated and referenced against the literature reported value for phenalenone of 98%.^{4,5} The following equation 1 was applied,

$$\phi_c = \phi_R \left(\frac{A_R}{A_C} \right) \left(\frac{I_C}{I_R} \right) \quad \text{eq. 1}$$

where ϕ_x is the quantum yield and A_x the absorbance of the respective substance (reference phenalenone (R) or compound (C)). I_x is the integrated detected emission of the singlet oxygen.⁶

Photocatalytic dehalogenation. An oven-dried vial was charged with BI₁H (0.2 mmol), the corresponding substrate Ar-X (0.10 mmol) and hexadecane (ca. 0.1 mmol) as internal standard in acetonitrile (3 mL). The vial was sealed with a rubber septum and purged with argon. The copper complex (0.001 mmol) was next added and the mixture was degassed again for 5 min. Then the reaction mixture was stirred under one blue LED (Figure S12.6) irradiation for 30 min to 3 h. The distance from light source irradiation to the vial was 0.3 cm without the use of any filters. The yield of Ar-H was determined by GC-MS analysis using hexadecane as internal standard.

DFT calculations. Quantum chemical calculations at the density functional theory (DFT) level were performed using the open source ORCA program package (Version 5.0.0).⁷ Geometry optimizations of the electronic ground state were performed using the BP86⁸ exchange-correlation functional for preoptimization. The B3LYP⁹ hybrid functional was then used for final optimization steps and for time-dependent density functional theory (TD-DFT) calculations. Dispersion effects were accounted for applying D3 correction by S. Grimme including Becke-Johnson (BJ) damping.¹⁰ As basis sets the Karlsruhe's valence triple-zeta polarization functions basis sets (def2-TZVP) were applied.¹¹ Solvation effects were treated with the conductor-like polarizable continuum model, CPCM.¹² Optimized geometries were verified as minima on the potential energy surface by frequency calculations in the simulated solvent (analytical frequency calculation, B3LYP-D3(BJ)/def2-TZVP, CPCM). Visualizations were evoked using the Chemcraft software package (Version 1.8).¹³ Isosurface values for orbital representation were 0.06.

2 Synthetic Details

All chemicals were acquired from commercial suppliers (*e.g.* Sigma-Aldrich, VWR, Acros Organics and ABCR) and directly used as received, if not stated otherwise. Precursors, ligands and complexes were synthesized according to the procedures described in the main text, in this supporting material or in the literature which is cited accordingly. 2,9-Dimethyl-4,7-diphenyl-1,10-phenanthroline (bathocuproine, termed as **LH** herein) was also acquired commercially (Sigma-Aldrich).

Solvents were purified and dried according to standard procedures.¹⁴ Dry dichloromethane (DCM) and dry tetrahydrofuran (THF) used for synthesis or complexation were purified by distillation over calcium hydride under argon atmosphere. Degassing solvents was performed by the freeze-pump-thaw degassing technique.¹⁵ Degassed water was prepared by intensively purging with argon inside a Schlenk tube for several hours.

Reaction utilizing with oxygen- and/or water-sensitive compounds were carried out in dried glassware and under argon atmosphere. Glassware was vacuum dried while heated with a heat gun at 500 °C for several minutes and flushed with argon three times. Column chromatography was performed using aluminum oxide (neutral or basic) or silica as stationary phase. Small overpressure to improve the purification step was applied by hand utilizing a pump ball.

2.1 Synthesis of the ligands $L(CF_3)_2$, LCF_3 , **LF**, and **LOMe**

General synthetic procedure for ligand preparation (GSP-L): A round bottomed flask was equipped with a magnetic stir bar and the precatalyst XPhos-Pd-G2 (0.04 eq.) was added. Then 4,7-dichloro-2,9-dimethyl-1,10-phenanthroline (1.0 eq.) and the corresponding boronic acid (3.0 eq.) were added. The vessel attached to a reflux cooler and the apparatus was evacuated and backfilled with argon three times. Degassed THF and degassed 1M Cs_2CO_3 aqueous solution were added in appropriate amounts (see below) *via* syringe and the reaction was stirred at 75 °C for 16 hours.

Then, THF was evaporated directly from the reaction mixture, which resulted in a precipitation of the product. The remaining basic aqueous phase was extracted with DCM three times. The combined organic layer was washed with saturated Na_2CO_3 solution, water, and brine. The solution was then passed through a small column of aluminum oxide (AlOx, basic) and the solvent was filtered through wool and finally removed to yield the corresponding crude product as foamy solid.

Synthesis of $L(CF_3)_2$

The reaction was conducted after the GSP-L using 3,5-bis-(trifluoromethyl)-phenylboronic acid ($(CF_3)_2$ -PBA) and 1 M Cs_2CO_3 aqueous solution as base.

$dmpCl_2$	$(CF_3)_2$ -PBA	Cat.	THF	Cs_2CO_3 (aq)	Yield
166 mg (0.82 mmol)	618 mg (2.46 mmol)	18.4.2 mg (0.033 mmol)	5 mL	6 mL $c = 1$ mol/L	270 mg (71%)

$C_{30}H_{16}F_2N_2$ (M = 632.45 g/mol): 1H NMR ($CDCl_3$, 400 MHz): $\delta = 7.98(s, 2H, Ar-H)$, $7.92(s, 4H, Ar-H)$, $7.58(s, 2H, Ar-H)$, $7.42(s, 2H, Ar-H)$, $3.06(s, 6H, CH_3)$. ^{19}F NMR ($CDCl_3$, 400 MHz): $\delta = -63.21$

Synthesis of LCF₃

The reaction was conducted after the GSP-L using *p*-trifluoromethylphenylboronic acid (CF₃-PBA) and 1 M CS₂CO₃ aqueous solution as base.

dmpCl ₂	MeO-PBA	Cat.	THF	CS ₂ CO ₃ (aq)	Yield
100 mg (0.36 mmol)	274 mg (1.44 mmol)	11.1 mg (0.014 mmol)	5 mL	6 mL <i>c</i> = 1 mol/L	176 mg (98%)

C₂₈H₁₈F₆N₂ (M = 496.46 g/mol): ¹H NMR (CDCl₃, 400 MHz): δ = 7.74 (*d*, *J* = 8.5, Hz, 4H, Ar-*H*), 7.61 (*d*, *J* = 8.5 Hz, 2H, Ar-*H*), 7.58 (*m*, 4H, Ar-*H*), 7.41 (*s*, 2H, Ar-*H*), 2.98 (*s*, 6H, CH₃). ¹⁹F NMR (CDCl₃, 400 MHz): δ = -63.01.

Synthesis of LF

The reaction was conducted after the GSP-L using *p*-fluorophenylboronic acid (F-PBA) and 1 M CS₂CO₃ aqueous solution as base.

dmpCl ₂	F-PBA	Cat.	THF	CS ₂ CO ₃ (aq)	Yield
100 mg (0.36 mmol)	202 mg (1.44 mmol)	11.1 mg (0.014 mmol)	5 mL	6 mL <i>c</i> = 1 mol/L	140 mg (98 %)

C₂₆H₁₈F₂N₂ (M = 396.44 g/mol): ¹H NMR (CDCl₃, 500 MHz): δ = 7.66 (*s*, 2H, Ar-*H*), 7.43 (*ddd*, *J* = 11.7 Hz, *J* = 5.2 Hz, *J* = 2.9 Hz, 4H, Ar-*H*), 7.38 (*s*, 2H, Ar-*H*), 7.16 (*tt*, *J* = 8.8 Hz, *J* = 2.5 Hz, 4H, Ar-*H*), 2.93 (*s*, 6H, CH₃).

Synthesis of LOMe

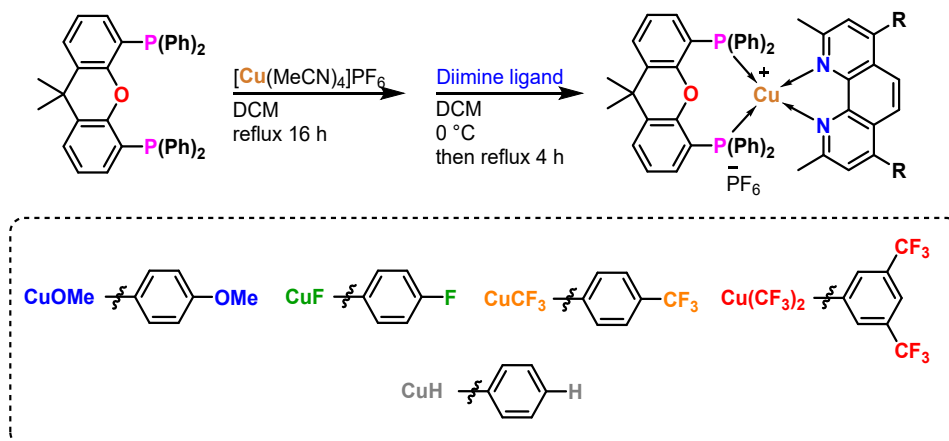
The reaction was conducted after the GSP-L using *p*-methoxyphenylboronic acid (OMe-PBA) and 1 M CS₂CO₃ aqueous solution as base.

dmpCl ₂	MeO-PBA	Cat.	THF	CS ₂ CO ₃ (aq)	Yield
130 mg (0.82 mmol)	214 mg (2.46 mmol)	14.4 mg (0.033 mmol)	5 mL	6 mL <i>c</i> = 1 mol/L	189 mg (96 %)

C₂₈H₂₄N₂O₂ (M = 420.50 g/mol): ¹H NMR (CDCl₃, 400 MHz): δ = 7.86 (*s*, 2H, Ar-*H*), 7.51 (*s*, 2H, Ar-*H*), 7.48 (*dt*, *J* = 9.4 Hz, 2.4 Hz, 4H, Ar-*H*), 7.08 (*dt*, *J* = 9.4 Hz, 2.4 Hz, 4H, Ar-*H*), 3.91 (*s*, 6H, OCH₃), 2.13 (*s*, 6H, CH₃). ¹³C NMR (CDCl₃, 400 MHz): δ = 159.78, 158.60, 148.35, 145.76, 130.93, 130.45, 124.82, 123.96, 122.90, 114.02, 55.39, 25.92. HRMS (ESI) *m/z*: calcd. for [C₂₈H₂₅N₂O₂]⁺: 421.1911; found: 421.1913.

2.2 Synthesis of the Complexes $\text{Cu}(\text{CF}_3)_2$, CuCF_3 , CuF and CuOMe

The complexation of the ligands $\text{L}(\text{CF}_3)_2$, LCF_3 , LF and LOMe towards the respective heteroleptic Cu(I) complexes were conducted as described before in the literature¹⁶, however, with slight modification concerning the addition of the diimine ligand. The general synthetic procedure is described hereafter, followed by details about chemical quantities used, yields obtained, and analytical data for each complex.



General procedure: into a dried Schlenk tube equipped with a magnetic stir bar solid tetrakis(acetonitrile)-copper(I) hexafluorophosphate ($[\text{Cu}(\text{MeCN})_4]\text{PF}_6$, 1.0 eq.) and xantphos (xant, 1.0 eq.) were added. The vessel was attached to a reflux cooler and the whole apparatus was flushed with argon three times. Dry and degassed DCM was added and the solution refluxed for 16 hours.

After cooling to 0 °C, a solution of the respective diimine ligand (1.0 eq.) in dry and degassed DCM was added dropwise very carefully using a syringe pump (pump rate 12 mL/h, unless otherwise stated). Then, the solution was stirred for another 1 hour at room temperature and finally refluxed for four hours. The heteroleptic complex was then precipitated by slowly adding *n*-hexane. The crystalline solid was collected and washed with *n*-hexane.

Cu(CF₃)₂: [Cu(L(CF₃)₂(xant))PF₆

[Cu(MeCN) ₄]PF ₆	Xantphos	Diimine L(CF ₃) ₂	DCM	Yield
130.5 mg (0.350 mmol)	202.5 mg (0.350 mmol)	221.4mg (0.350 mmol)	30 mL + 30 mL	388 mg (78 %)

C₆₉H₄₈CuF₁₈N₂OP₃ (M = 1419.60 g/mol). ¹H NMR (CD₃CN, 500 MHz): δ = 8.22 (s, 2H, Ar-H), 8.08 (s, 4H, Ar-H), 7.78 (dd, J = 7.8 Hz, J = 1.4 Hz, 2H, Ar-H), 7.64 (d, J = 12.0 Hz, 4H, Ar-H), 7.28 (m, 6H, Ar-H), 7.13 (m, 16H, Ar-H), 7.02 (m, 2H, Ar-H), 2.36 (s, 6H, CH₃), 1.74 (s, 6H, CH₃). ¹³C NMR (CD₃CN, 500 MHz): δ = 159.71, 155.92, 147.44, 144.33, 139.96, 135.01, 134.03, 132.75, 132.45, 131.30, 131.19, 131.11, 129.72, 129.09, 127.47, 126.49, 126.26, 125.52, 124.31, 124.19, 123.35, 122.50, 121.19, 36.98, 28.94, 27.93. ³¹P NMR (CD₃CN, 500 MHz): -12.92 (s, Ar-P), -144.63 (qi, J = 708 Hz, PF₆). ¹⁹F NMR (CD₃CN, 500 MHz): -62.29 (s, CF₃). HRMS (ESI) m/z: calcd. for [C₆₉H₄₈CuF₁₂N₂OP₂]⁺: 1273.2341; found: 1273.2358

CuCF₃: [Cu(LCF₃)(xant)]PF₆

[Cu(MeCN) ₄]PF ₆	Xantphos	Diimine LCF ₃	DCM	Yield
75.5 mg (0.200 mmol)	115.7 mg (0.200 mmol)	94.3 mg (0.200 mmol)	15 mL + 15 mL	178 mg (75 %)

C₆₇H₅₀CuF₁₂N₂OP₃ (M = 1283.60 g/mol). ¹H NMR (CD₃CN, 500 MHz): δ = 7.91 (d, J = 8.2 Hz, 4H, Ar-H), 7.78 (dd, J = 7.6 Hz, J = 1.5 Hz, 2H, Ar-H), 7.91 (d, J = 7.9 Hz, 4H, Ar-H), 7.65 (s, 2H, Ar-H), 7.56 (s, 2H, Ar-H), 7.29 (t, J = 7.1 Hz, 4H, Ar-H), 7.28 (t, J = 7.8 Hz, 2H, Ar-H), 7.15 (m, 8H, Ar-H), 7.10 (m, 8H, Ar-H), 7.06 (m, 2H, Ar-H), 2.34 (s, 6H, CH₃), 1.73 (s, 6H, CH₃). ¹³C NMR (CD₃CN, 500 MHz): δ = 158.06, 154.55, 147.87, 143.07, 140.43, 133.62, 132.67, 131.16, 130.21, 130.00, 129.92, 129.70, 128.31, 127.67, 125.53, 125.45, 125.09, 124.99, 123.99, 122.91, 121.21, 35.64, 27.60, 26.55. ³¹P NMR (CD₃CN, 500 MHz): -12.86 (s, Ar-P), -144.63 (qi, J = 708 Hz, PF₆). ¹⁹F NMR (CD₃CN, 500 MHz): -62.12 (s, CF₃). HRMS (ESI) m/z: calcd. for [C₆₇H₅₀CuF₆N₂OP₂]⁺: 1137.2593; found: 1137.2606

CuF: [Cu(LF)(xant)]PF₆

[Cu(MeCN) ₄]PF ₆	Xantphos	Diimine LF	DCM	Yield
130.5 mg (0.350 mmol)	202.5 mg (0.350 mmol)	138.8 mg (0.350 mmol)	30 mL + 30 mL	314 mg (76 %)

C₆₅H₅₀CuF₈N₂OP₃ (M = 1183.58 g/mol). ¹H NMR (CD₃CN, 500 MHz): δ = 7.77 (dd, J = 7.8 Hz, J = 1.4 Hz, 2H, Ar-H); 7.70 (s, 2H, Ar-H), 7.55 (td, J = 8.6 Hz, J = 5.5 Hz, 4H, Ar-H), 7.51 (s, 2H, Ar-H), 7.34 (tt, J = 8.9 Hz, J = 2.6 Hz, 4H, Ar-H), 7.27 (dt, J = 13.1 Hz, J = 7.4 Hz, 6H, Ar-H), 7.14 (m, 8H, Ar-H), 7.09 (m, 8H, Ar-H), 7.04 (m, 2H, Ar-H), 2.32(s, 6H, CH₃), 1.723(s, 6H, CH₃). ¹³C NMR (CD₃CN, 500 MHz): δ = 165.24, 163.27, 159.19, 155.93, 149.72, 144.49, 134.97, 134.01, 132.78, 132.70, 132.57, 132.45, 131.27, 131.03, 129.64, 128.98, 126.77, 126.58, 126.42, 124.22, 122.64, 116.86, 37.02, 28.95, 27.92. ³¹P NMR (CD₃CN, 500 MHz): -13.04 (s, Ar-P), -144.63 (qi, J = 708 Hz, PF₆). ¹⁹F NMR (CD₃CN, 500 MHz): -113.02 (s, Ar-F). HRMS (ESI) m/z: calcd. for [C₆₅H₅₀CuF₂N₂OP₂]⁺: 1037.2657; found: 1037.2670

CuOMe: [Cu(LOMe)(xant)]PF₆

[Cu(MeCN)₄]PF₆	Xantphos	Diimine LOMe	DCM	Yield
186.4 mg (0.500 mmol)	289.3 mg (0.500 mmol)	210.3 mg (0.500 mmol)	60 mL + 20 mL	512.1 mg (85 %)

C₆₇H₅₆CuF₆N₂O₃P₃ (M = 1207.65 g/mol). ¹H NMR (CD₃CN, 500 MHz): δ = 7.77 (s, 2H, Ar-H); 7.76 (dd, J = 7.8 Hz, J = 1.4 Hz, 2H, Ar-H), 7.48 (m, 6H, Ar-H), 7.27 (dt, J = 13.3 Hz, J = 7.5 Hz, 6H, Ar-H), 7.13 (m, 12H, Ar-H), 7.08 (dd, J = 8.0 Hz, J = 7.3 Hz, 8H, Ar-H), 7.03 (m, 2H, Ar-H), 3.88 (s, 6H, OCH₃), 2.29 (s, 6H, CH₃), 1.72 (s, 6H, CH₃). ¹³C NMR (CD₃CN, 500 MHz): δ = 161.58, 158.94, 155.98, 150.54, 144.67, 134.97, 134.02, 132.64, 132.09, 131.26, 131.00, 129.88, 129.61, 128.91, 126.61, 126.42, 124.24, 122.73, 115.38, 56.25, 36.99, 28.96, 27.92. ³¹P NMR (CD₃CN, 400 MHz): -13.12 (s, Ar-P), -144.63 (qi, J = 708 Hz, PF₆). HRMS (ESI) m/z: calcd. for [C₆₇H₅₆CuN₂O₃P₂]⁺: 1061,3057; found: found: 1061.3066

3 NMR spectra

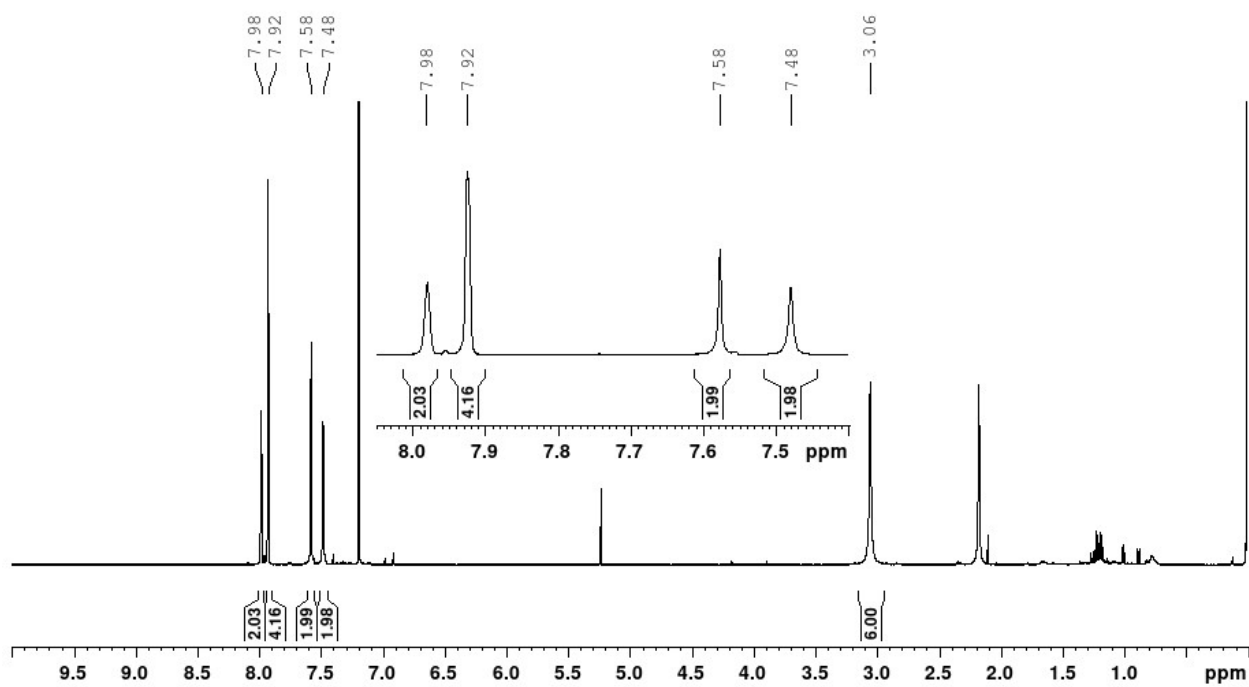


Figure S3.1. ^1H NMR spectrum of ligand $\text{L}(\text{CF}_3)_2$ in CDCl_3 .

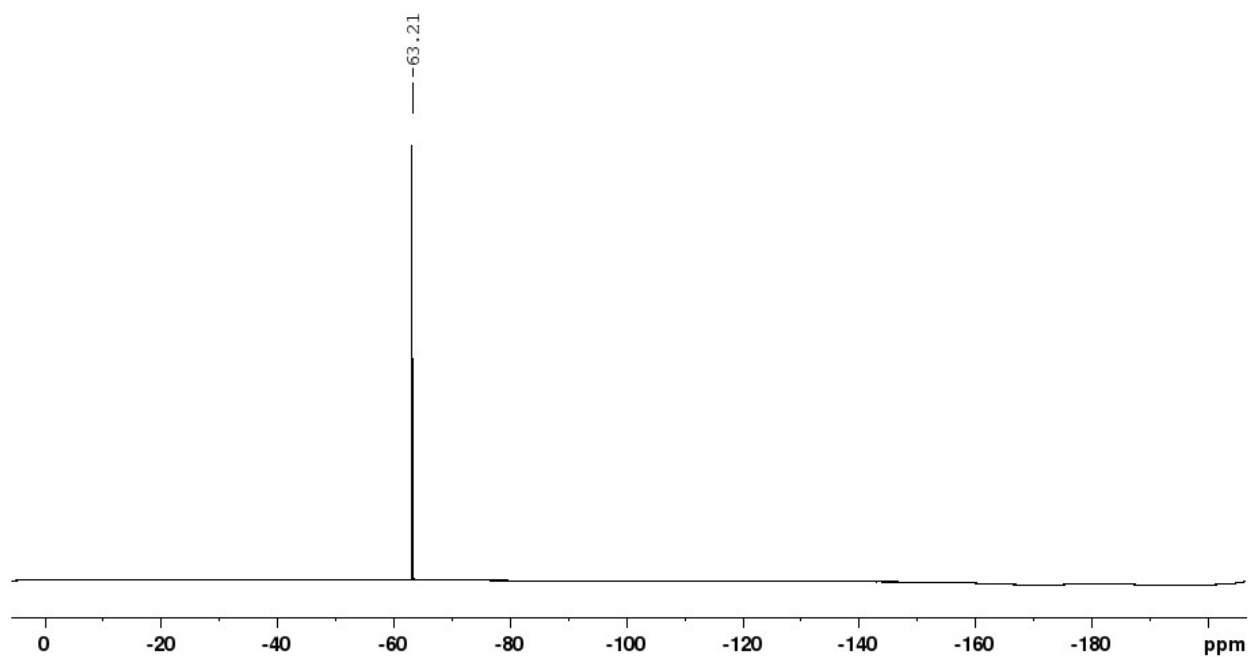


Figure S3.2. ^{19}F NMR spectrum of ligand $\text{L}(\text{CF}_3)_2$ in CDCl_3 .

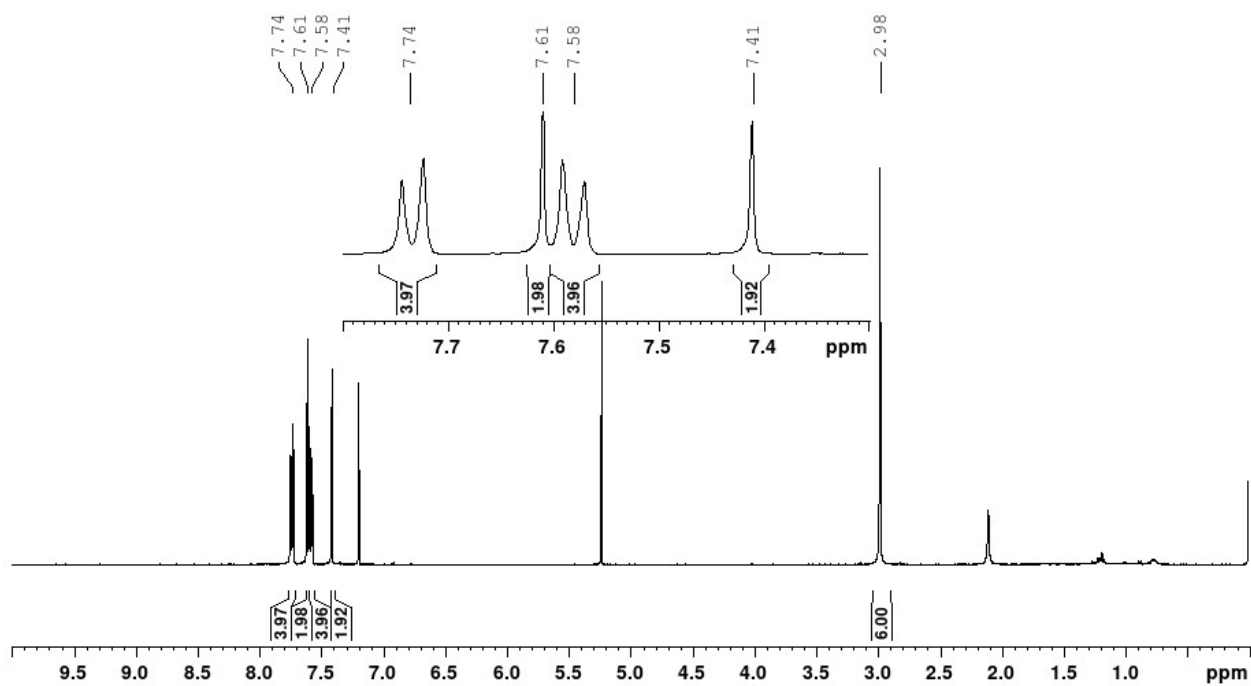


Figure S3.3. ^1H NMR spectrum of ligand LCF_3 in CDCl_3 .

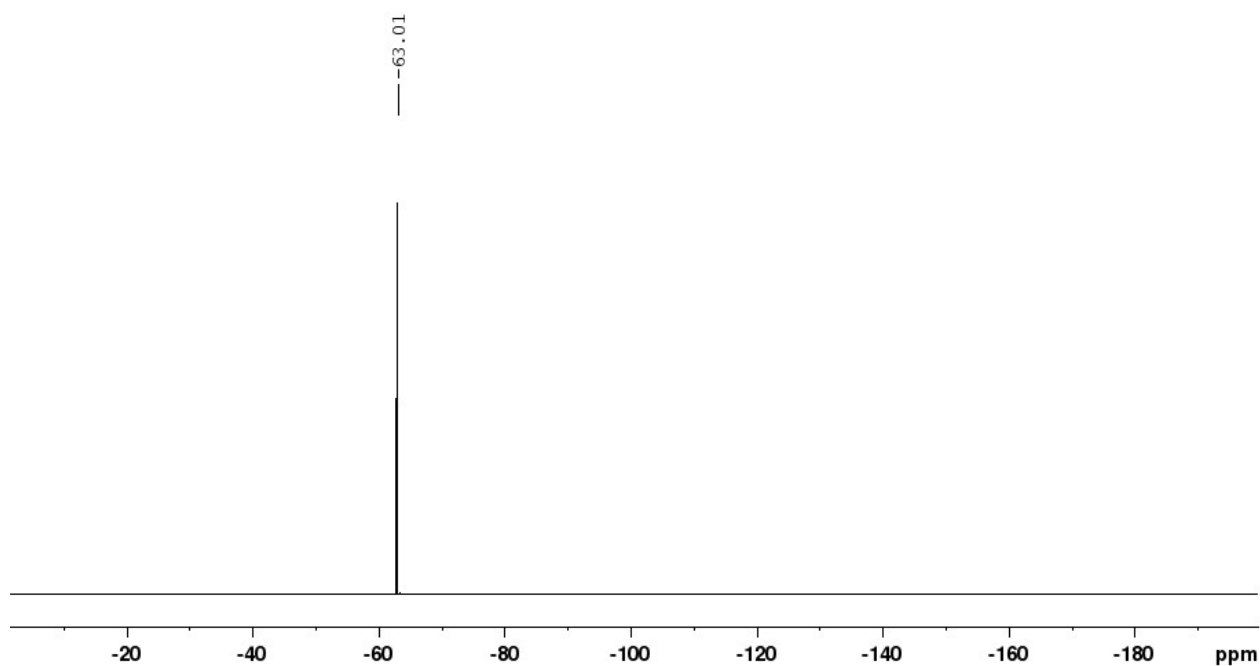


Figure S3.4. ^{19}F NMR spectrum of ligand LCF_3 in CDCl_3 .

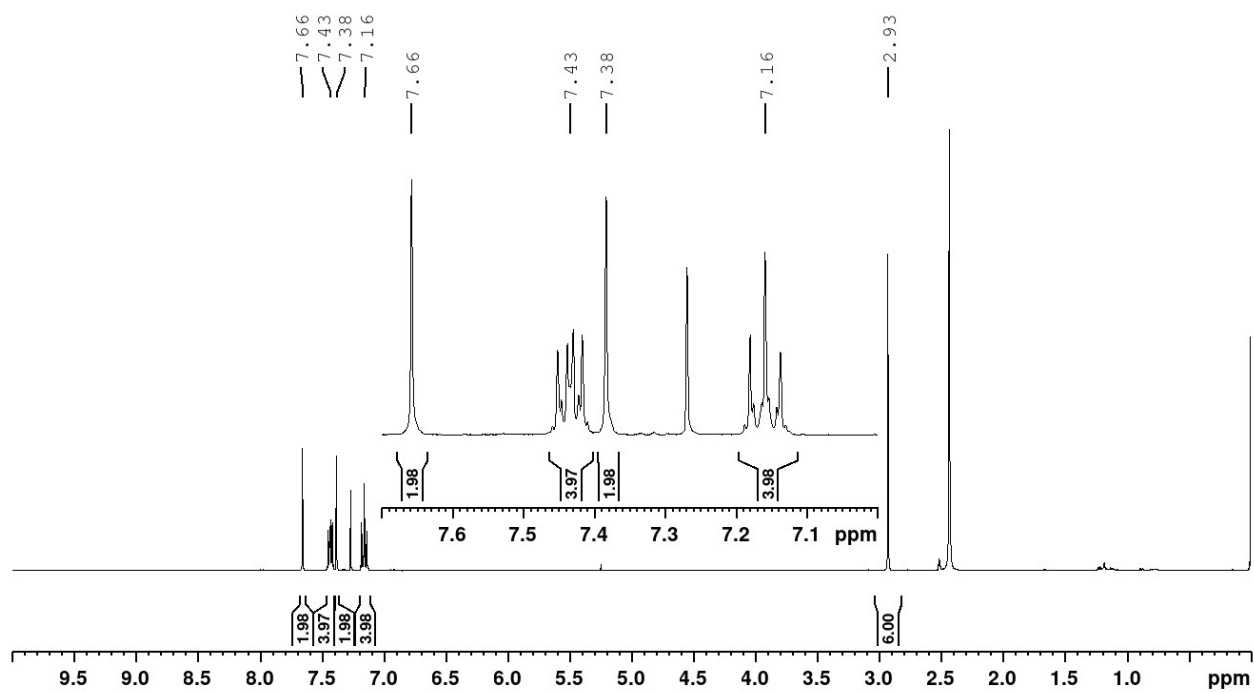


Figure S3.5. ^1H NMR spectrum of ligand LF in CDCl_3 .

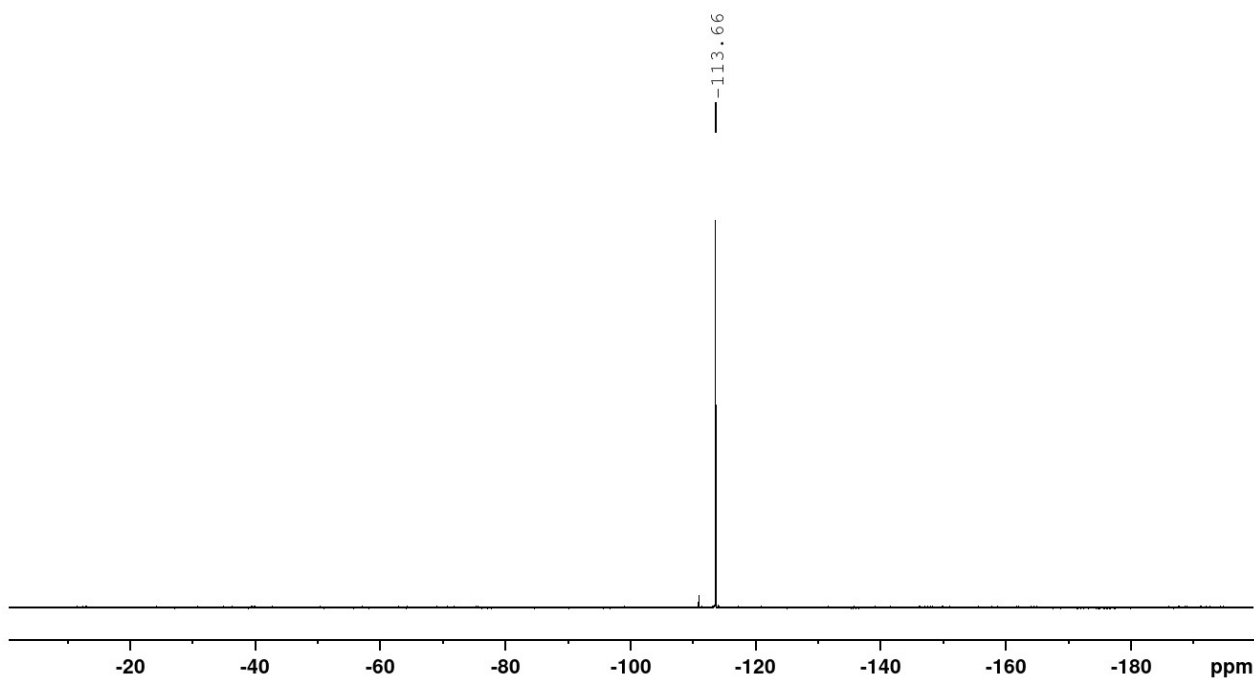


Figure S3.6. ^{19}F NMR spectrum of ligand LF in CDCl_3 .

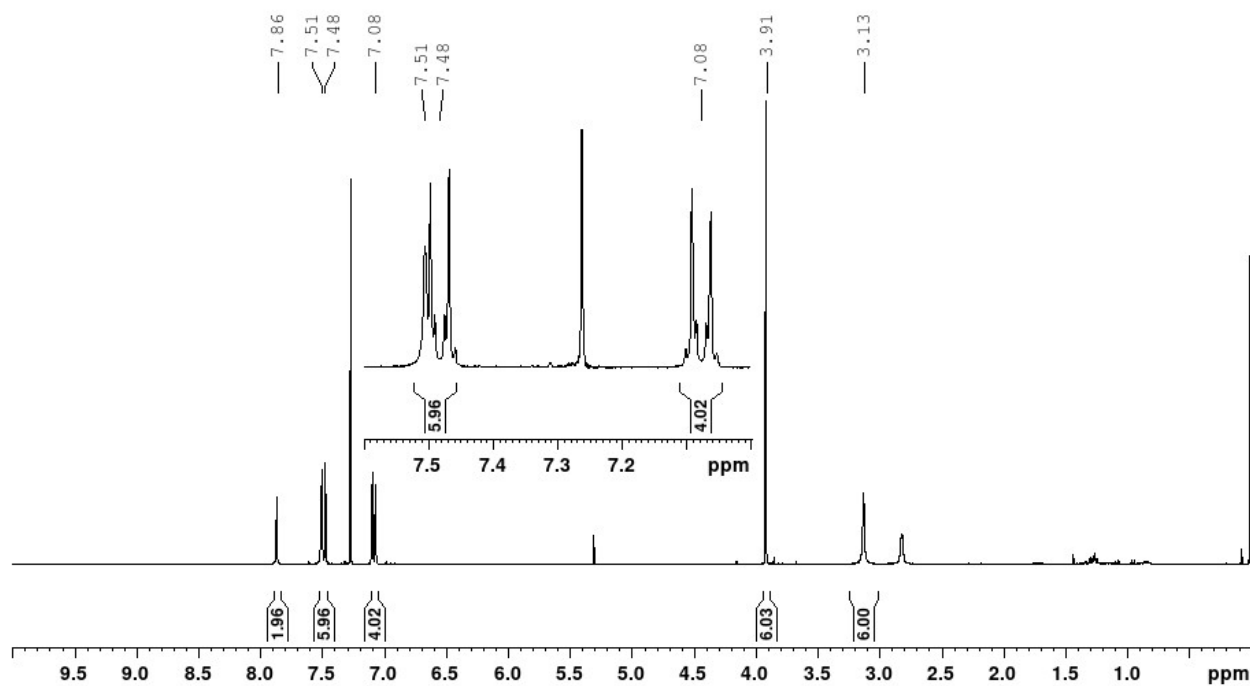


Figure S3.7. ^1H NMR spectrum of ligand **LOMe** in CDCl_3 .

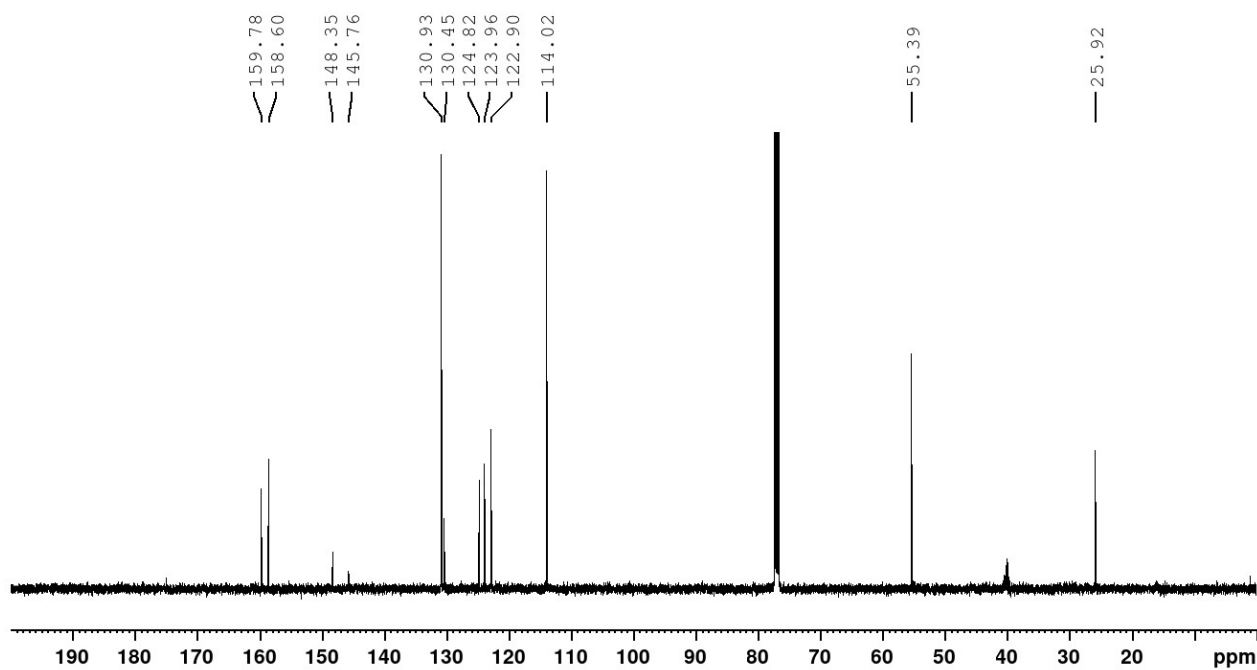


Figure S3.8. ^{13}C NMR spectrum of ligand **LOMe** in CDCl_3 .

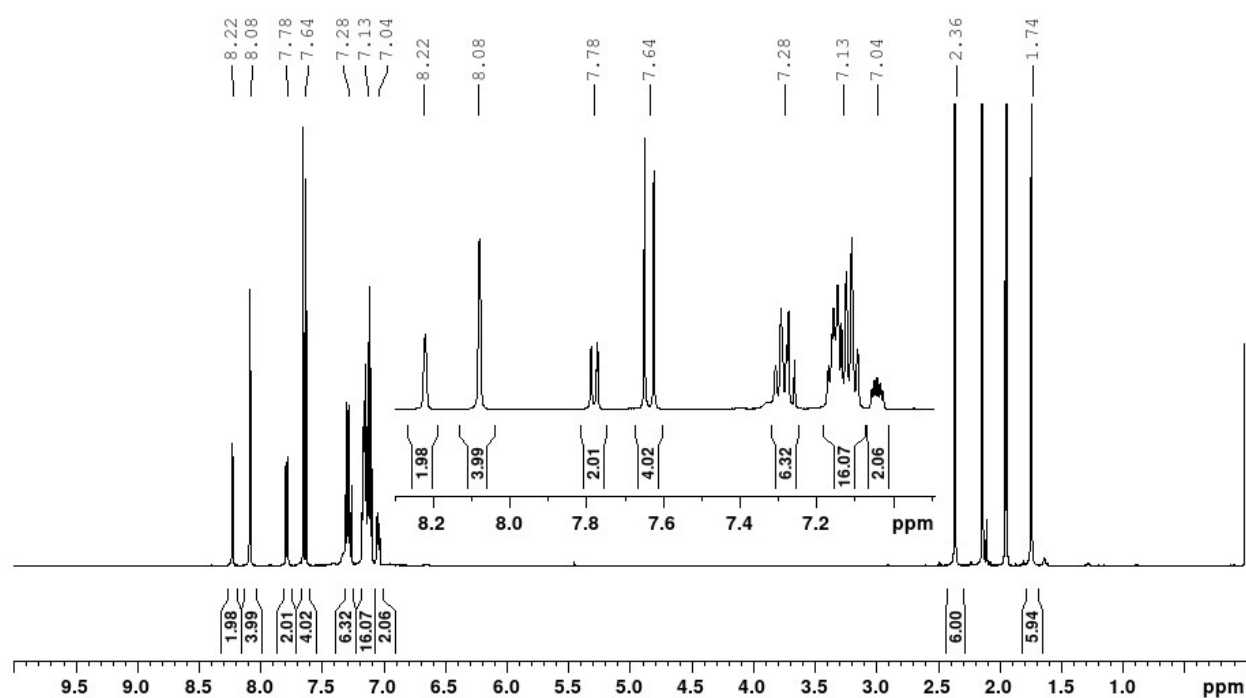


Figure S3.9. ^1H NMR spectrum of $\text{Cu}(\text{CF}_3)_2$ in CD_3CN .

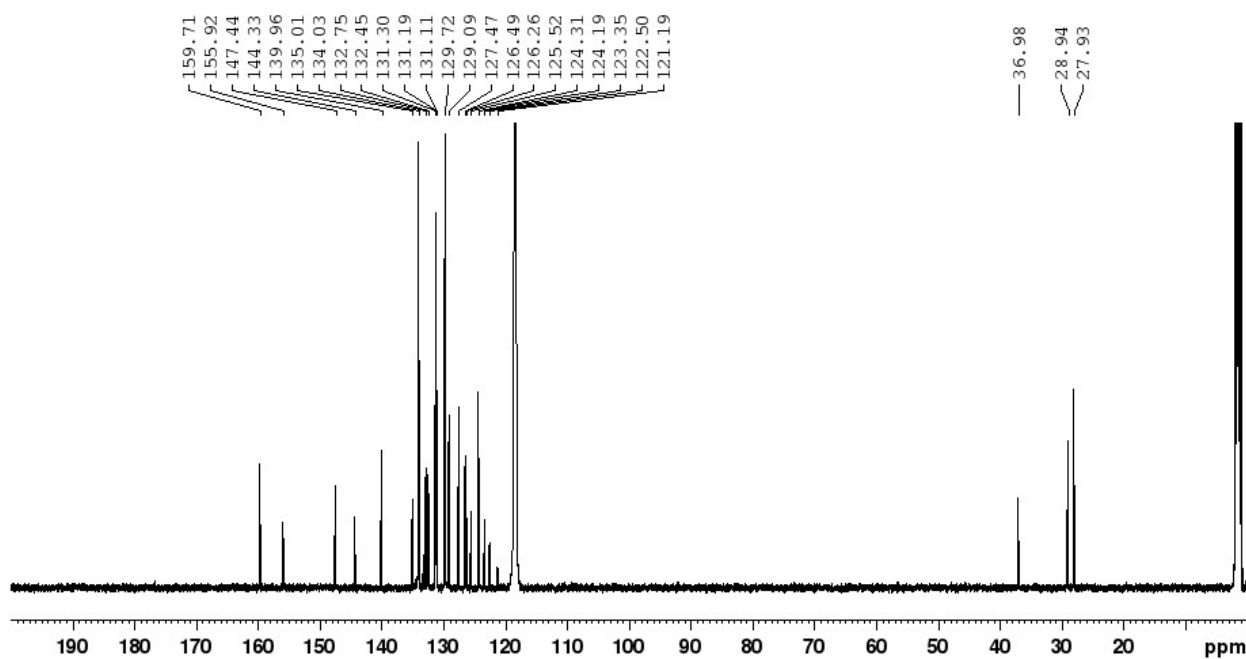


Figure S3.10. ^{13}C NMR spectrum of $\text{Cu}(\text{CF}_3)_2$ in CD_3CN .

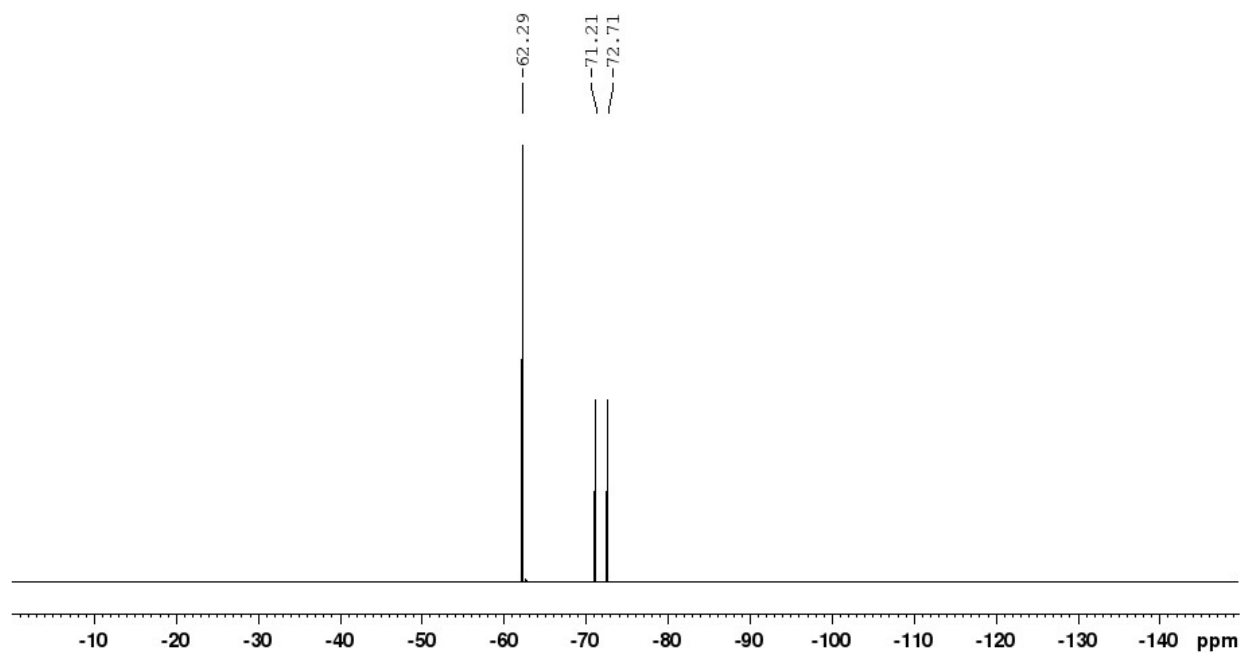


Figure S3.11. ^{19}F NMR spectrum of $\text{Cu}(\text{CF}_3)_2$ in CD_3CN .

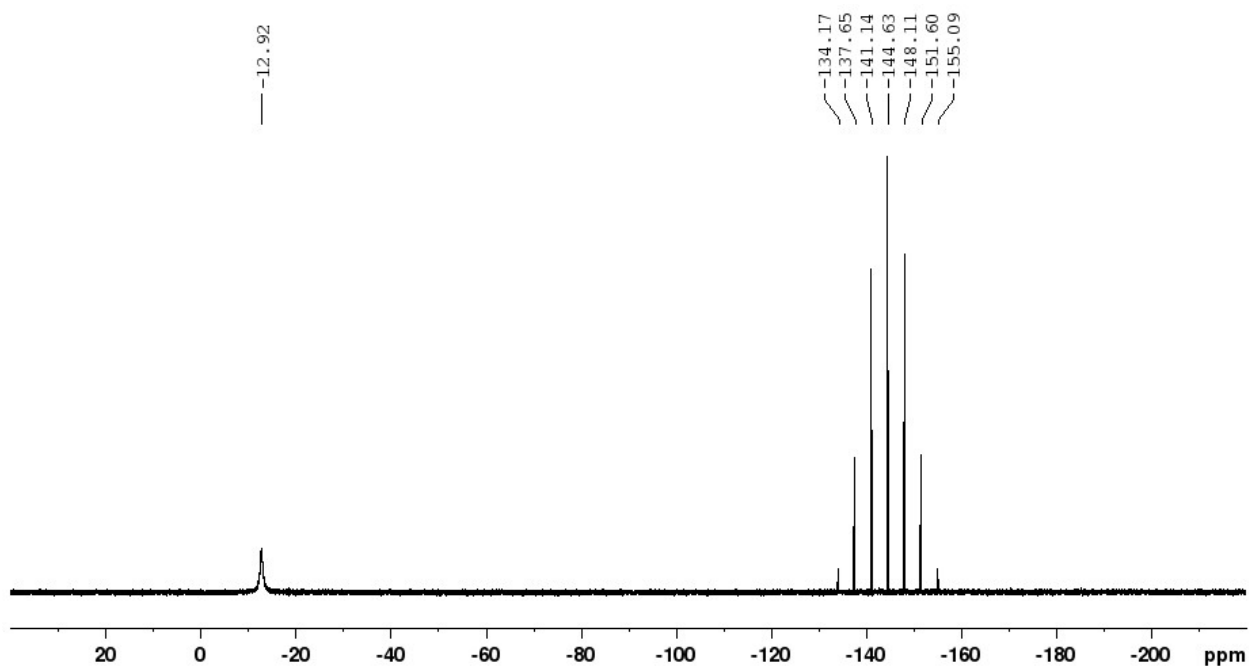


Figure S3.12. ^{31}P NMR spectrum of $\text{Cu}(\text{CF}_3)_2$ in CD_3CN .

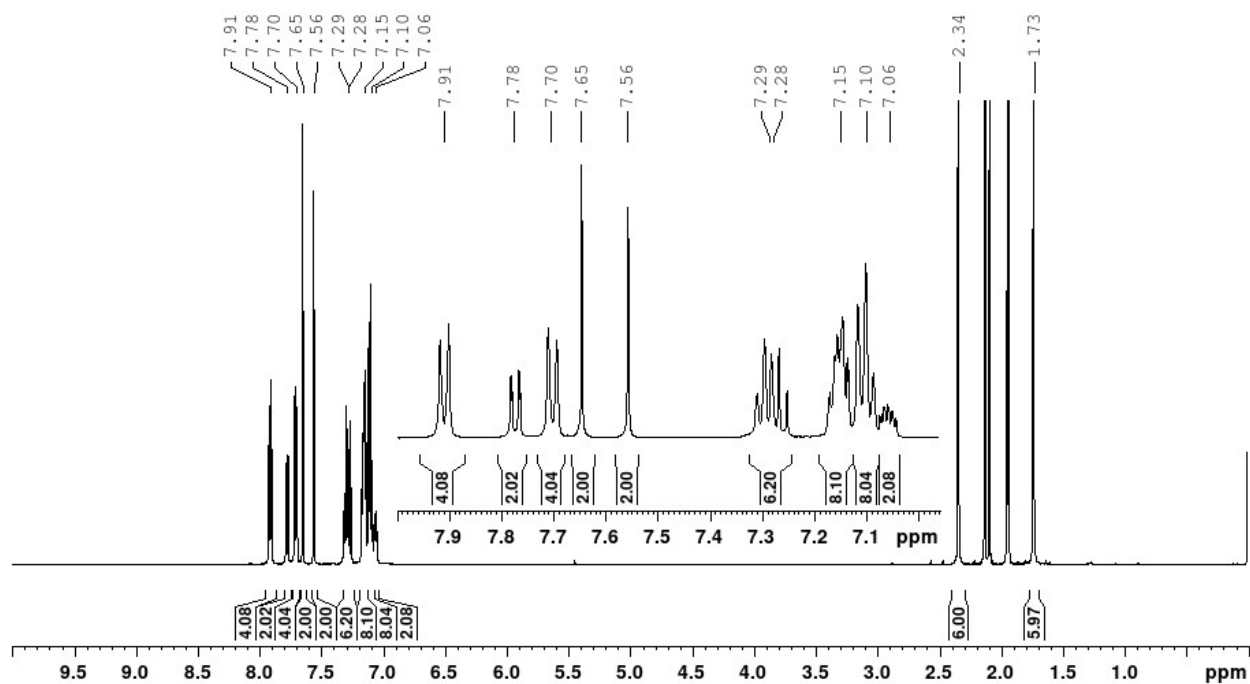


Figure S3.13. ^1H NMR spectrum of CuCF_3 in CD_3CN .

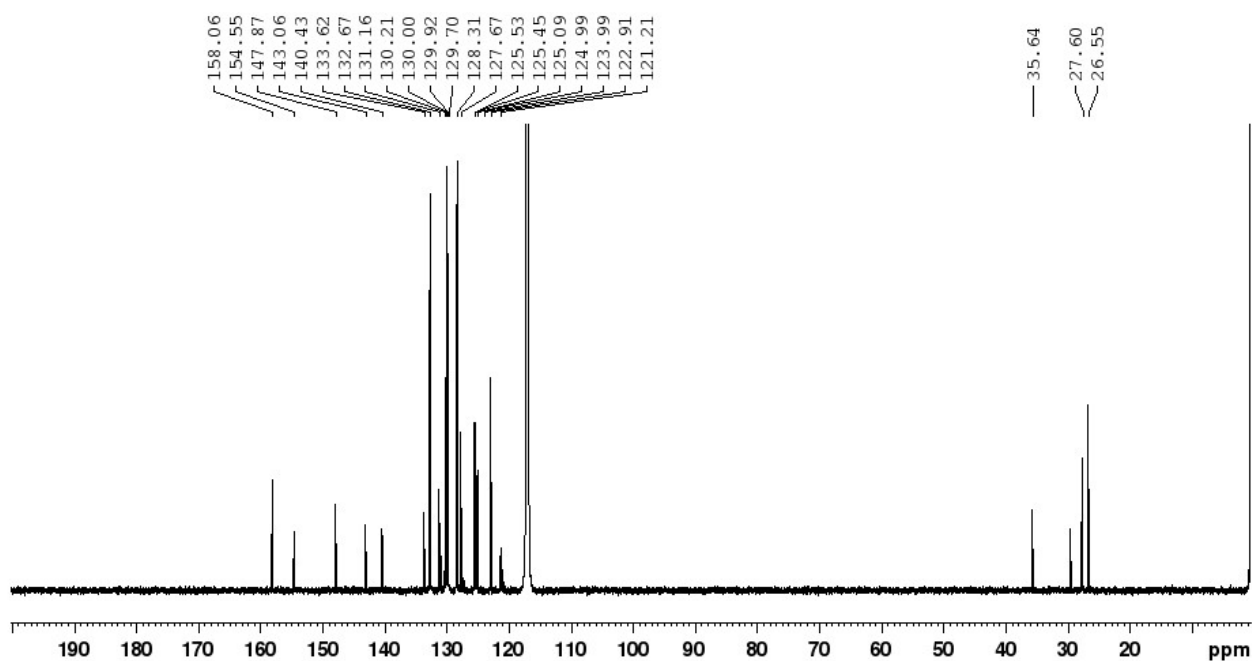


Figure S3.14. ^{13}C NMR spectrum of CuCF_3 in CD_3CN .

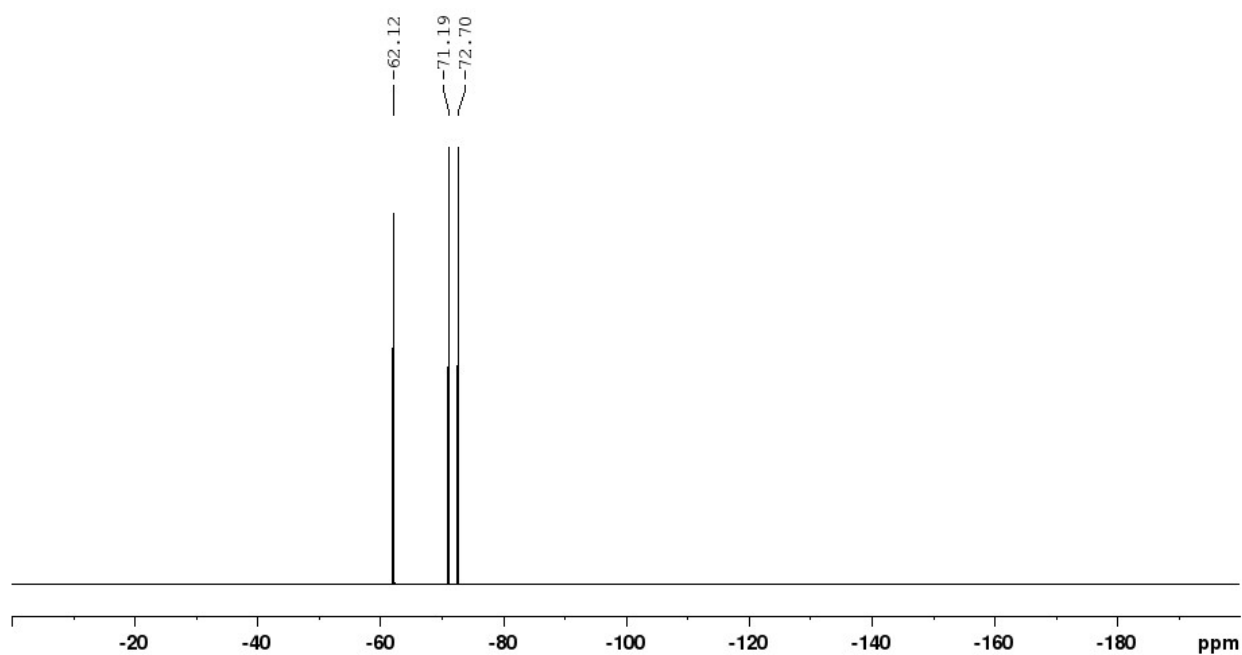


Figure S3.15. ^{19}F NMR spectrum of CuCF_3 in CD_3CN .

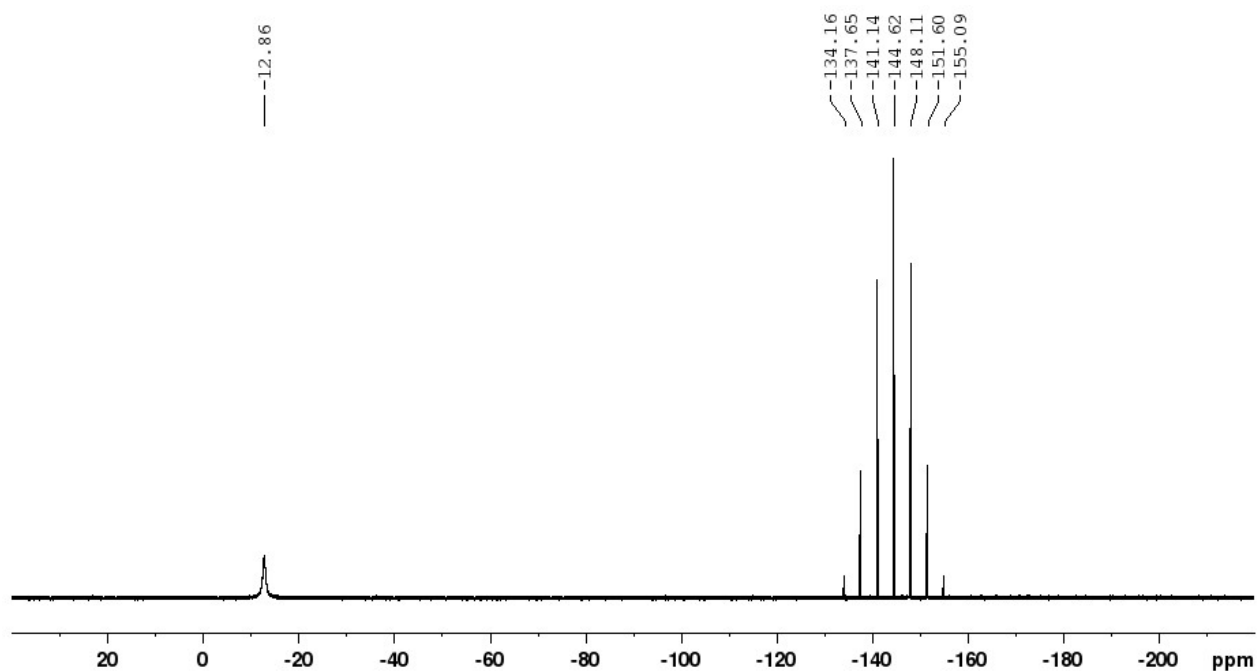


Figure S3.16. ^{31}P NMR spectrum of CuCF_3 in CD_3CN .

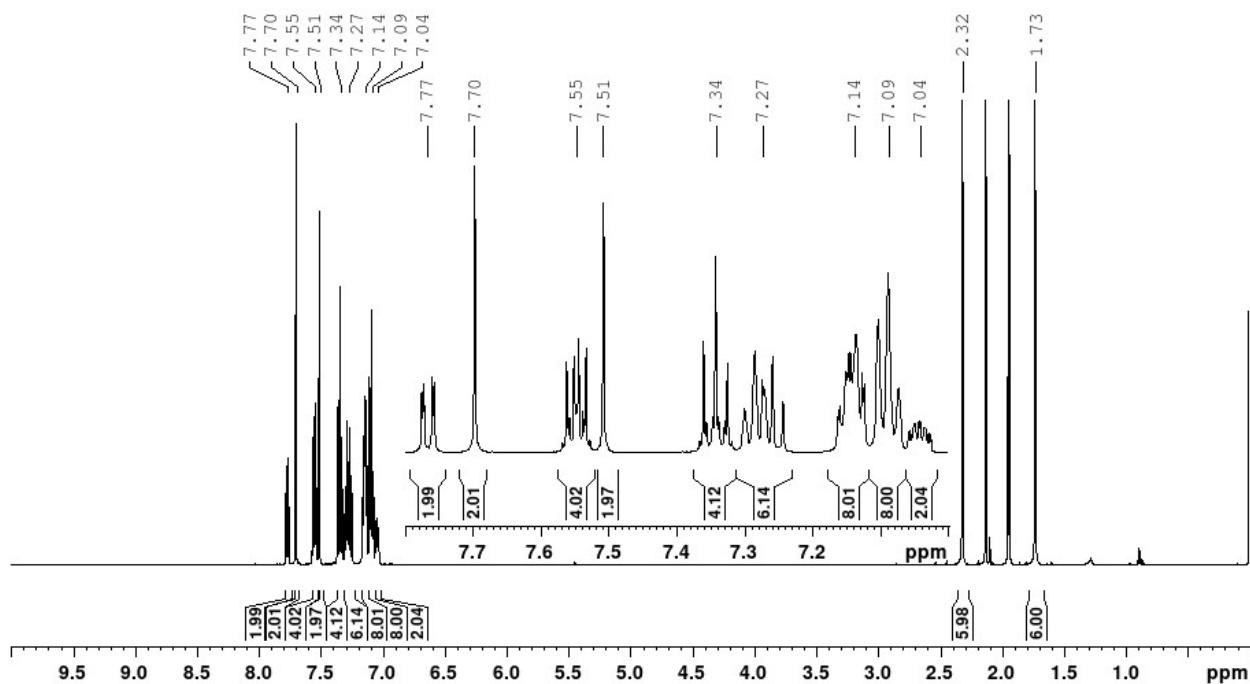


Figure S3.17. ^1H NMR spectrum of CuF in CD_3CN .

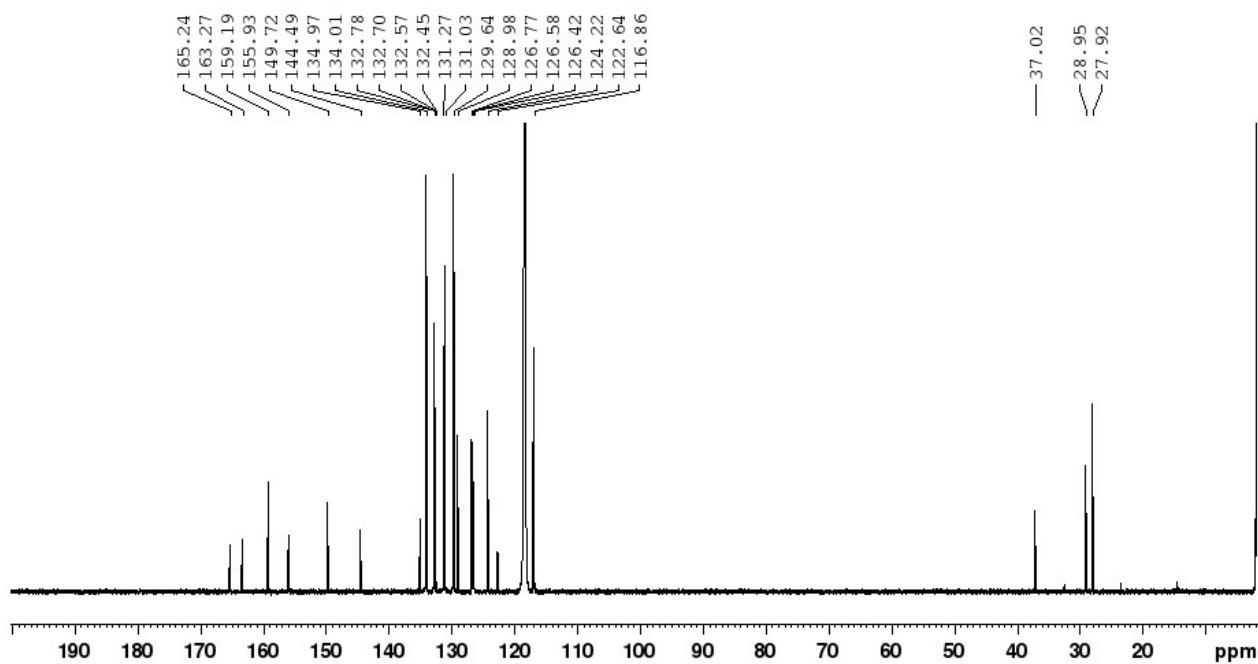


Figure S3.18. ^{13}C NMR spectrum of CuF in CD_3CN .

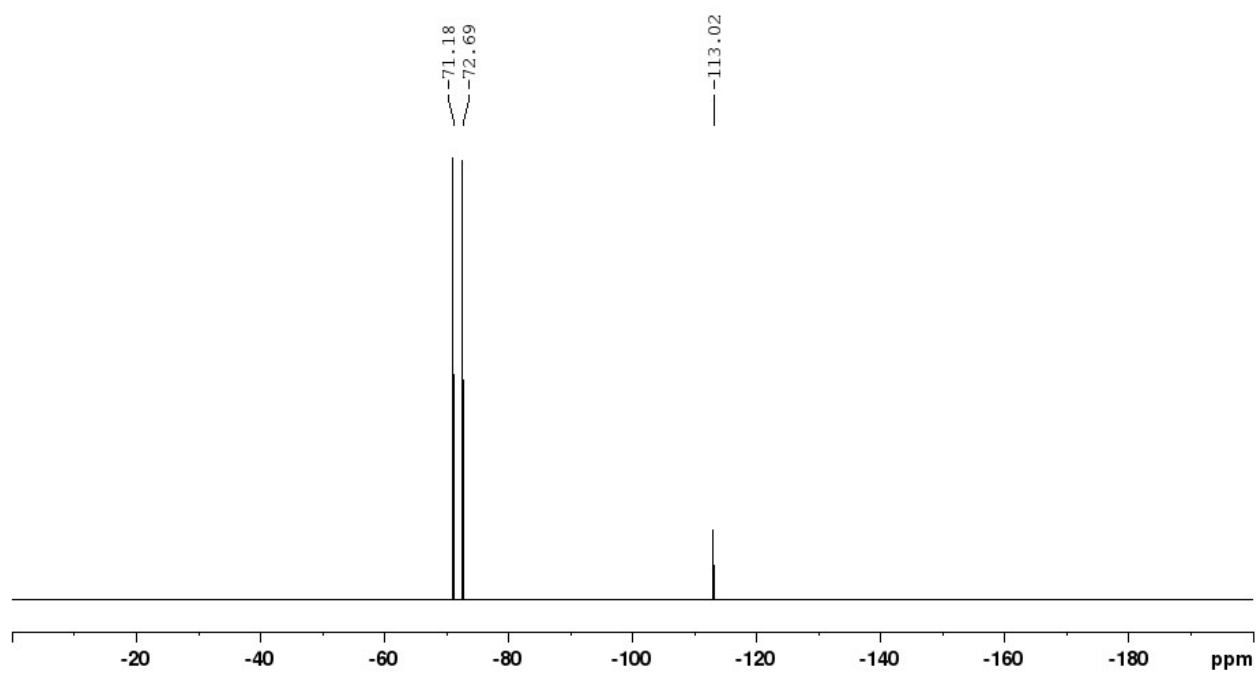


Figure S3.19. ^{19}F NMR spectrum of CuF in CD_3CN .

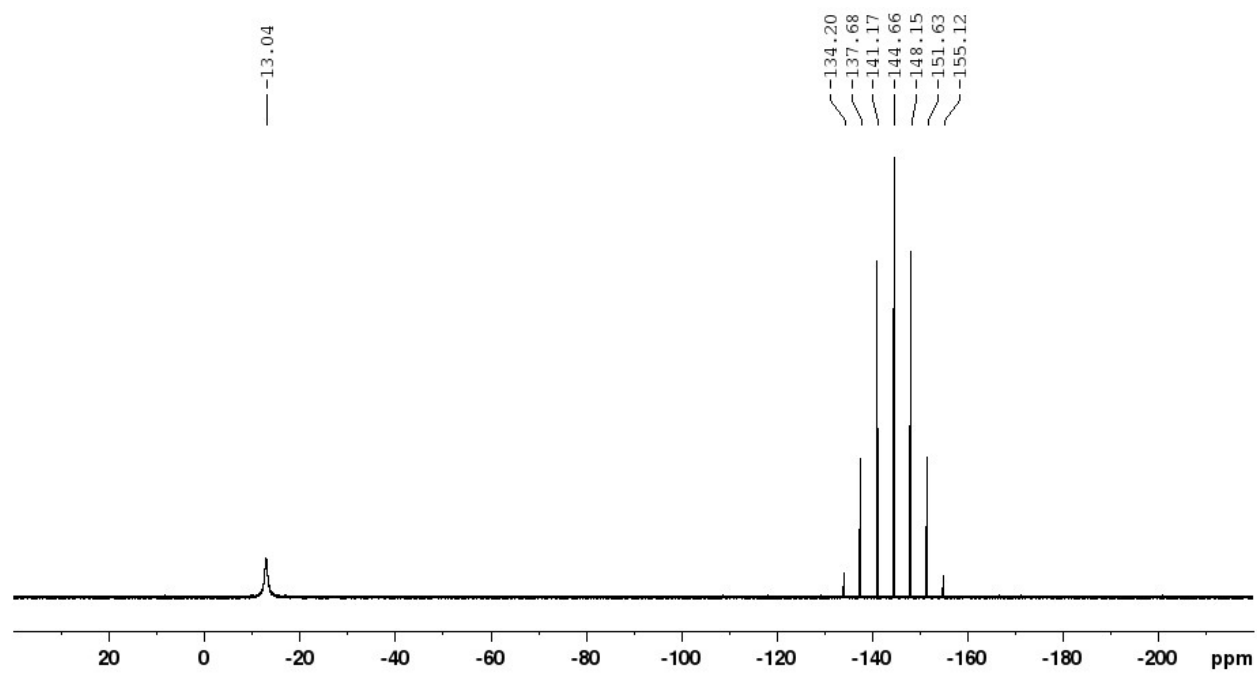


Figure S3.20. ^{31}P NMR spectrum of CuF in CD_3CN .

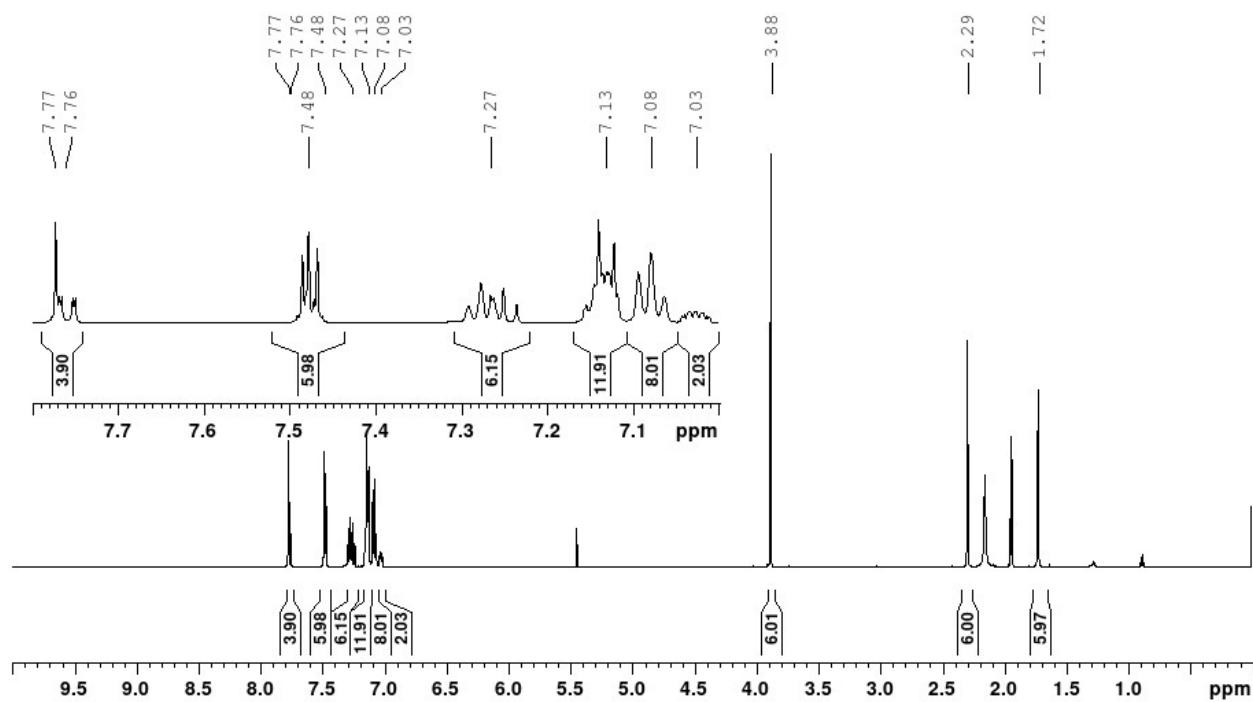


Figure S3.21. ^1H NMR spectrum of CuOMe in CD_3CN .

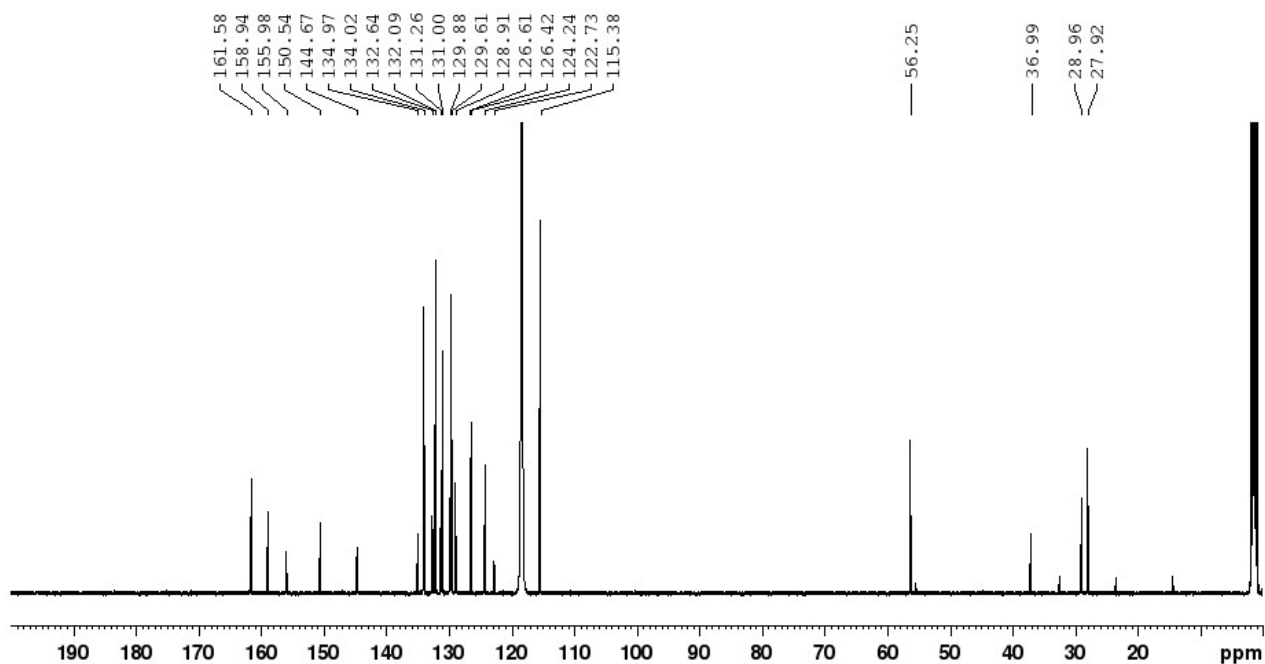


Figure S3.22. ^{13}C NMR spectrum of CuOMe in CD_3CN .

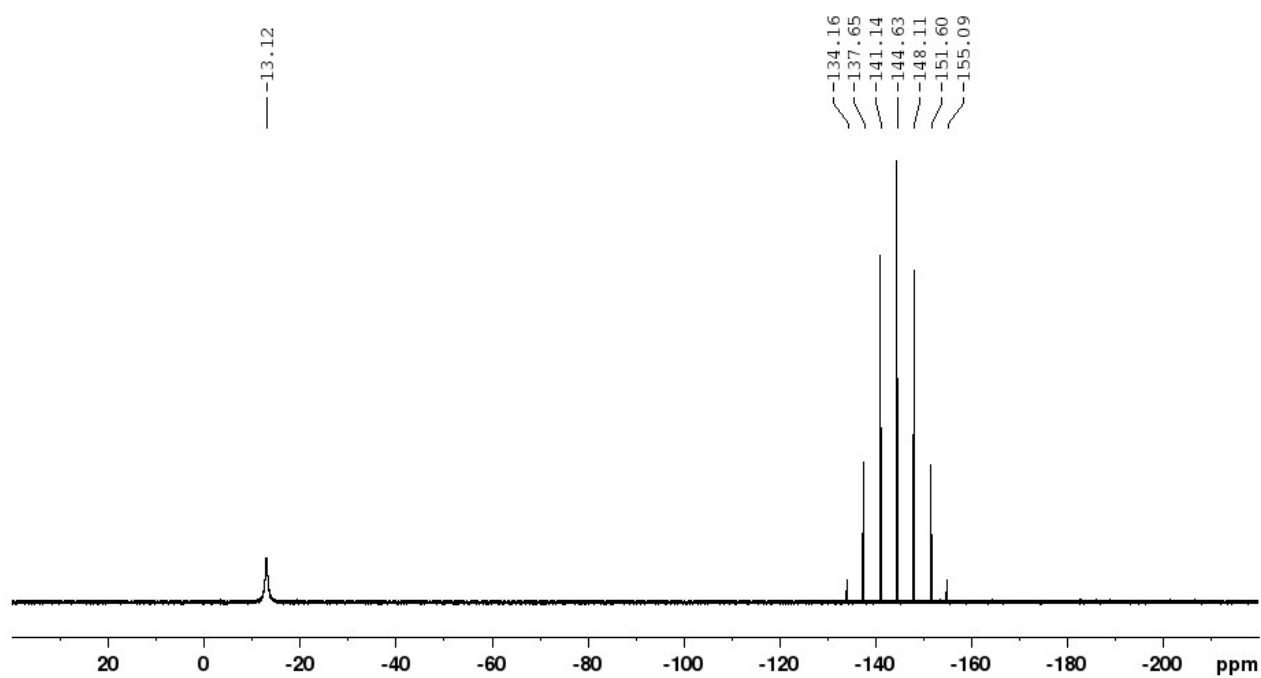
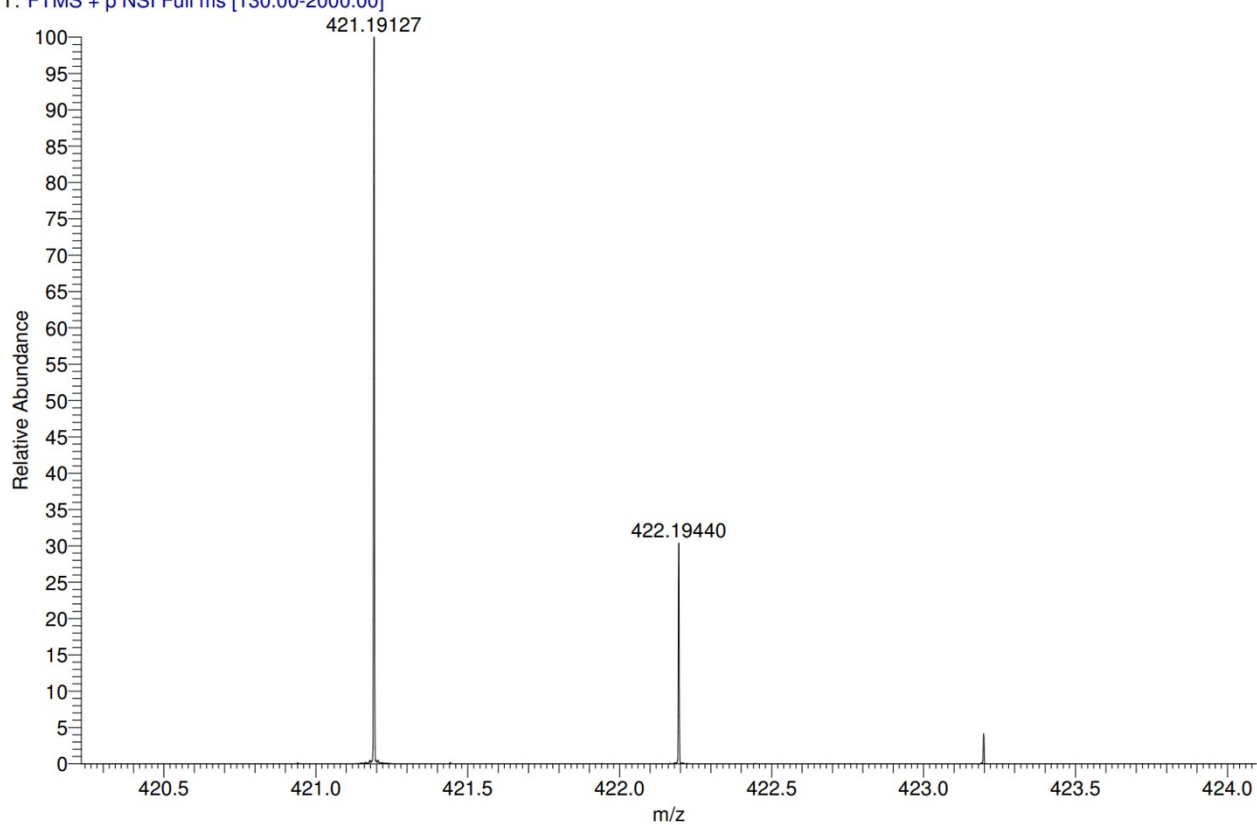


Figure S3.23. ^{31}P NMR spectrum of **CuOMe** in CD_3CN .

4 MS spectra

LTQOT15630 #5-20 RT: 0.11-0.53 AV: 16 NL: 1.65E8
T: FTMS + p NSI Full ms [130.00-2000.00]



LTQOT15630 #5-20 RT: 0.11-0.53 AV: 16 NL: 1.65E8
T: FTMS + p NSI Full ms [130.00-2000.00]

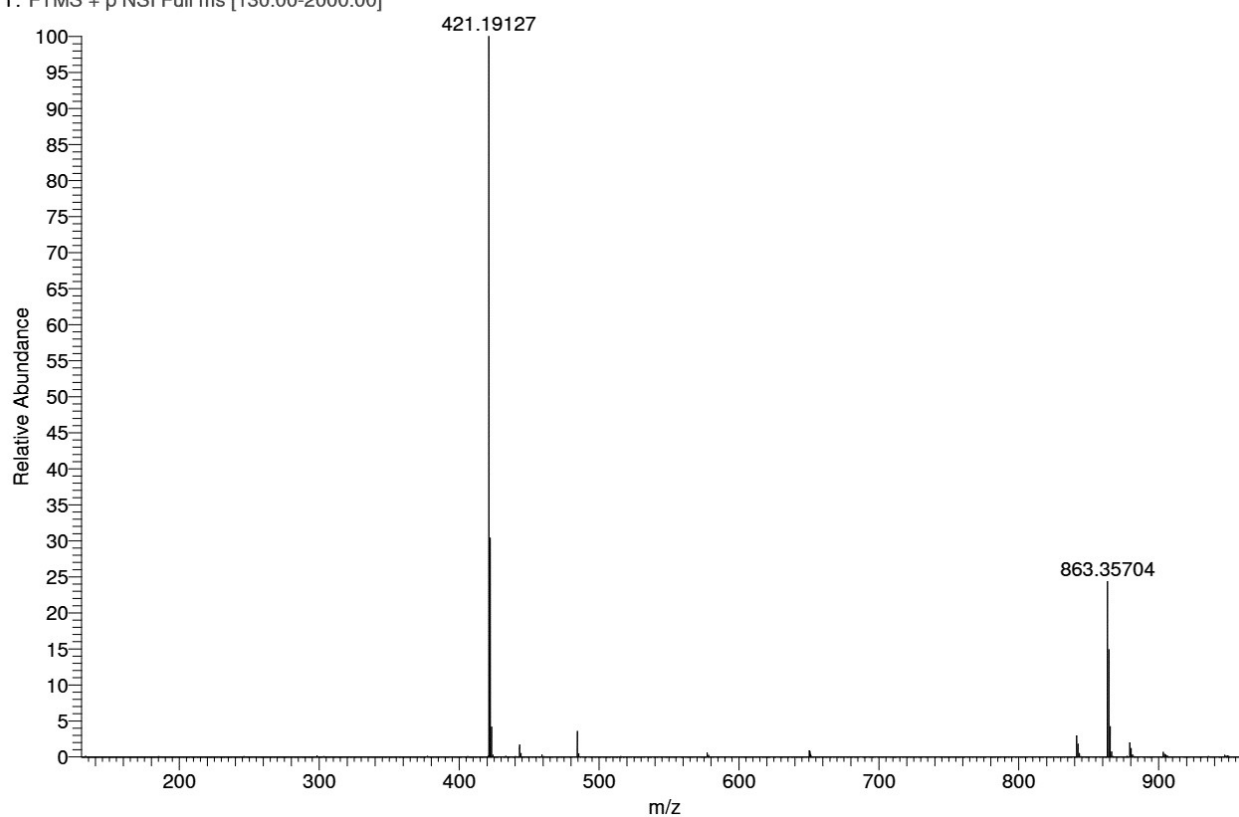
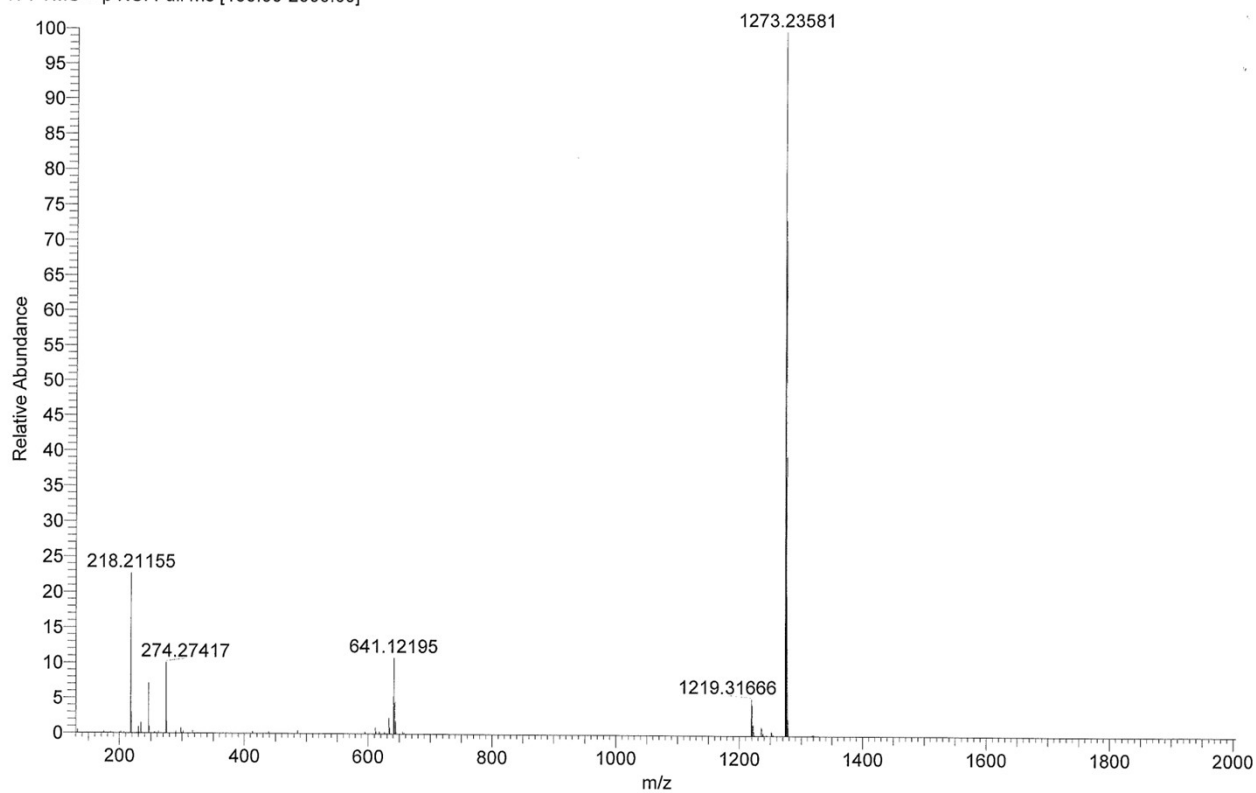


Figure S4.1. Experimental high resolution ESI mass spectrum of **LOMe**. m/z : calcd. for $[C_{28}H_{25}N_2O_2]^+$: 421.1911; found: 421.1913 (top: whole measurement range; bottom: zoomed excerpt).

LTQOT13938 #1-5 RT: 0.01-0.12 AV: 5 NL: 1.36E8
T: FTMS + p NSI Full ms [130.00-2000.00]



LTQOT13938 #1-5 RT: 0.01-0.12 AV: 5 NL: 1.36E8
T: FTMS + p NSI Full ms [130.00-2000.00]

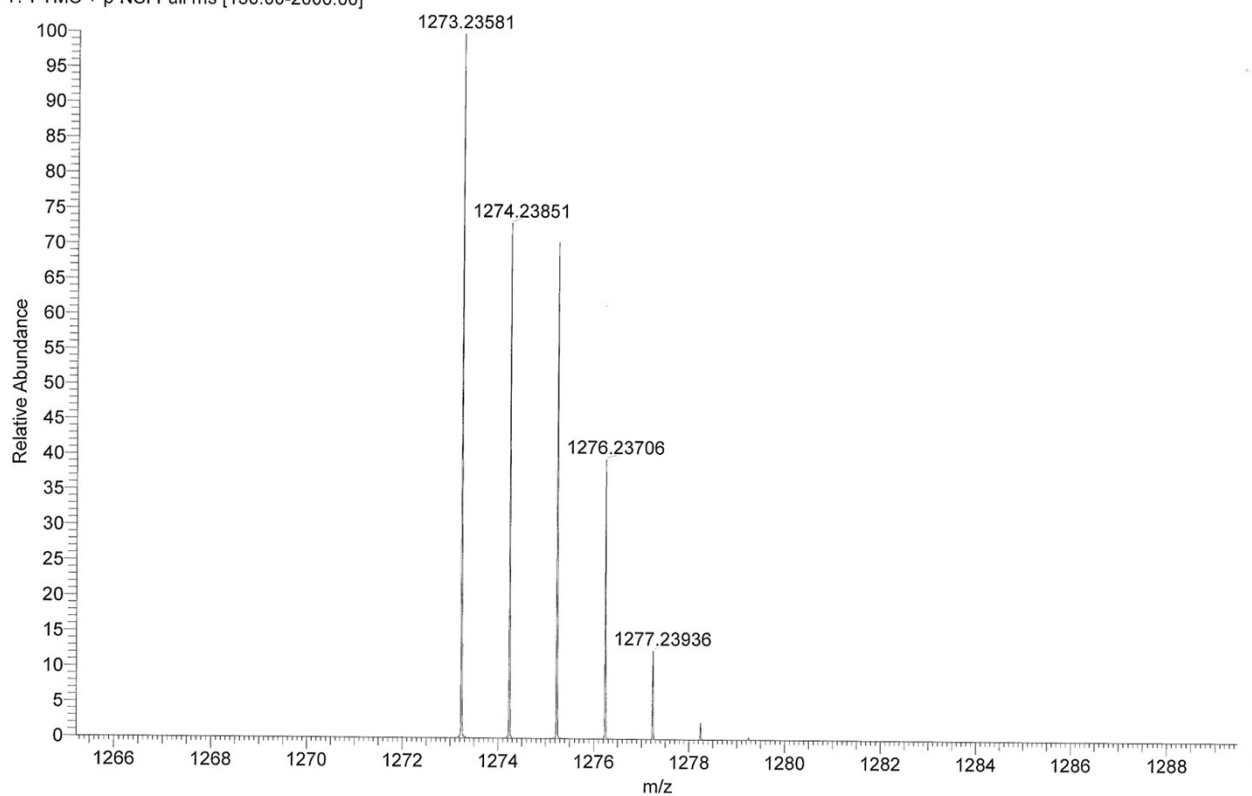


Figure S4.2. Experimental high resolution ESI mass spectrum of $\text{Cu}(\text{CF}_3)_2$. m/z : calcd. for $[\text{C}_{69}\text{H}_{48}\text{CuF}_{12}\text{N}_2\text{OP}_2]^+$: 1273.2341; found: 1273.2358 (top: whole measurement range; bottom: zoomed excerpt).

LTQOT13937 #2-4 RT: 0.04-0.10 AV: 3 NL: 1.45E8
T: FTMS + p NSI Full ms [130.00-2000.00]

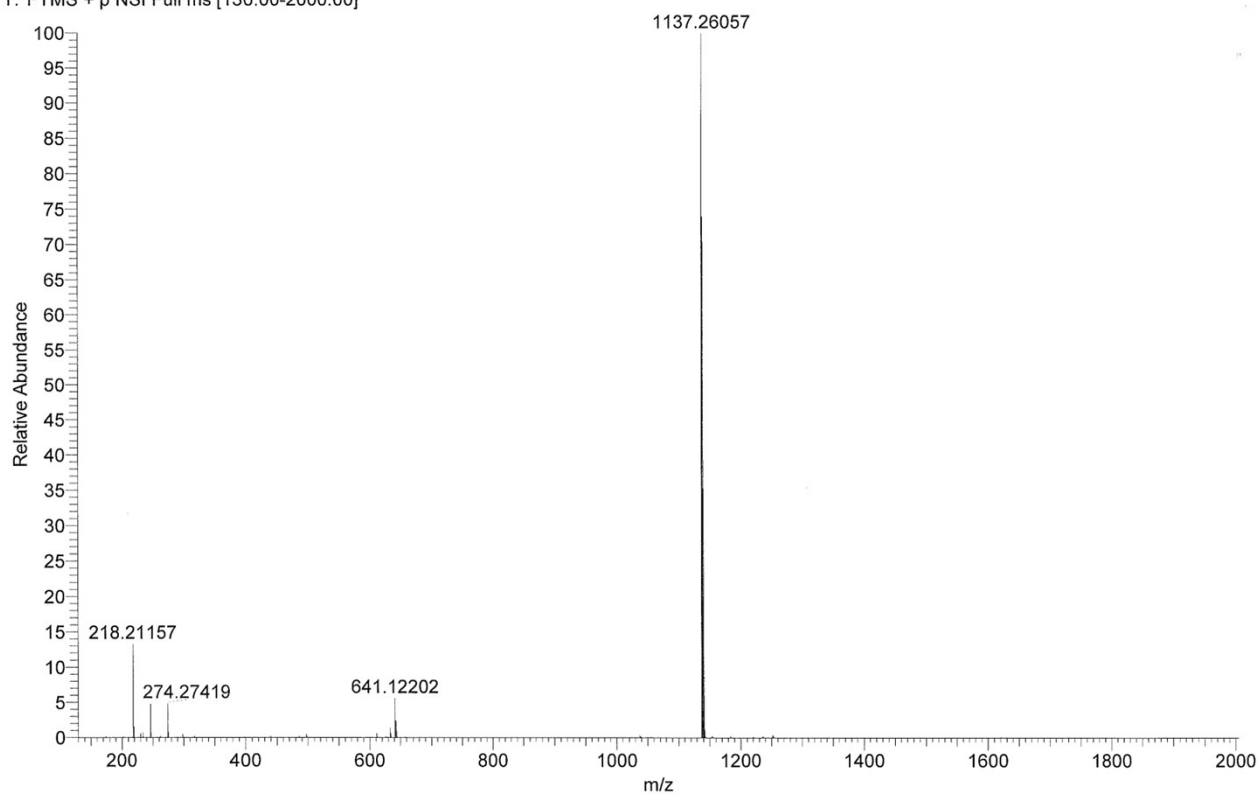
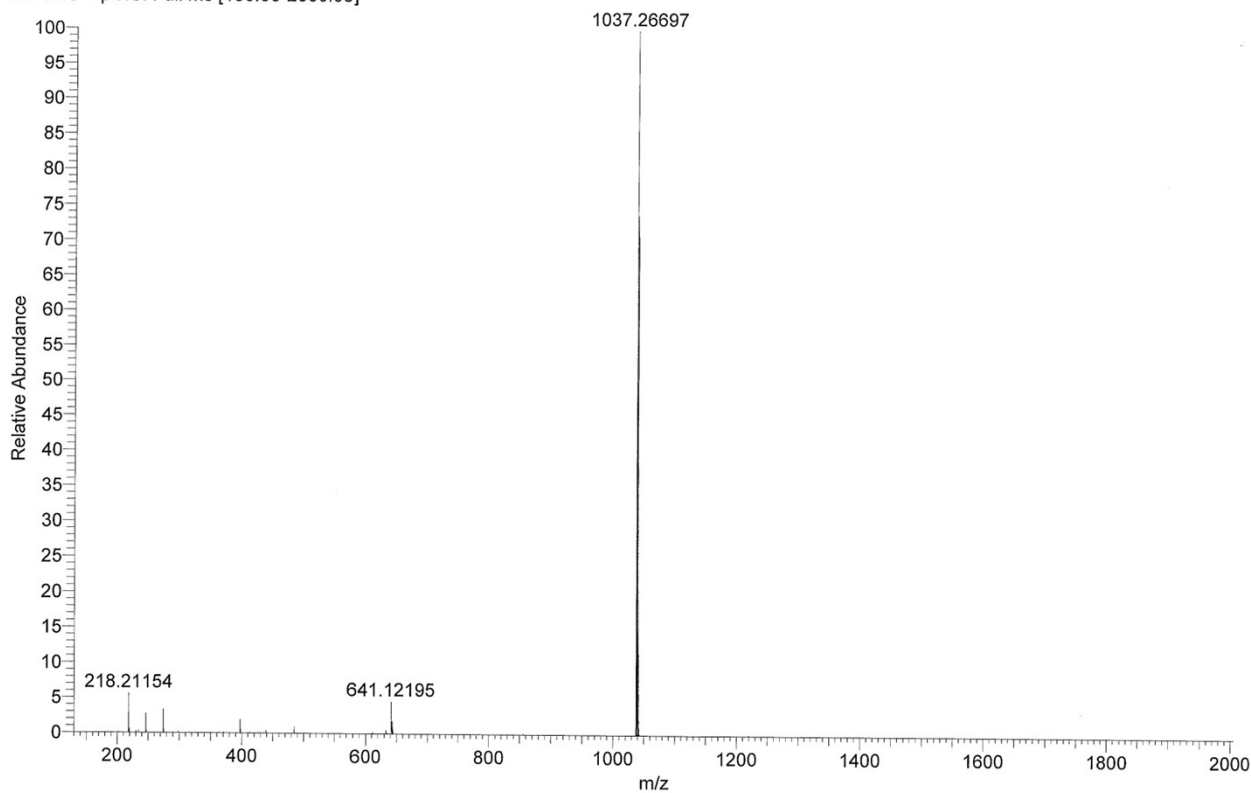


Figure S4.3. Experimental high resolution ESI mass spectrum of CuCF_3 . m/z : calcd. for $[\text{C}_{67}\text{H}_{50}\text{CuF}_6\text{N}_2\text{OP}_2]^+$: 1137.2593; found: 1137.2606.

LTQOT13936 #1-4 RT: 0.02-0.11 AV: 4 NL: 2.27E8
T: FTMS + p NSI Full ms [130.00-2000.00]



LTQOT13936 #1-4 RT: 0.02-0.11 AV: 4 NL: 2.27E8
T: FTMS + p NSI Full ms [130.00-2000.00]

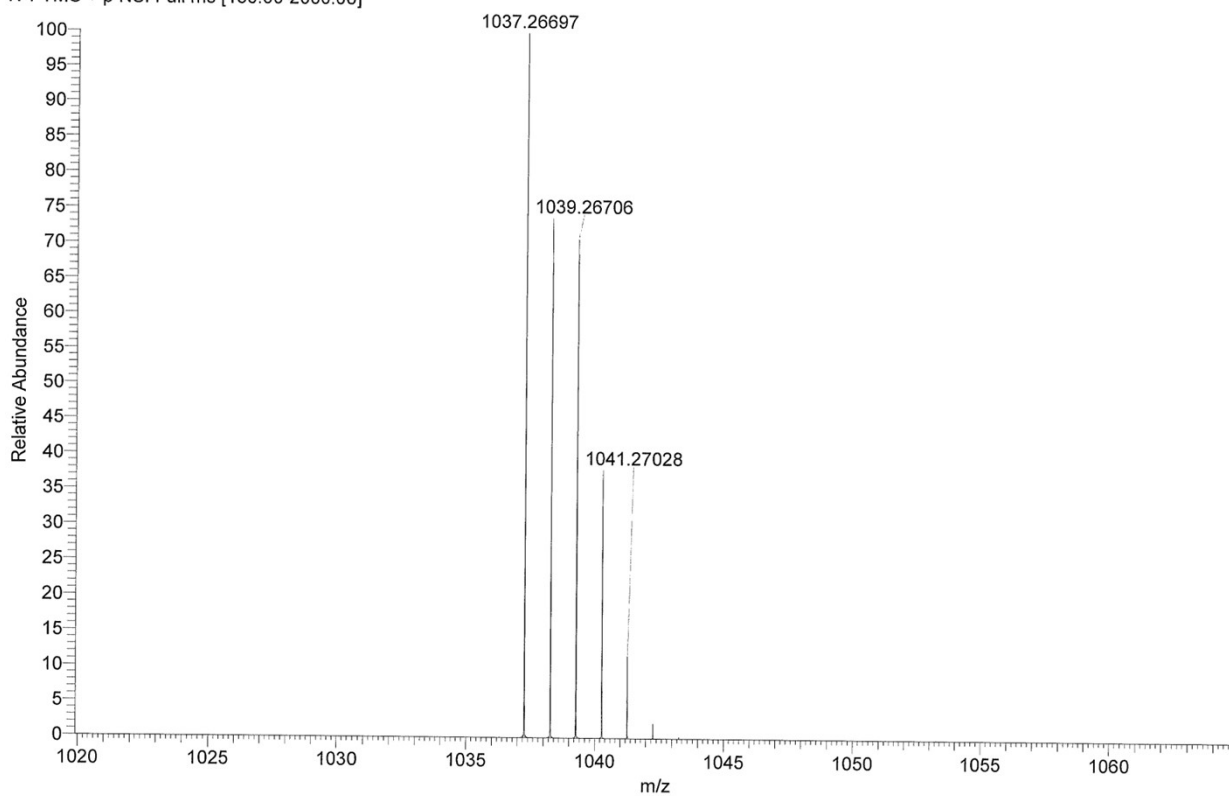
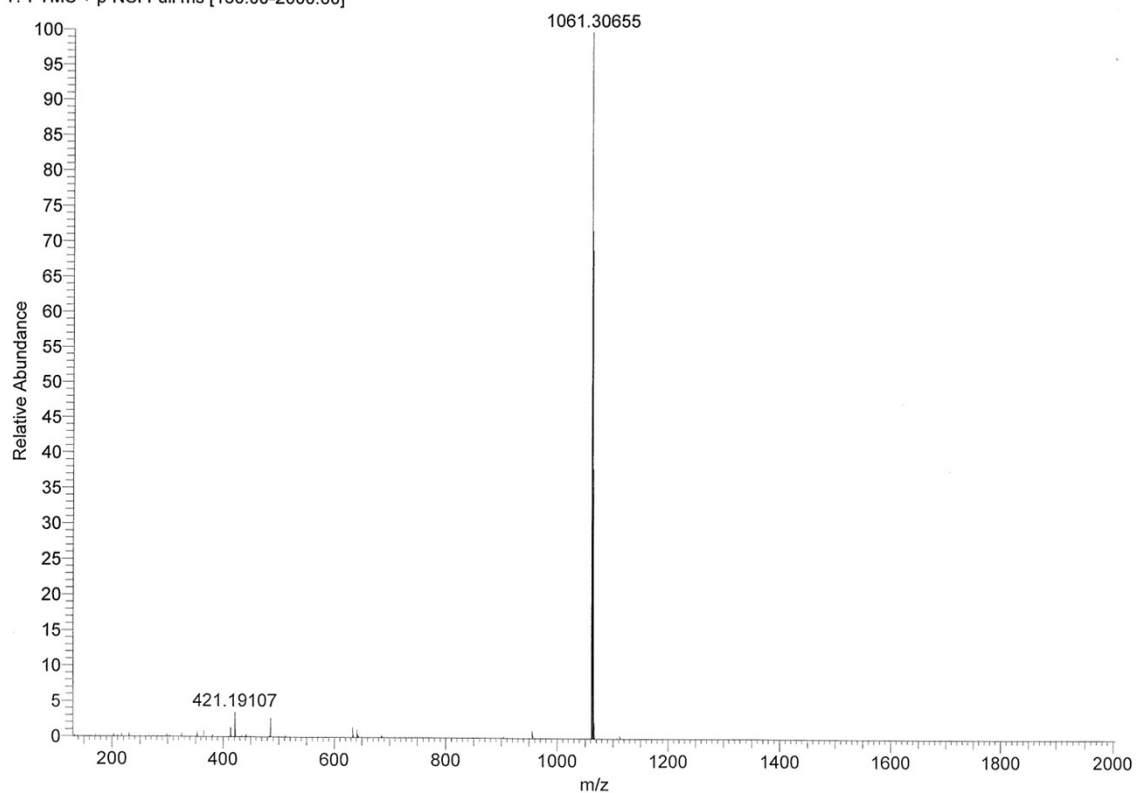


Figure S4.4. Experimental high resolution ESI mass spectrum of **CuF**. m/z : calcd. for $[C_{65}H_{50}CuF_2N_2OP_2]^+$: 1037.2657; found: 1037.2670 (top: whole measurement range; bottom: zoomed excerpt).

LTQOT15622 #2-11 RT: 0.03-0.27 AV: 10 NL: 2.91E7
T: FTMS + p NSI Full ms [130.00-2000.00]



LTQOT15622 #2-11 RT: 0.03-0.27 AV: 10 NL: 2.91E7
T: FTMS + p NSI Full ms [130.00-2000.00]

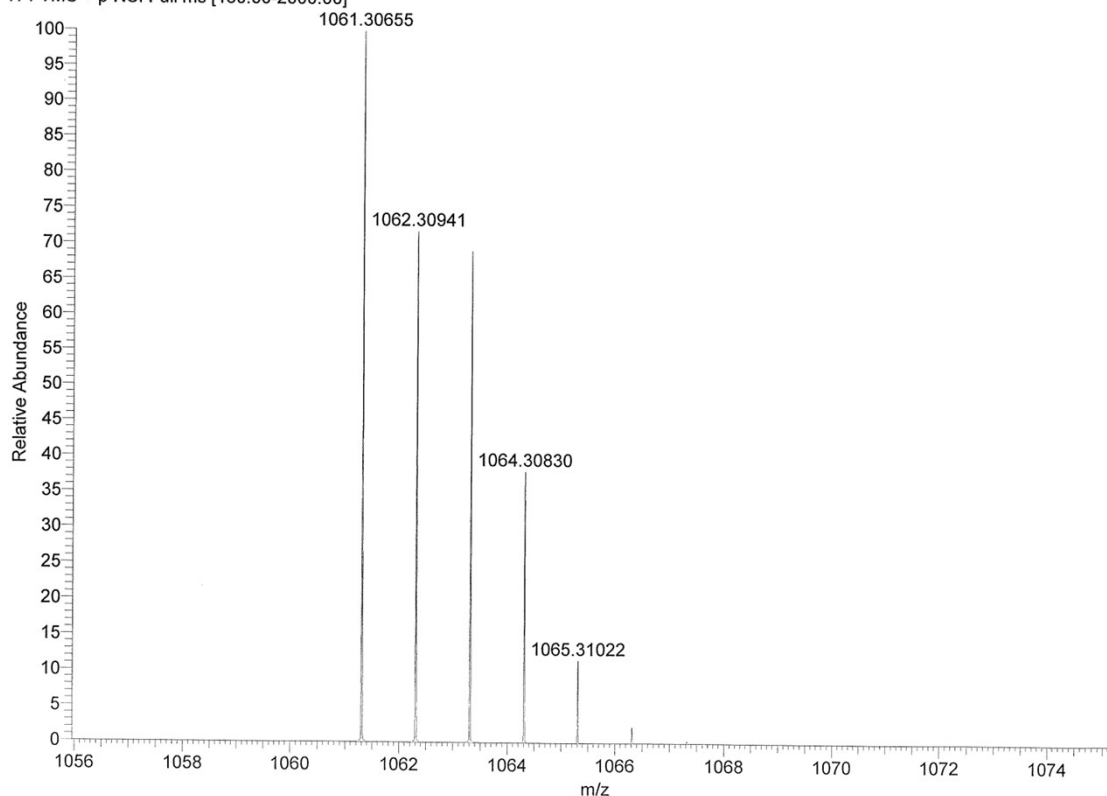


Figure S4.5. Experimental high resolution ESI mass spectrum of **CuOMe**. m/z : calcd. for $[C_{67}H_{56}CuN_2O_3P_2]^+$: 1061,3057; found: 1061.3066 (top: whole measurement range; bottom: zoomed excerpt).

5 Crystallographic Data and Solid State Molecular Structures

Single crystals of the solvate $[\text{Cu}(\text{MeCN})_2(\text{xant})][\text{PF}_6](\text{CH}_2\text{Cl}_2)_2(\text{C}_6\text{H}_{14})_{1/2}$ were obtained by crystallization from a concentrated dichloromethane/*n*-hexane solution at room temperature. Single crystals of **CuOMe** as solvate (*vide infra*) were obtained by crystallization from a concentrated 1,2-dichloroethane solution. The solution was carefully layered with a thin film of ethanol and secondly with *n*-heptane. Crystal growth was completed after 3-6 days at room temperature.

Table S5.1. Crystallographic data of the structures determinations of $[\text{Cu}(\text{MeCN})_2(\text{xant})][\text{PF}_6](\text{CH}_2\text{Cl}_2)_2(\text{C}_6\text{H}_{14})_{1/2}$ and a solvate of **CuOMe**.

	$[\text{Cu}(\text{MeCN})_2(\text{xant})][\text{PF}_6](\text{CH}_2\text{Cl}_2)_2(\text{C}_6\text{H}_{14})_{1/2}$ ^a	CuOMe ^b
Chemical Formula	$\text{C}_{48}\text{H}_{49}\text{Cl}_4\text{CuF}_6\text{N}_2\text{O}_3\text{P}_3$	$\text{C}_{67}\text{H}_{56}\text{CuF}_6\text{N}_2\text{O}_3\text{P}_3$
Formula mass	1082.14 g mol ⁻¹	1207.58 g mol ⁻¹
Crystal shape, colour	fragment, light yellow	fragment of plate, clear yellow
Crystal size	0.320 × 0.180 × 0.150 mm ³	0.188 × 0.152 × 0.069 mm ³
Temperature, Radiation	100 K, 1.54184 Å (CuK _α)	100 K, 1.54184 Å (CuK _α)
Abs. coefficient (corr.)	4.102 mm ⁻¹ (Gaussian)	1.750 mm ⁻¹ (Gaussian)
Crystal system	Triclinic	Monoclinic
Space group type (no.)	$P\bar{1}$ (2)	$P2/n$ (13)
Z, Z'	2, 1	4, 1
a, b, c	9.7521(1) Å, 15.5514(2) Å, 16.6886(3) Å	12.8402(2) Å, 19.2826(3) Å, 25.7915(3) Å
α, β, γ	94.049(1)°, 99.373(1)°, 100.684(1)°	90°, 101.171 (1)°, 90°
Volume	2440.59(6) Å ³	6264.8(2) Å ³
Refl. collected	14083	186131
unique	10316	13292
observed [<i>I</i> > 2σ(<i>I</i>)]	9809	11739
Data collection ranges	-12 ≤ <i>h</i> ≤ 12 / -19 ≤ <i>k</i> ≤ 19 / -21 ≤ <i>l</i> ≤ 21	-16 ≤ <i>h</i> ≤ 16 / -24 ≤ <i>k</i> ≤ 24 / -32 ≤ <i>l</i> ≤ 31
Completeness (to θ)	99.0% (77.69°)	99.2% (77.74°)
Data / restr. / param.	10316 / 0 / 604	13292 / 73 / 780
<i>R</i> _{int}	0.0554	0.0520
<i>R</i> ₁ [<i>I</i> > 2σ(<i>I</i>)]	0.0463	0.0374
<i>wR</i> ₂ (all data)	0.1268	0.0972
GoF on F ²	1.037	1.039
Largest peak/hole	0.981/-0.783 Å ⁻³	0.414/-0.634 Å ⁻³
CCDC Number ^c	2237581	2237580

^a A disordered $[\text{PF}_6]^-$ ion was refined using a split atom model (0.891(3) SOF of main component); a common ADP were refined for each disordered atom pair (EADP).

^b No appropriate model could be established for cocrystallised solvent molecules; the data were processed using the BYPASS algorithm as implemented in OLEX² (reference ¹⁷). A $[\text{PF}_6]^-$ was refined using a split atom model (0.619(5) SOF of main component); similarity and isotropicity restraints were applied (SADI, ISOR).

^c The CCDC reference numbers shown contain the supplementary crystallographic data for this paper. The data can be accessed free of charge at the Cambridge Crystallographic Data Centre via www.ccdc.cam.ac.uk/data_request/cif

6 Calculated Ground State Structures

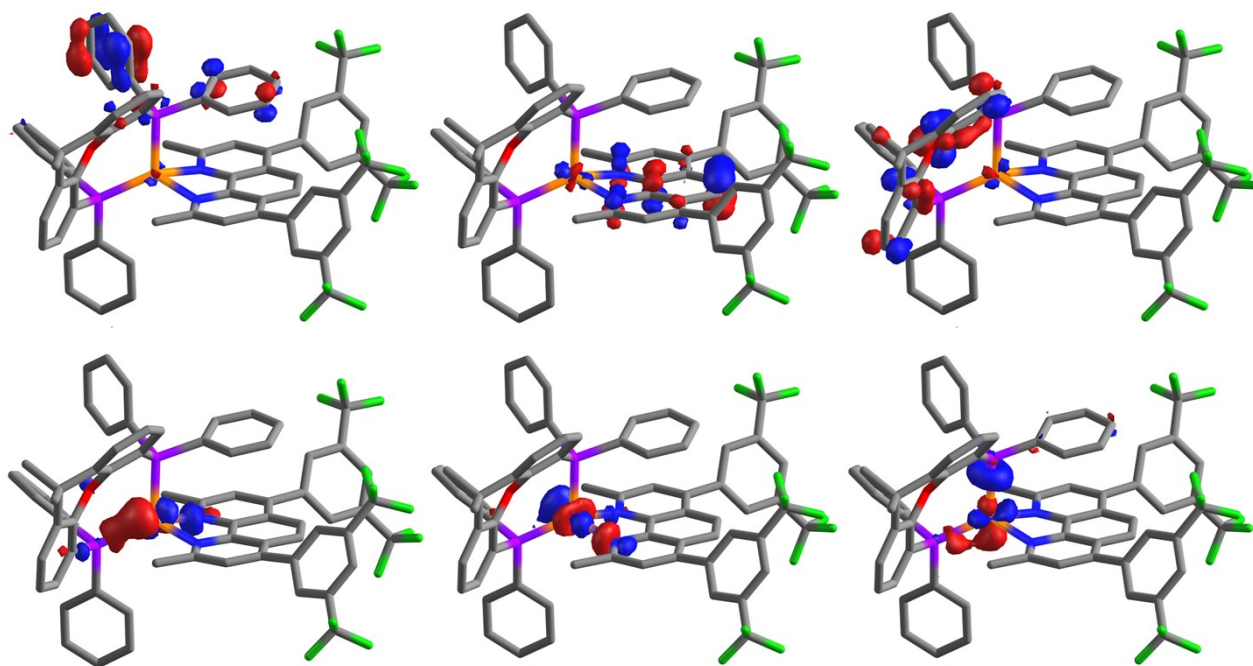


Figure S6.1. Orbital representation of the complex $\text{Cu}(\text{CF}_3)_2$. Left to right, top to bottom: HOMO-5, HOMO-4, HOMO-3, HOMO-2, HOMO-1, HOMO.

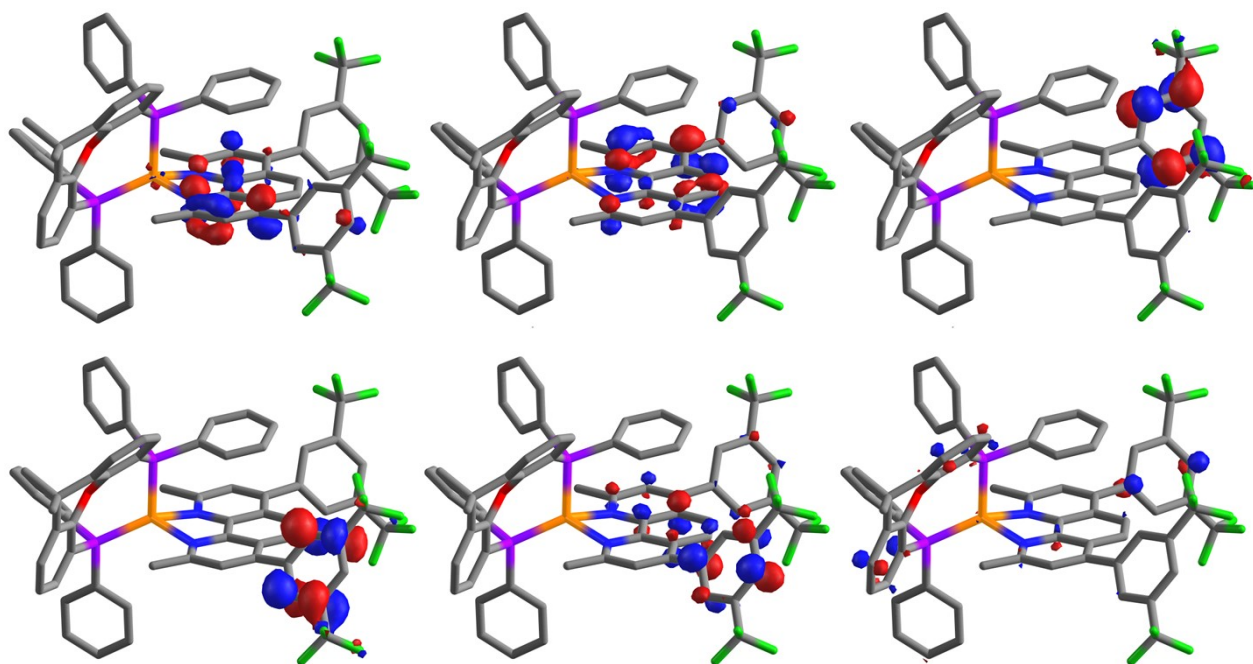


Figure S6.2. Orbital representation of the complex $\text{Cu}(\text{CF}_3)_2$. Left to right, top to bottom: LUMO, LUMO+1, LUMO+2, LUMO+3, LUMO+4, LUMO+5.

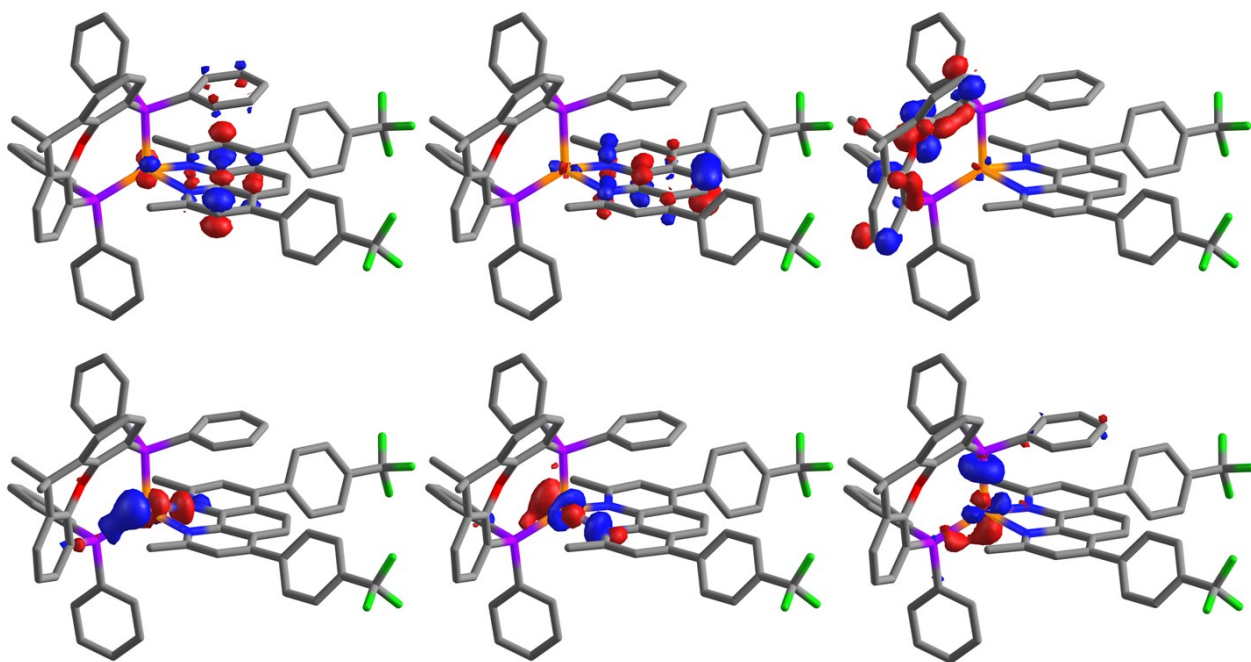


Figure S6.3. Orbital representation of the complex CuCF_3 . Left to right, top to bottom: HOMO-5, HOMO-4, HOMO-3, HOMO-2, HOMO-1, HOMO.

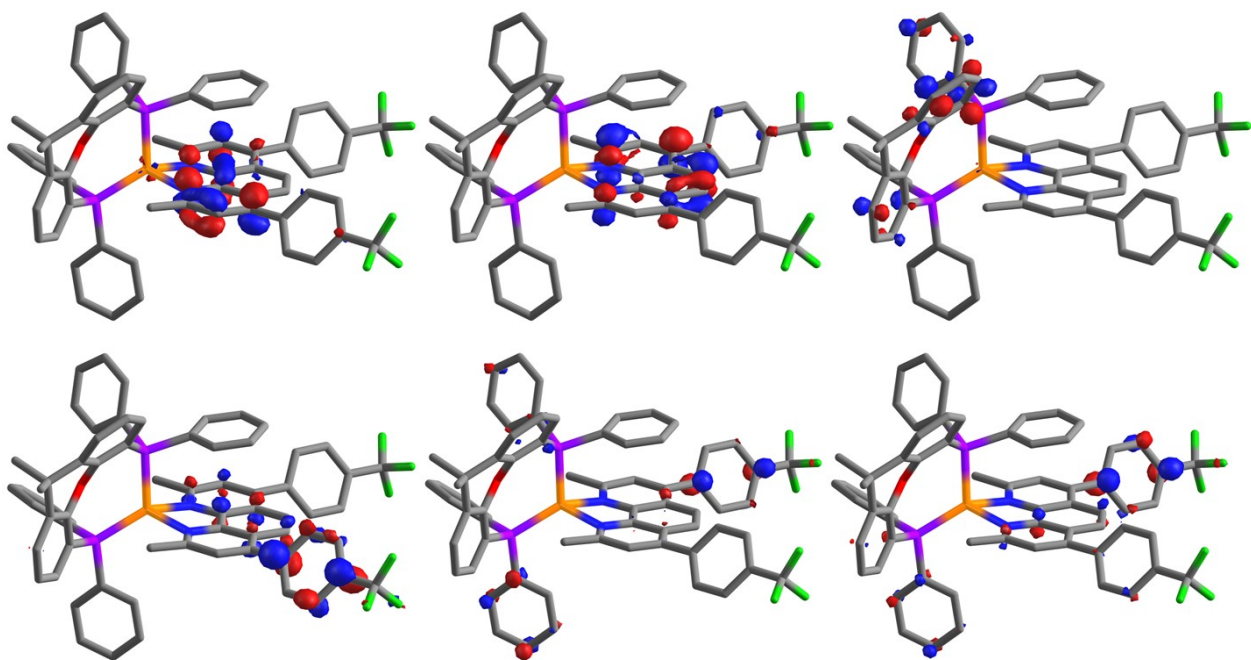


Figure S6.4. Orbital representation of the complex CuCF_3 . Left to right, top to bottom: LUMO, LUMO+1, LUMO+2, LUMO+3, LUMO+4, LUMO+5.

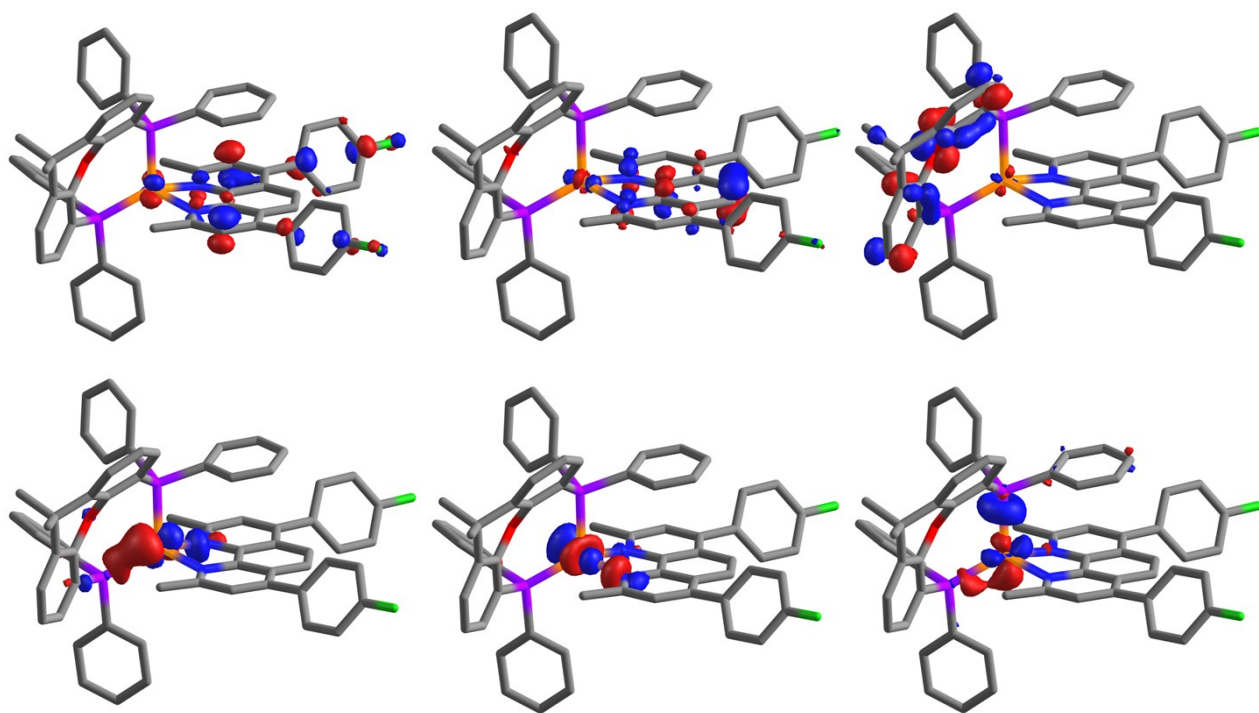


Figure S6.5. Orbital representation of the complex **CuF**. Left to right, top to bottom: HOMO-5, HOMO-4, HOMO-3, HOMO-2, HOMO-1, HOMO.

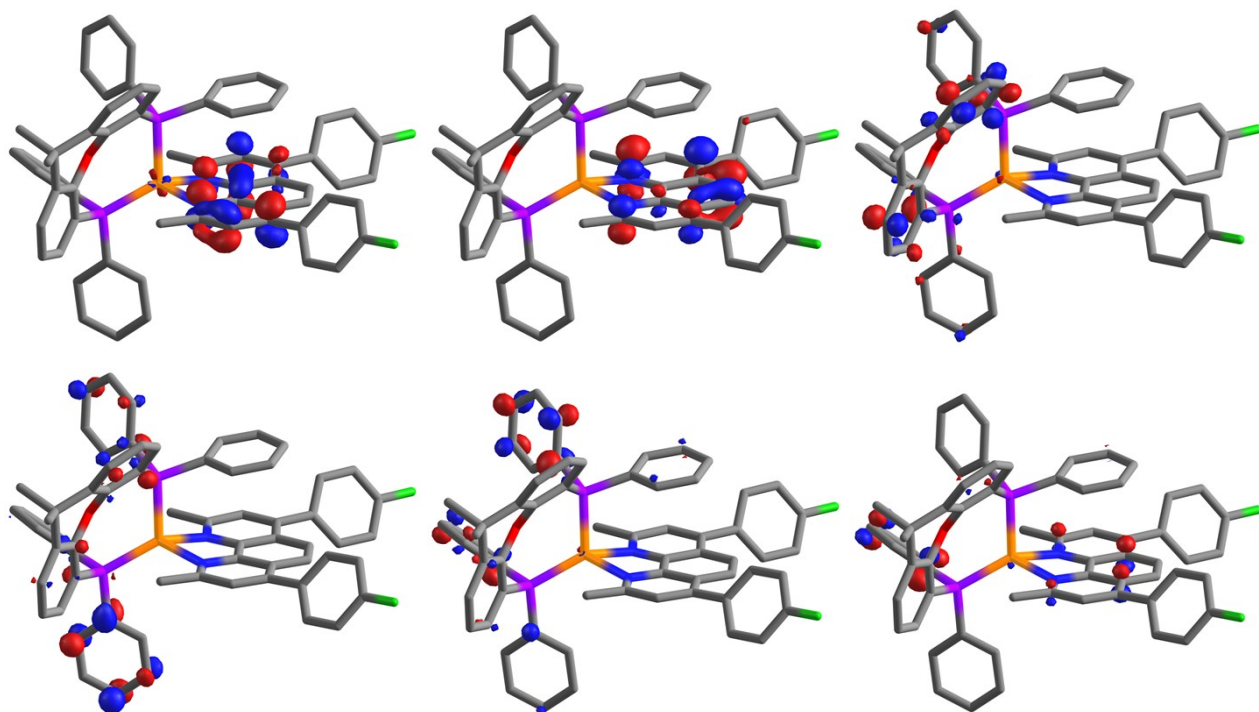


Figure S6.6. Orbital representation of the complex **CuF**. Left to right, top to bottom: LUMO, LUMO+1, LUMO+2, LUMO+3, LUMO+4, LUMO+5.

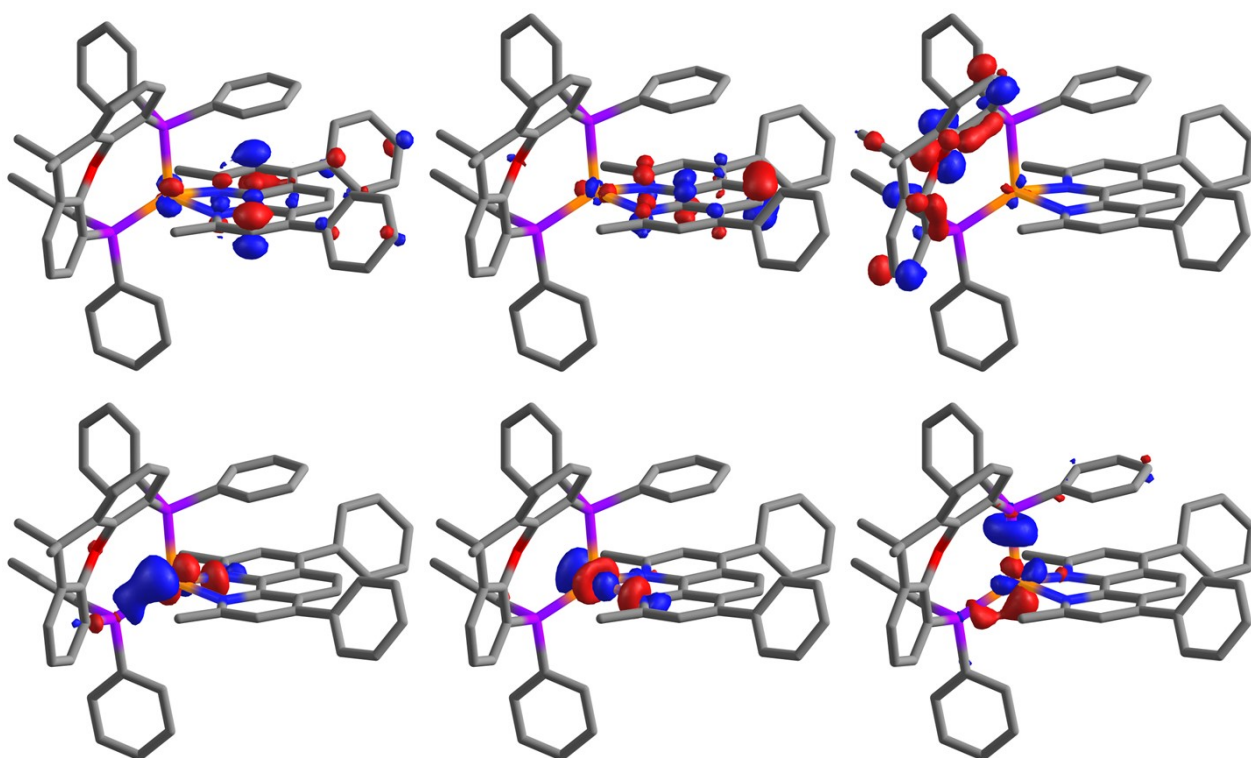


Figure S6.7. Orbital representation of the complex **CuH**. Left to right, top to bottom: HOMO-5, HOMO-4, HOMO-3, HOMO-2, HOMO-1, HOMO.

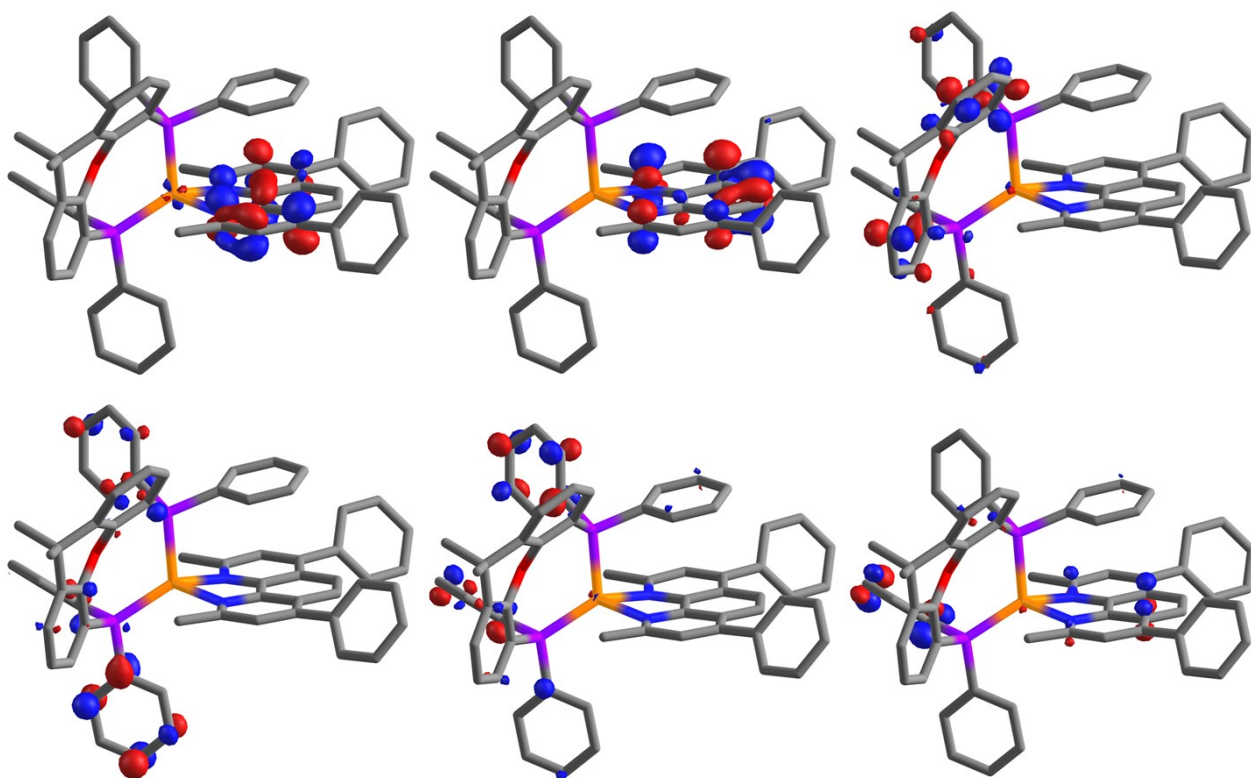


Figure S6.8. Orbital representation of the complex **CuH**. Left to right, top to bottom: LUMO, LUMO+1, LUMO+2, LUMO+3, LUMO+4, LUMO+5.

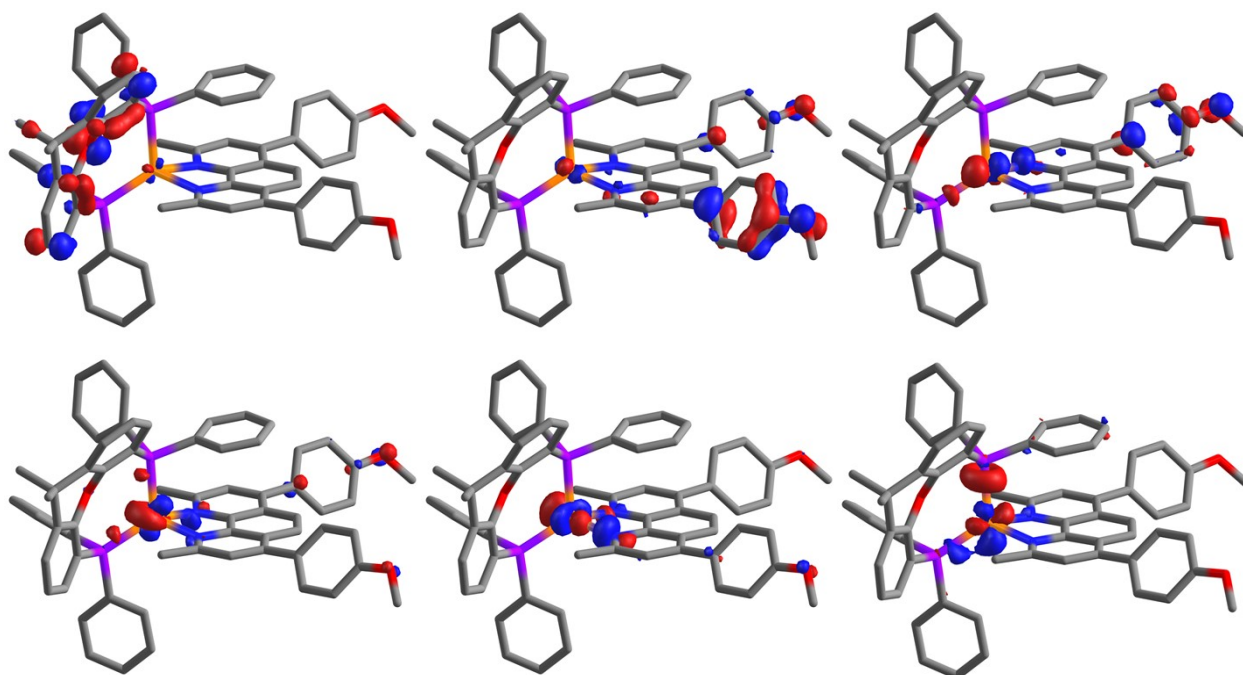


Figure S6.9. Orbital representation of the complex **CuOMe**. Left to right, top to bottom: HOMO-5, HOMO-4, HOMO-3, HOMO-2, HOMO-1, HOMO.

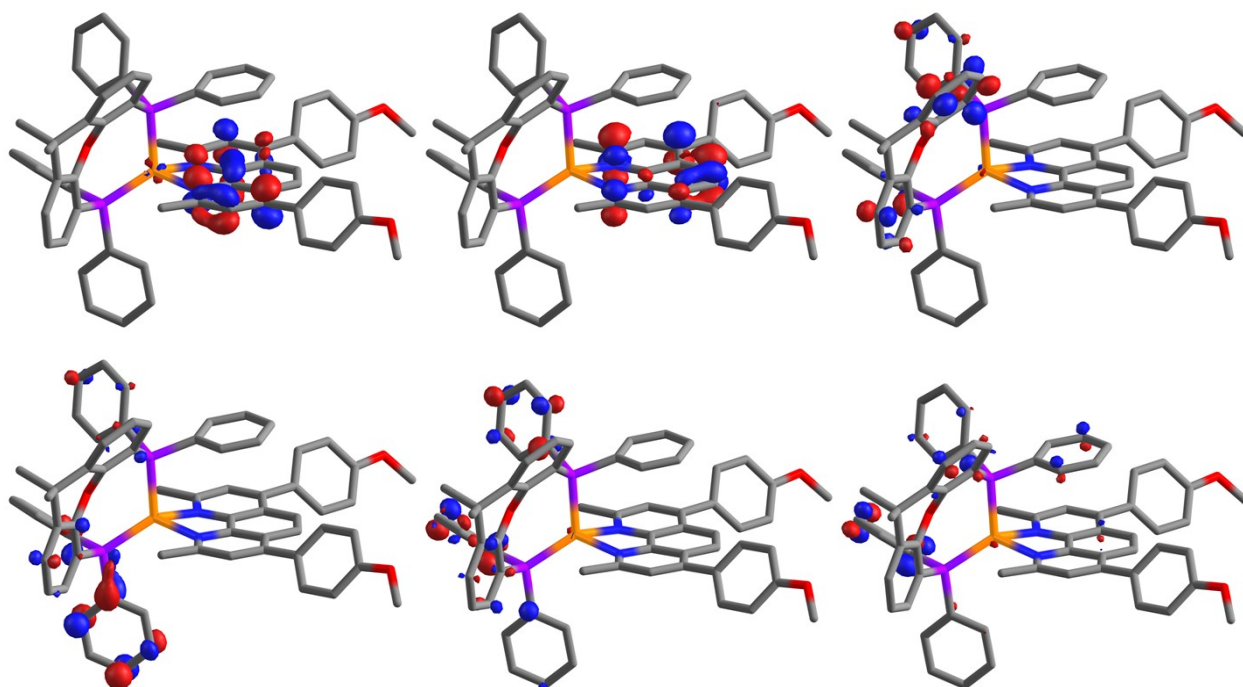


Figure S6.10. Orbital representation of the complex **CuOMe**. Left to right, top to bottom: LUMO, LUMO+1, LUMO+2, LUMO+3, LUMO+4, LUMO+5.

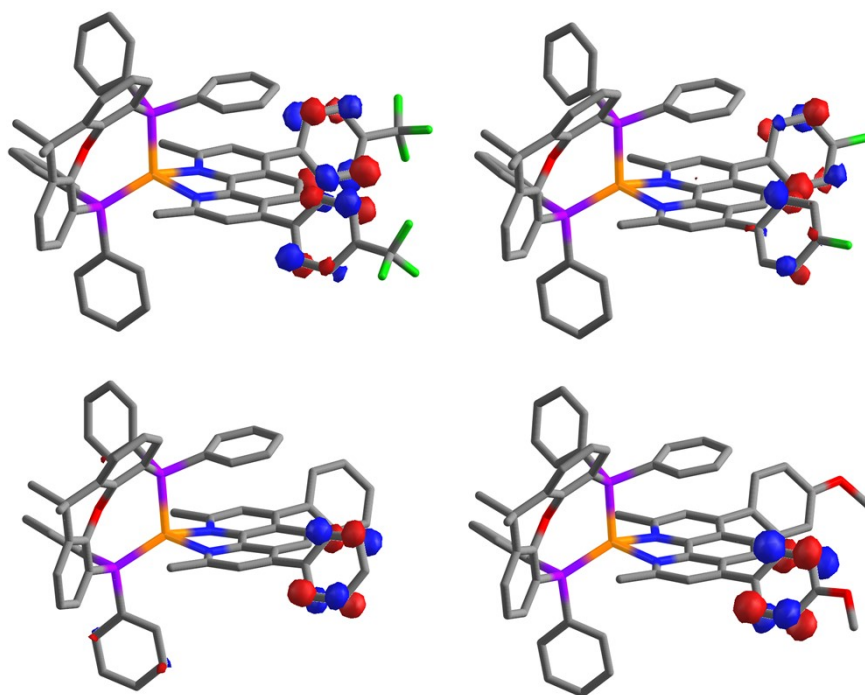


Figure S6.11. Selected orbitals of the complexes (left to right, top to bottom) **CuCF₃**, **CuF**, **CuH** and **CuOMe** showing the LUMO+10, LUMO+7, LUMO+12 and LUMO+10, respectively. Energies are -7.137 eV, -6.988 eV, -7.165 eV and -7.042 eV.

7 Electrochemical Data

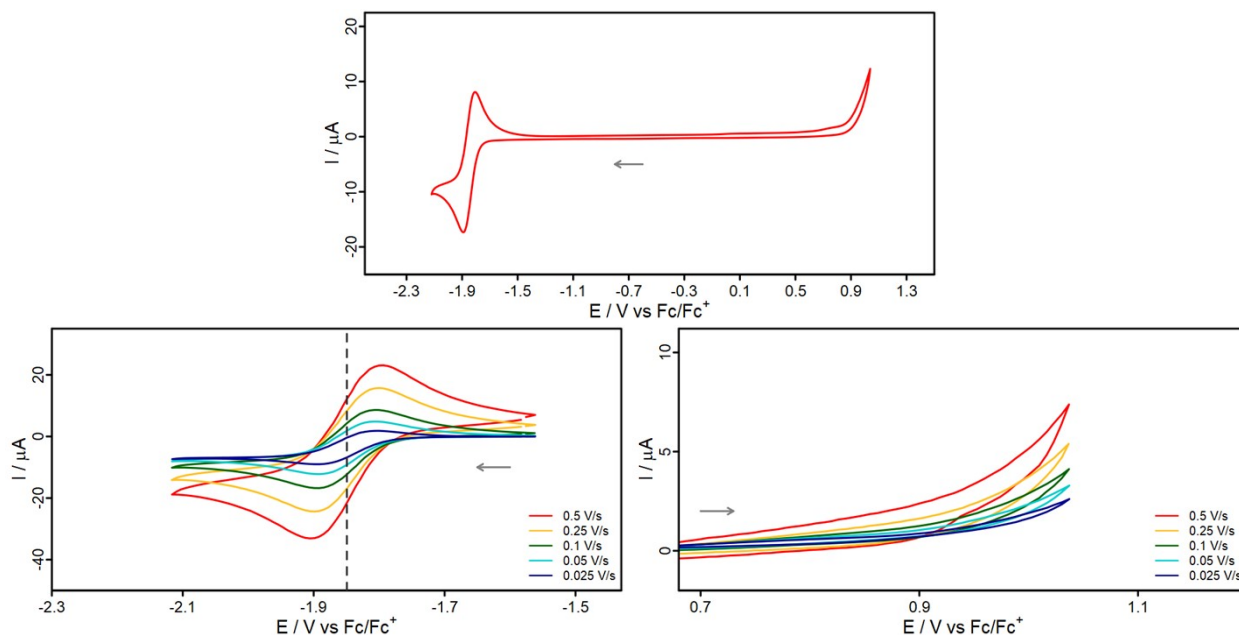


Figure S7.1. Cyclic voltammogram of $\text{Cu}(\text{CF}_3)_2$ (top, red, 1 mM) in acetonitrile solution referenced vs. the ferrocene/ferricenium (Fc/Fc^+) couple. Conditions: scan rate of 100 mVs^{-1} with $0.1 \text{ M} [\text{Bu}_4\text{N}][\text{PF}_6]$ as supporting electrolyte. Reductive (bottom left) and oxidative (bottom right) events of the cyclic voltammograms of $\text{Cu}(\text{CF}_3)_2$ at different scan rates: 25 mVs^{-1} (blue), 50 mVs^{-1} (teal), 100 mVs^{-1} (green), 250 mVs^{-1} (yellow) and 500 mVs^{-1} (red). The arrow illustrates the initial scan direction.

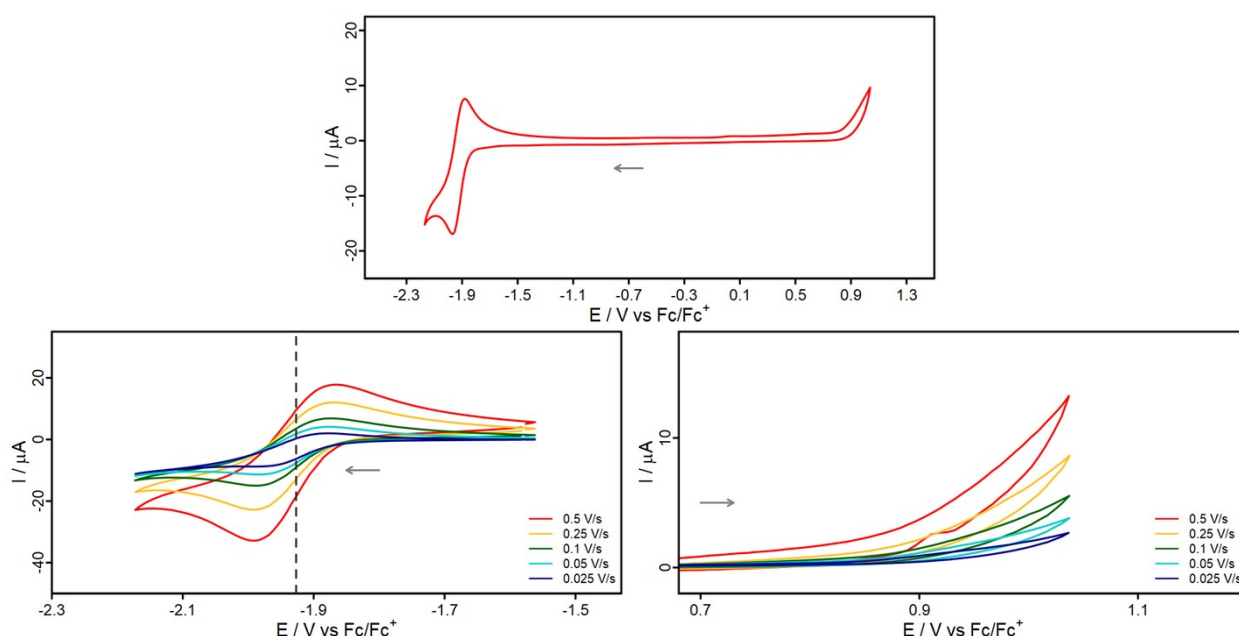


Figure S7.2. Cyclic voltammogram of CuCF_3 (top, red, 1 mM) in acetonitrile solution referenced vs. the ferrocene/ferricenium (Fc/Fc^+) couple. Conditions: scan rate of 100 mVs^{-1} with $0.1 \text{ M} [\text{Bu}_4\text{N}][\text{PF}_6]$ as supporting electrolyte. Reductive (bottom left) and oxidative (bottom right) events of the cyclic voltammograms of CuCF_3 at different scan rates: 25 mVs^{-1} (blue), 50 mVs^{-1} (teal), 100 mVs^{-1} (green), 250 mVs^{-1} (yellow) and 500 mVs^{-1} (red). The arrow illustrates the initial scan direction.

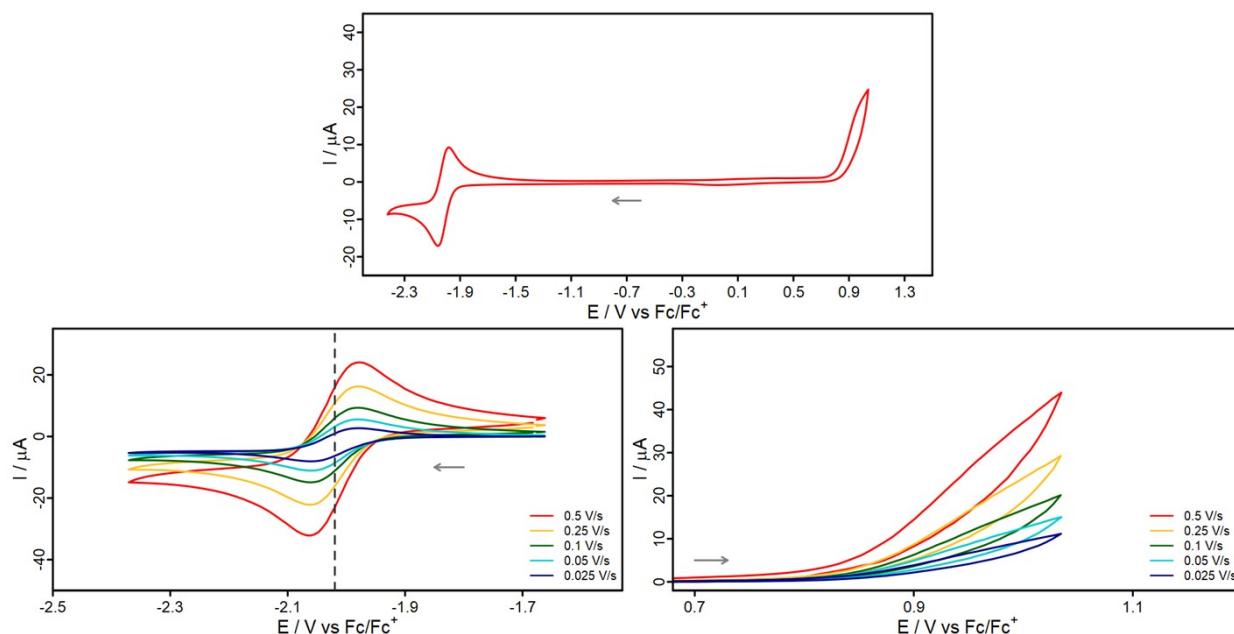


Figure S7.3. Cyclic voltammogram of **CuF** (top, red, 1 mM) in acetonitrile solution referenced vs. the ferrocene/ferricenium (Fc/Fc^+) couple. Conditions: scan rate of 100 mVs^{-1} with $0.1 \text{ M } [\text{Bu}_4\text{N}][\text{PF}_6]$ as supporting electrolyte. Reductive (bottom left) and oxidative (bottom right) events of the cyclic voltammograms of **CuF** at different scan rates: 25 mVs^{-1} (blue), 50 mVs^{-1} (teal), 100 mVs^{-1} (green), 250 mVs^{-1} (yellow) and 500 mVs^{-1} (red). The arrow illustrates the initial scan direction.

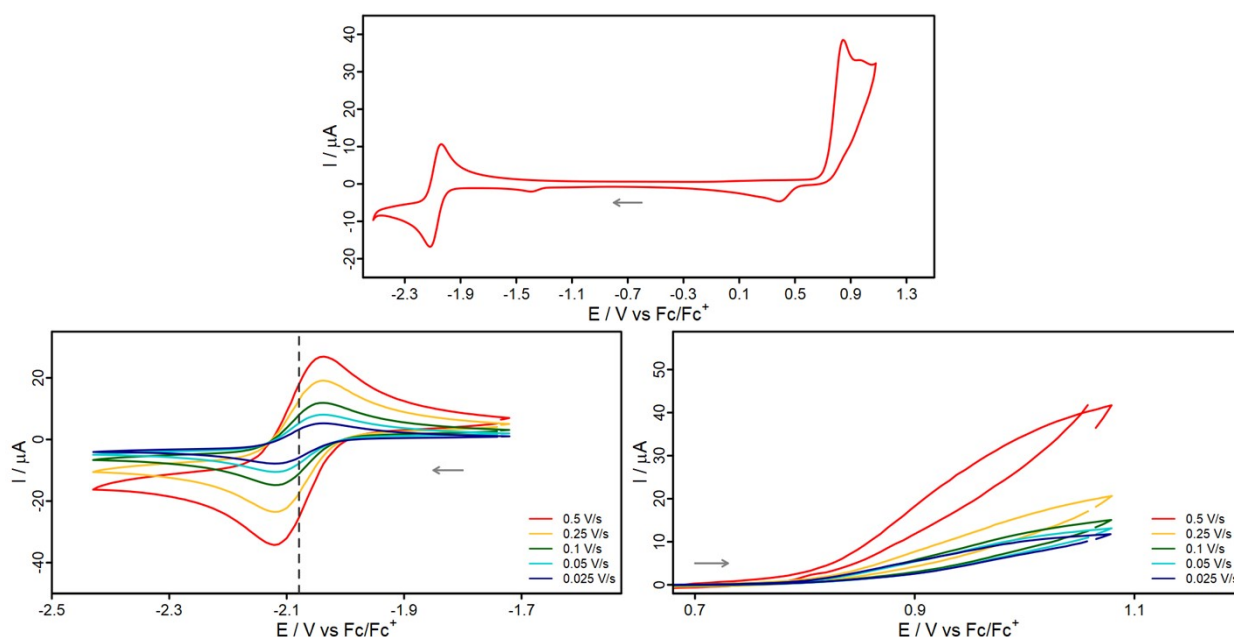


Figure S7.4. Cyclic voltammogram of **CuOME** (top, red, 1 mM) in acetonitrile solution referenced vs. the ferrocene/ferricenium (Fc/Fc^+) couple. Conditions: scan rate of 100 mVs^{-1} with $0.1 \text{ M } [\text{Bu}_4\text{N}][\text{PF}_6]$ as supporting electrolyte. Reductive (bottom left) and oxidative (bottom right) events of the cyclic voltammograms of **CuOME** at different scan rates: 25 mVs^{-1} (blue), 50 mVs^{-1} (teal), 100 mVs^{-1} (green), 250 mVs^{-1} (yellow) and 500 mVs^{-1} (red). The arrow illustrates the initial scan direction.

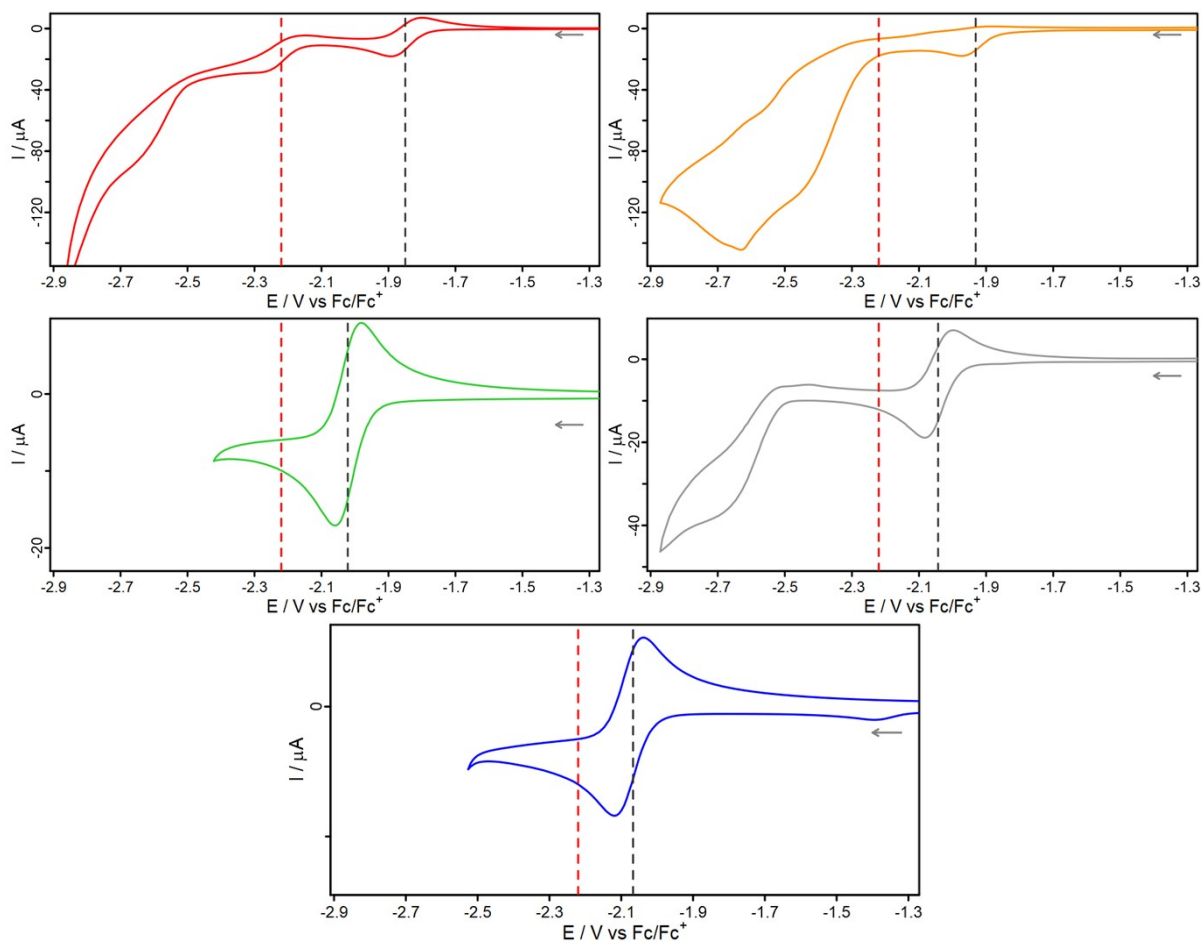


Figure S7.5. Cyclic voltammograms of all complexes **Cu(CF₃)₂**, **CuCF₃**, **CuF**, **CuH** and **CuOMe** (from top left to bottom right: red, orange, green, grey, blue) in acetonitrile solution (1 mM) referenced vs. the ferrocene/ferricenium (Fc/Fc⁺) couple. Conditions: scan rate of 100 mVs⁻¹ with 0.1 M [Bu₄N][PF₆] as supporting electrolyte. All voltammograms are plotted in the same potential window for comparison. Further, the left vertical line (red, dashed) represents the potential where the second reduction of **Cu(CF₃)₂** was detected. The right vertical line (black, dashed) represents the reduction potential of each complex of the respectively shown voltammogram (e.g. **CuOMe**, bottom center). At potentials more negative than -2.5 V the solvent acetonitrile is being reduced, which marks the measurable potential window of the solvent (prominent in the voltammograms of **Cu(CF₃)₂** and **CuH**). In **CuCF₃**, another reduction event onsets at -2.3 V already, indicating a possible reduction at the trifluoromethylphenyl substituent. This reduction, however, would be irreversible (note for example the strong negative current of up to -110 μA).

8 Time-resolved Spectroscopy

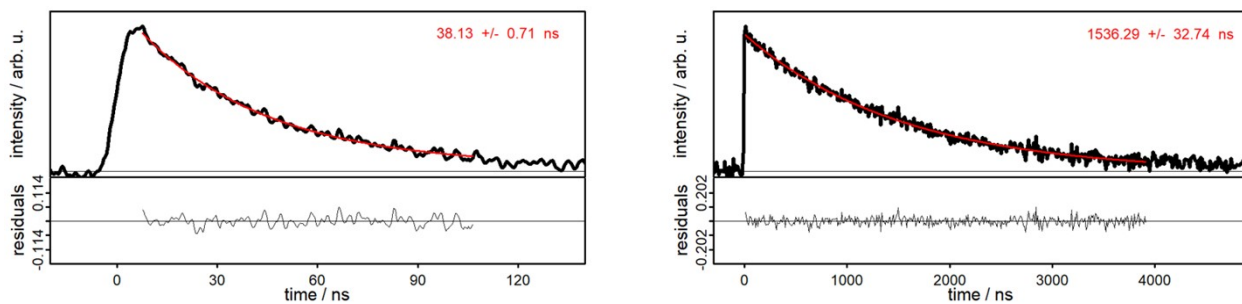


Figure S8.1. Decay curves obtained from time-resolved emission spectroscopy of $\text{Cu}(\text{CF}_3)_2$ measured in inert acetonitrile (left) and inert dichloromethane (right). Luminescence lifetimes after fitting (red curve) are denoted in ns with estimated error.

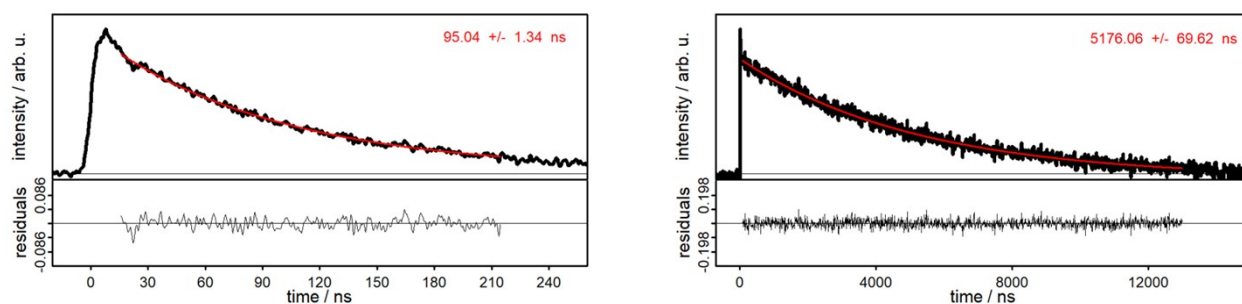


Figure S8.2. Decay curves obtained from time-resolved emission spectroscopy of CuCF_3 measured in inert acetonitrile (left) and inert dichloromethane (right). Luminescence lifetimes after fitting (red curve) are denoted in ns with estimated error.

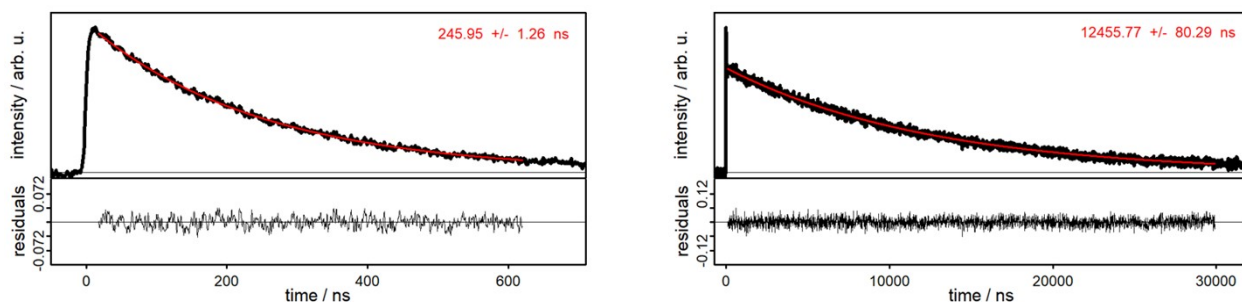


Figure S8.3. Decay curves obtained from time-resolved emission spectroscopy of CuF measured in inert acetonitrile (left) and inert dichloromethane (right). Luminescence lifetimes after fitting (red curve) are denoted in ns with estimated error.

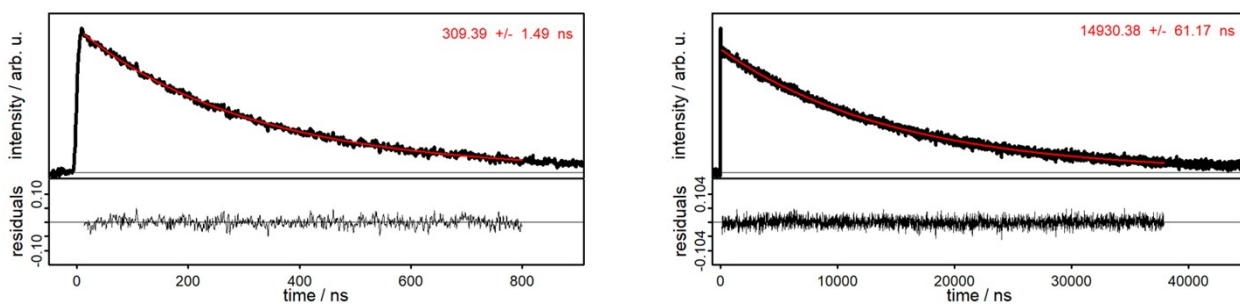


Figure S8.4. Decay curves obtained from time-resolved emission spectroscopy of **CuH** measured in inert acetonitrile (left) and inert dichloromethane (right). Luminescence lifetimes after fitting (red curve) are denoted in ns with estimated error.

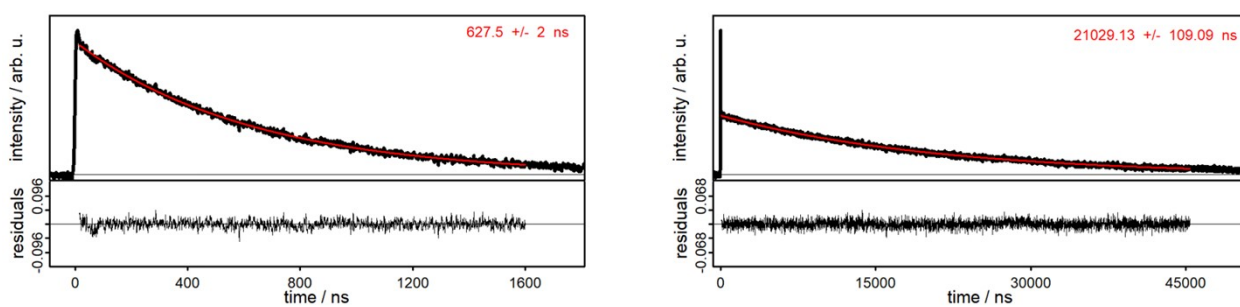


Figure S8.5. Decay curves obtained from time-resolved emission spectroscopy of **CuOMe** measured in inert acetonitrile (left) and inert dichloromethane (right). Luminescence lifetimes after fitting (red curve) are denoted in ns with estimated error.

9 Radiative and Non-Radiative Rate Constants

The k_r and k_{nr} were approximated using the respective formalism:^{18,19}

$$k_r = \frac{\phi_{em}}{\tau_{em}} \quad \text{and} \quad k_{nr} = \frac{1}{\tau_{em}} - k_r$$

Note, that for k_{nr} , the reverse-intersystem crossing rate k_{RISC} was neglected. The results are gathered below.

Table S9.1. Summary of the determined emission lifetimes τ_{em} , emission quantum yields ϕ_{em} and the approximated radiative (k_r) and non-radiative (k_{nr}) rate constants for the complexes **Cu(CF₃)₂-CuOMe** and their 5,6-disubstituted counterparts.

Functional Group	Acetonitrile				Dichloromethane	
	k_r [10^4 s ⁻¹]		k_{nr} [10^6 s ⁻¹]		k_r [10^4 s ⁻¹]	k_{nr} [10^6 s ⁻¹]
	4,7	5,6 ^{a)}	4,7	5,6 ^{a)}	4,7	
-(CF ₃) ₂	5.0	5.3	25.0	17.2	4.0	0.63
-CF ₃	4.0	1.0	10	2.6	3.7	0.16
-F	4.4	0.8	4.0	2.0	3.6	0.044
-H	4.4	0.4	3.2	2.0	3.6	0.032
-OMe	3.3	14.5	1.6	90.8	3.0	0.017

^{a)} emission lifetimes and emission quantum yields taken from ^{16c}.

10 Excited State Reduction Potentials

For determination of the excited state potential the simplified Rehm-Weller^{19,20} equation 2 was applied:

$$E_{1/2}^{*red} = E_{1/2}^{red} + E_{0,0} \quad \text{eq. 2}$$

Table S10.1. Determined and calculated values for $E_{1/2}^{*red}$.

Compound	$E_{1/2}^{red}$ [V]	$E_{0,0}$ [nm]	$E_{0,0}$ [eV]	$E_{1/2}^{*red}$ [V vs. Fc/Fc ⁺]
Cu(CF ₃) ₂	-1.85	510	2.431	0.581
CuCF ₃	-1.93	501	2.475	0.545
CuF	-2.02	490	2.530	0.510
CuH	-2.04	489	2.535	0.495
CuOMe	-2.08	484	2.562	0.482

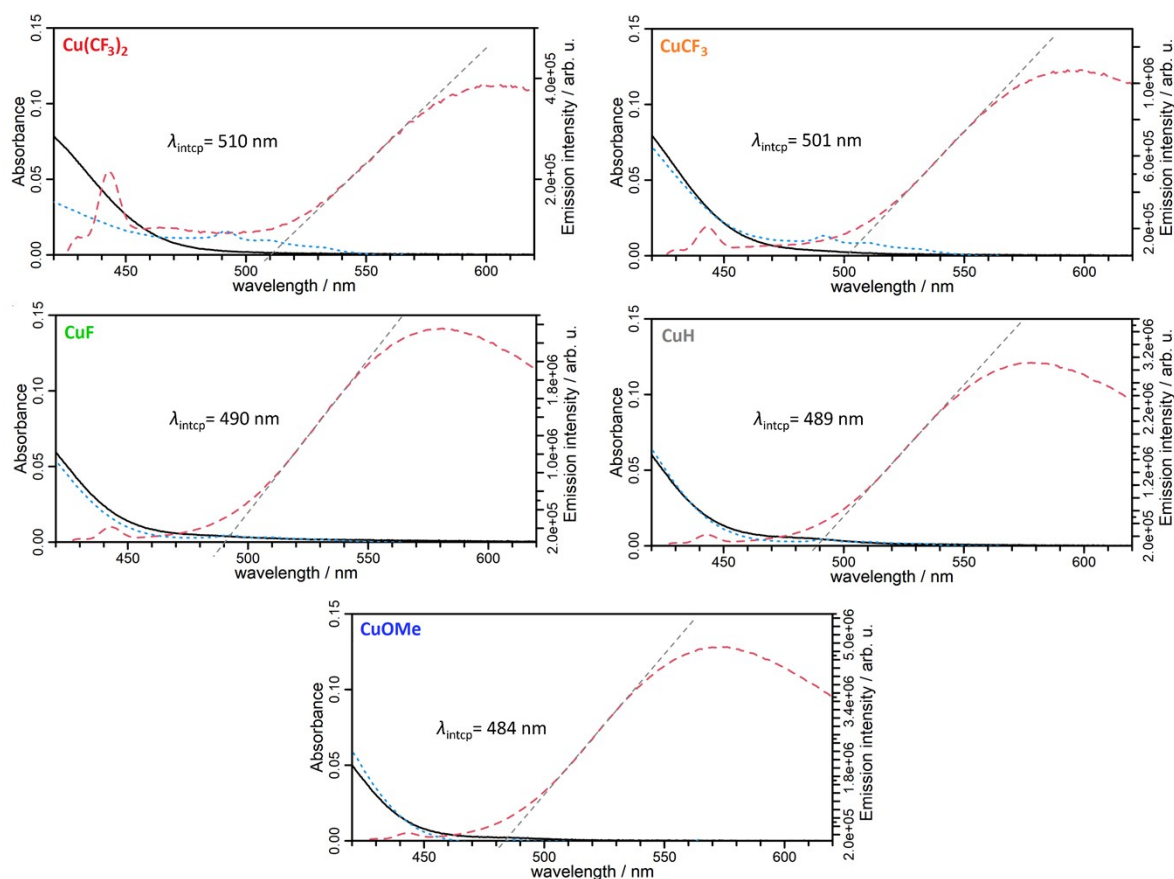


Figure S10.1. Determination of the intercept wavelength which was used for the determination of $E_{0,0}$.

11 Singlet Oxygen Generation and Catalytic Oxygenation

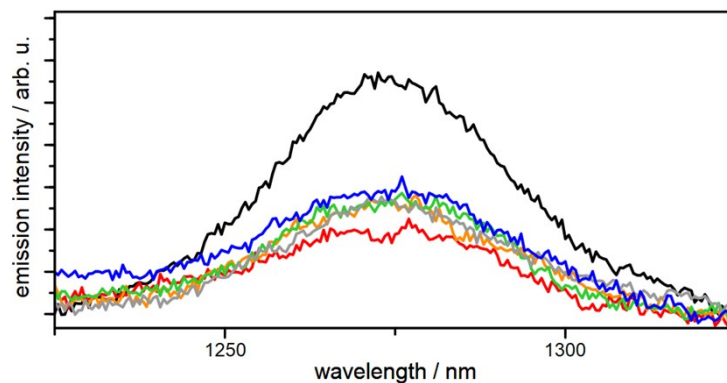


Figure S11.1. Emission spectra of the emission induced by the decay of catalytically generated $^1\text{O}_2$ which is commonly centered at 1275 nm. The spectra are baseline corrected at 1322 nm. Integration of the area under the emission curves was conducted from 1225 to 1322 nm. Emissions were evaluated for **Cu(CF₃)₂**, **CuCF₃**, **CuF**, **CuH**, **CuOMe** (red, orange, green, grey and blue, respectively) and the reference phenalenone PN (black).

Table S11.1. Summary of the determined singlet oxygen quantum yields $\phi_{1\text{O}_2}$ the complexes **Cu(CF₃)₂**-**CuOMe**. Phenalenone (PN) was used as referenced standard with an $\phi_{1\text{O}_2}$ of 0.95.

Compound	Integrated emission	$\phi_{1\text{O}_2}$ [%]
PN	6611	0.95
Cu(CF ₃) ₂	2607	0.37
CuCF ₃	3249	0.47
CuF	3313	0.48
CuH	3210	0.46
CuOMe	3763	0.54

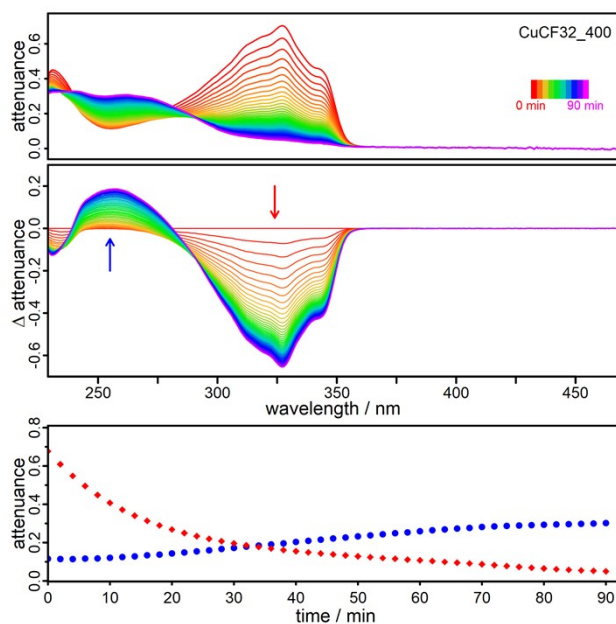


Figure S11.2. Top: Spectra evolution of the reaction of DPF ($c = 2 \cdot 10^{-5}$ M) with singlet oxygen sensitized by $\text{Cu}(\text{CF}_3)_2$ (DPF: $\text{Cu}(\text{CF}_3)_2 = 10:1$) in aerated dichloromethane. **Center:** Difference spectra of the recorded spectra shown above (arrows indicate the direction and the selected wavelengths 255 nm, blue, and 324 nm, red). **Bottom:** Kinetic traces of the two selected wavelengths 324 nm (absorption maximum DPF, red arrow top and dots bottom) and 255 nm (absorption maximum DBE, blue arrow top and dots bottom).

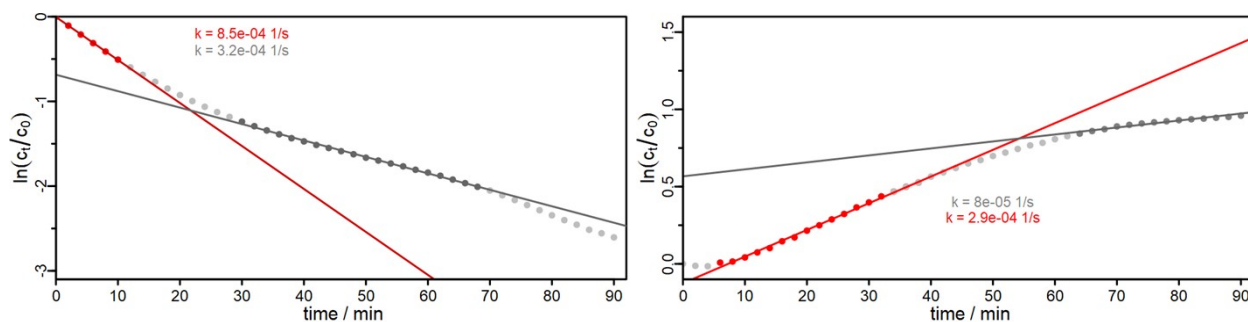


Figure S11.3. Logarithmic plots of the kinetic trace of the consumption of DPF ($\lambda = 324$ nm, left) and the formation of the product DBE ($\lambda = 255$ nm, right) yielding the corresponding rate constants k for an assumed first order kinetic behavior in the photosensitization using $\text{Cu}(\text{CF}_3)_2$.

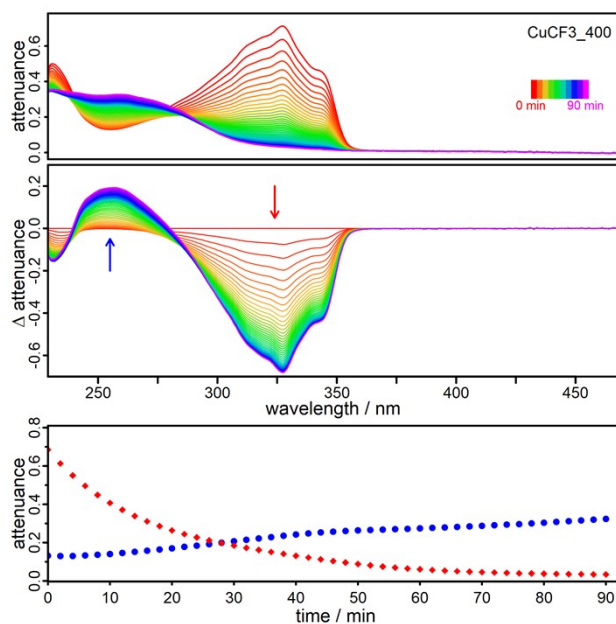


Figure S11.4. Top: Spectra evolution of the reaction of DPF ($c = 2 \cdot 10^{-5}$ M) with singlet oxygen sensitized by CuCF_3 (DPF: $\text{CuCF}_3 = 10:1$) in aerated dichloromethane. **Center:** Difference spectra of the recorded spectra shown above (arrows indicate the direction and the selected wavelengths 255 nm, blue, and 324 nm, red). **Bottom:** Kinetic traces of the two selected wavelengths 324 nm (absorption maximum DPF, red arrow top and dots bottom) and 255 nm (absorption maximum DBE, blue arrow top and dots bottom).

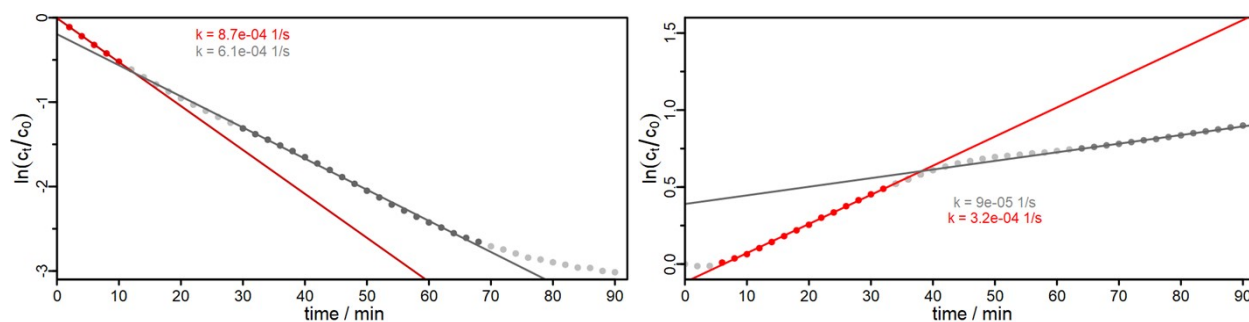


Figure S11.5. Logarithmic plots of the kinetic trace of the consumption of DPF ($\lambda = 324$ nm, left) and the formation of the product DBE ($\lambda = 255$ nm, right) yielding the corresponding rate constants k for an assumed first order kinetic behavior in the photosensitization using CuCF_3 .

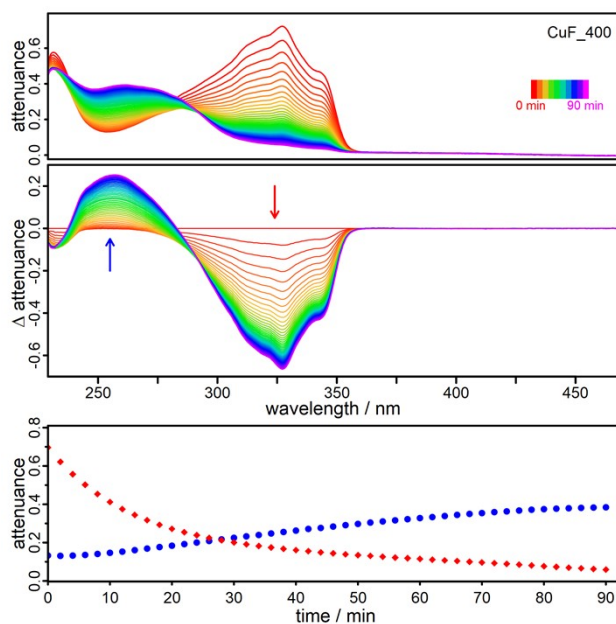


Figure S11.6. Top: Spectra evolution of the reaction of DPF ($c = 2 \cdot 10^{-5}$ M) with singlet oxygen sensitized by **CuF** (DPF:CuF = 10:1) in aerated dichloromethane. **Center:** Difference spectra of the recorded spectra shown above (arrows indicate the direction and the selected wavelengths 255 nm, blue, and 324 nm, red). **Bottom:** Kinetic traces of the two selected wavelengths 324 nm (absorption maximum DPF, red arrow top and dots bottom) and 255 nm (absorption maximum DBE, blue arrow top and dots bottom).

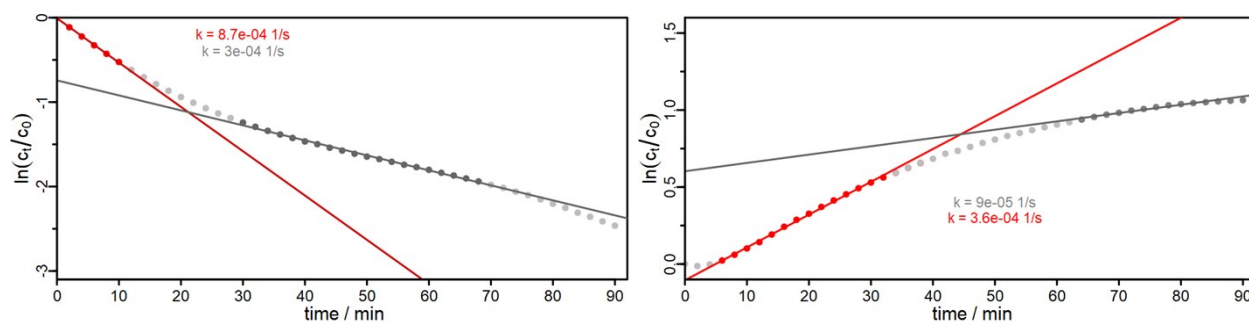


Figure S11.7. Logarithmic plots of the kinetic trace of the consumption of DPF ($\lambda = 324$ nm, left) and the formation of the product DBE ($\lambda = 255$ nm, right) yielding the corresponding rate constants k for an assumed first order kinetic behavior in the photosensitization using **CuF**.

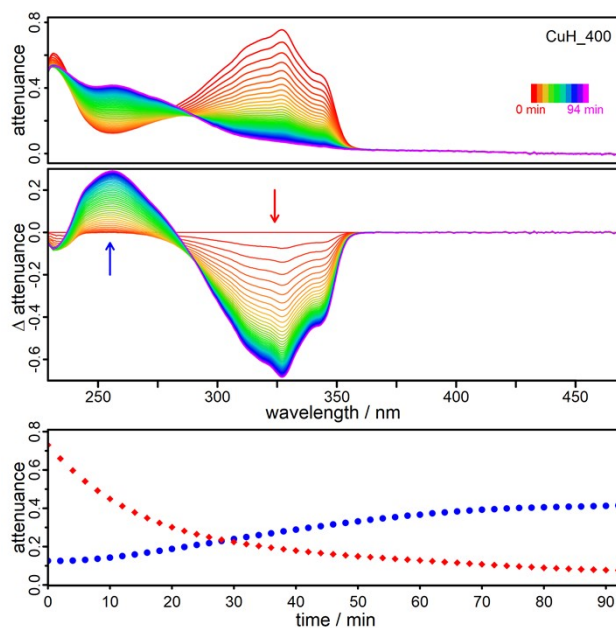


Figure S11.8. Top: Spectra evolution of the reaction of DPF ($c = 2 \cdot 10^{-5}$ M) with singlet oxygen sensitized by **CuH** (DPF:CuH = 10:1) in aerated dichloromethane. **Center:** Difference spectra of the recorded spectra shown above (arrows indicate the direction and the selected wavelengths 255 nm, blue, and 324 nm, red). **Bottom:** Kinetic traces of the two selected wavelengths 324 nm (absorption maximum DPF, red arrow top and dots bottom) and 255 nm (absorption maximum DBE, blue arrow top and dots bottom).

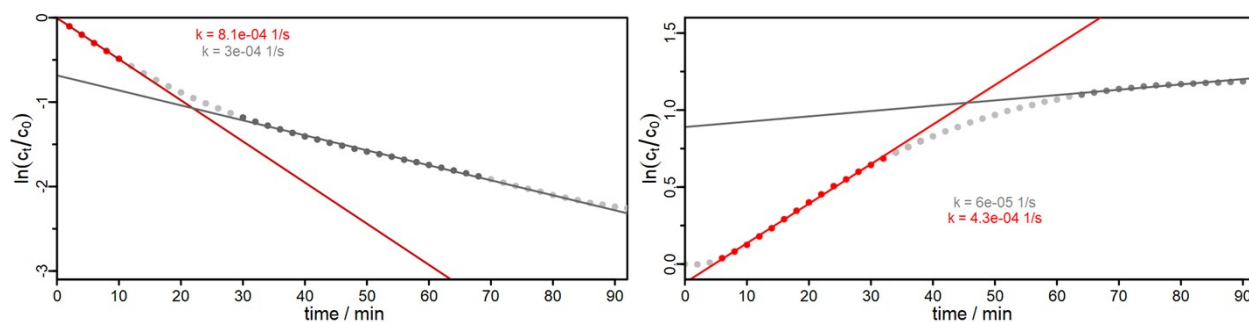


Figure S11.9. Logarithmic plots of the kinetic trace of the consumption of DPF ($\lambda = 324$ nm, left) and the formation of the product DBE ($\lambda = 255$ nm, right) yielding the corresponding rate constants k for an assumed first order kinetic behavior in the photosensitization using **CuH**.

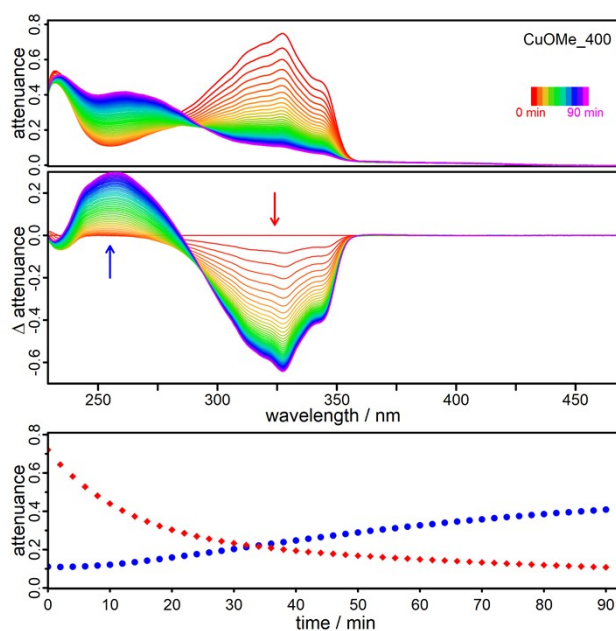


Figure S11.10. Top: Spectra evolution of the reaction of DPF ($c = 2 \cdot 10^{-5}$ M) with singlet oxygen sensitized by **CuOMe** (DPF: CuOMe = 10:1) in aerated dichloromethane. **Center:** Difference spectra of the recorded spectra shown above (arrows indicate the direction and the selected wavelengths 255 nm, blue, and 324 nm, red). **Bottom:** Kinetic traces of the two selected wavelengths 324 nm (absorption maximum DPF, red arrow top and dots bottom) and 255 nm (absorption maximum DBE, blue arrow top and dots bottom).

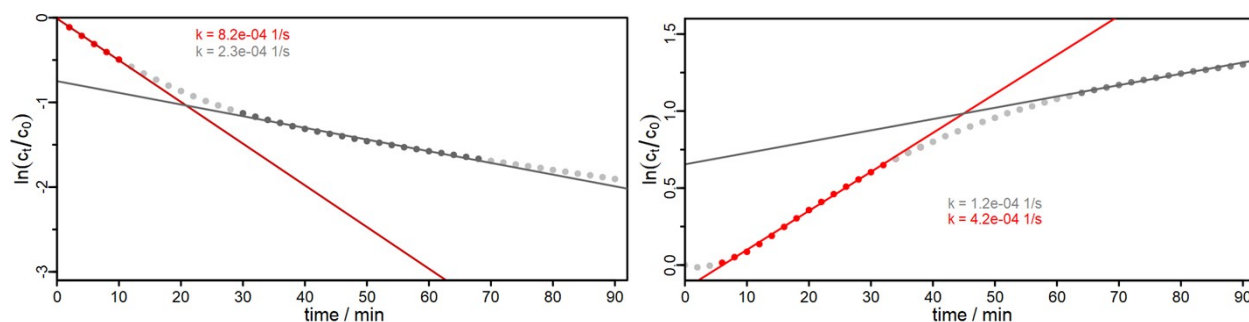


Figure S11.11. Logarithmic plots of the kinetic trace of the consumption of DPF ($\lambda = 324$ nm, left) and the formation of the product DBE ($\lambda = 255$ nm, right) yielding the corresponding rate constants k for an assumed first order kinetic behavior in the photosensitization using **CuOMe**.

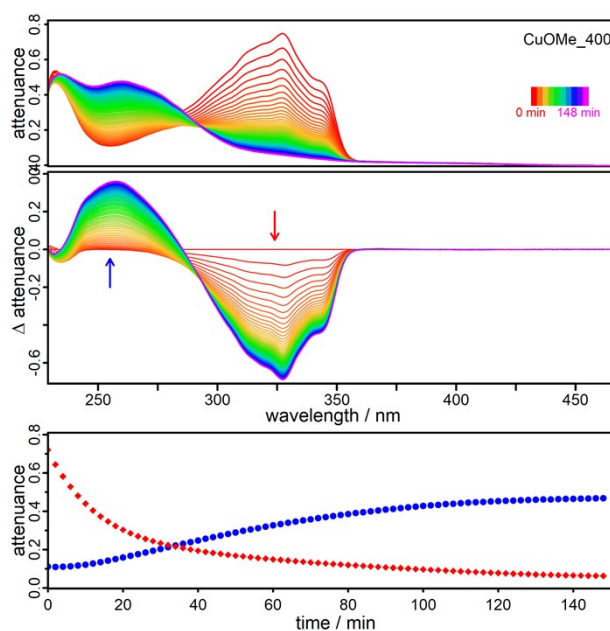


Figure S11.12. Top: Spectra evolution of the reaction of DPF ($c = 2 \cdot 10^{-5}$ M) with singlet oxygen sensitized by **CuOMe** (DPF:CuOMe = 10:1) in aerated dichloromethane followed until completion. **Center:** Difference spectra of the recorded spectra shown above (arrows indicate the direction and the selected wavelengths 255 nm, blue, and 324 nm, red). **Bottom:** Kinetic traces of the two selected wavelengths 324 nm (absorption maximum DPF, red arrow top and dots bottom) and 255 nm (absorption maximum DBE, blue arrow top and dots bottom).

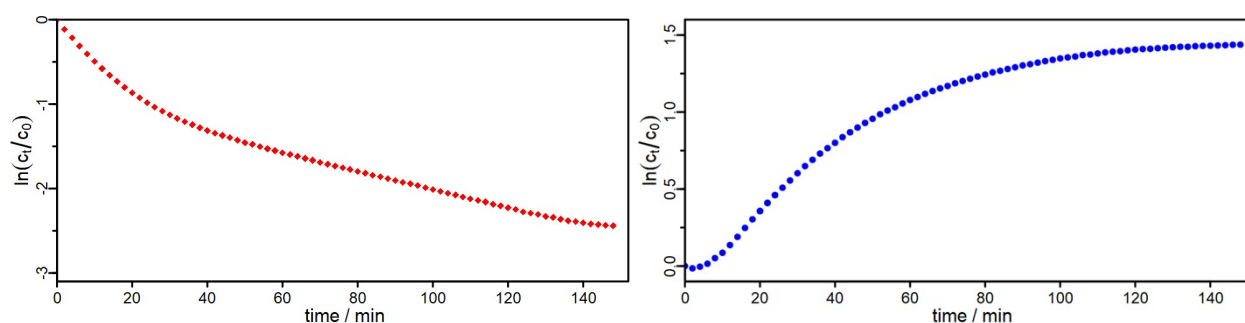


Figure S11.13. Logarithmic plots of the kinetic trace of the consumption of DPF ($\lambda = 324$ nm, left, red) and the formation of the product DBE ($\lambda = 255$ nm, right, blue) using **CuOMe**. The logarithmic plots reveal that a first order kinetic is valid for the DPF consumption, the formation of DBE clearly follows a different order. The reaction is completed after around 120 minutes.

Table S11.2. Calculation of yields of DBE in % after $t = 90$ min.. From the change in attenuation at 255 nm after 90 minutes, Δ_{att} , the concentration of DBE c_{DBE} was calculated using the attenuation coefficient of DBE ($\epsilon = 18.1 \cdot 10^3 \text{ M}^{-1}$)^{21,22}. As control experiment, yield was also calculated from the fully completed reaction (**CuOMe***, $t = 130$ min).

	Cu(CF₃)₂	CuCF₃	CuF	CuH	CuOMe	CuOMe*
Δ_{att} []	0.19	0.20	0.26	0.29	0.30	0.36
c_{DBE} [%]	$1.0 \cdot 10^{-5}$	$1.1 \cdot 10^{-5}$	$1.4 \cdot 10^{-5}$	$1.6 \cdot 10^{-5}$	$1.7 \cdot 10^{-5}$	$2.0 \cdot 10^{-5}$
yield [%]	52	54	70	80	83	99

Table S11.3. Summary of the first order rate constants of each reaction obtained from the respective logarithmic plots. Rate constants k_1 are marked in red in each plot shown above.

	Cu(CF₃)₂	CuCF₃	CuF	CuH	CuOMe
$k_{DPF,1}$ [10^{-4} s^{-1}]	8.5	8.7	8.7	8.1	8.2
$k_{DPF,2}$ [10^{-4} s^{-1}]	3.2	6.1	3.0	3.0	2.3
$k_{DBE,1}$ [10^{-4} s^{-1}]	2.9	3.2	3.6	4.3	4.2
$k_{DBE,2}$ [10^{-4} s^{-1}]	0.8	0.9	0.9	0.6	1.2

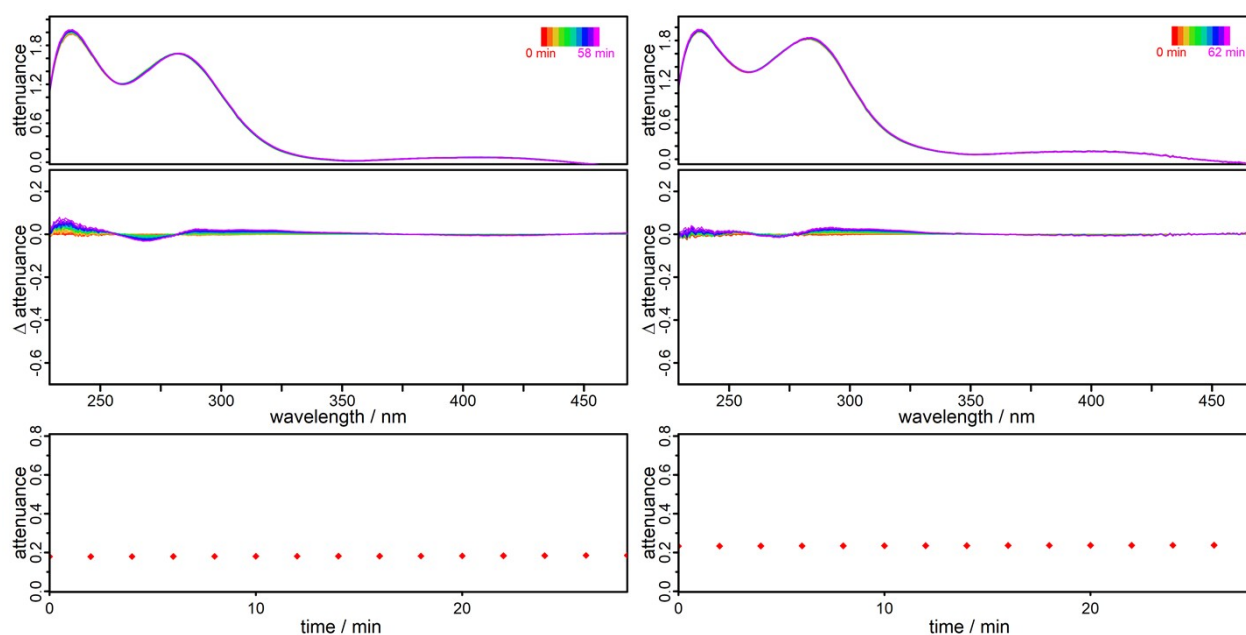


Figure S11.14. Top: Photostability experiment of the complex **Cu(CF₃)₂** (left) and **CuCF₃** (right) ($c = 2 \cdot 10^{-5} \text{ M}$) in aerated dichloromethane. **Center:** Difference spectra of the recorded spectra shown above. **Bottom:** Kinetic traces of the selected wavelength $\lambda = 400$ nm.

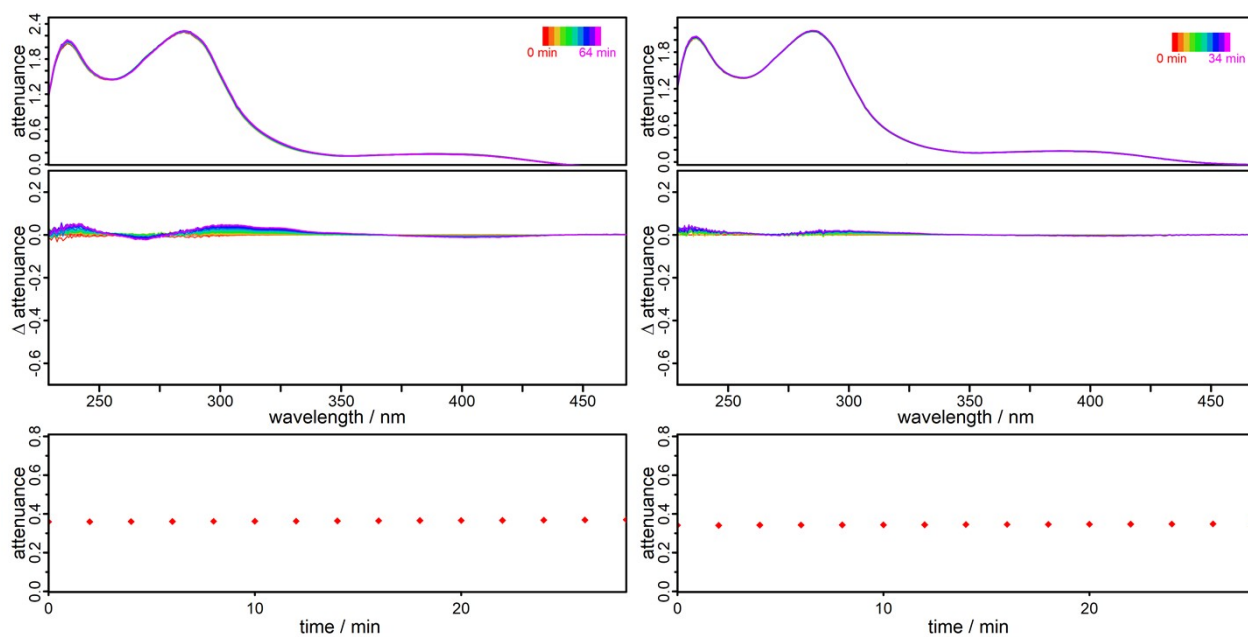


Figure S11.15. Top: Photostability experiment of the complex **CuF** (left) and **CuH** (right) ($c = 2 \cdot 10^{-5}$ M) in aerated dichloromethane. **Center:** Difference spectra of the recorded spectra shown above. **Bottom:** Kinetic traces of the selected wavelength $\lambda = 400$ nm.

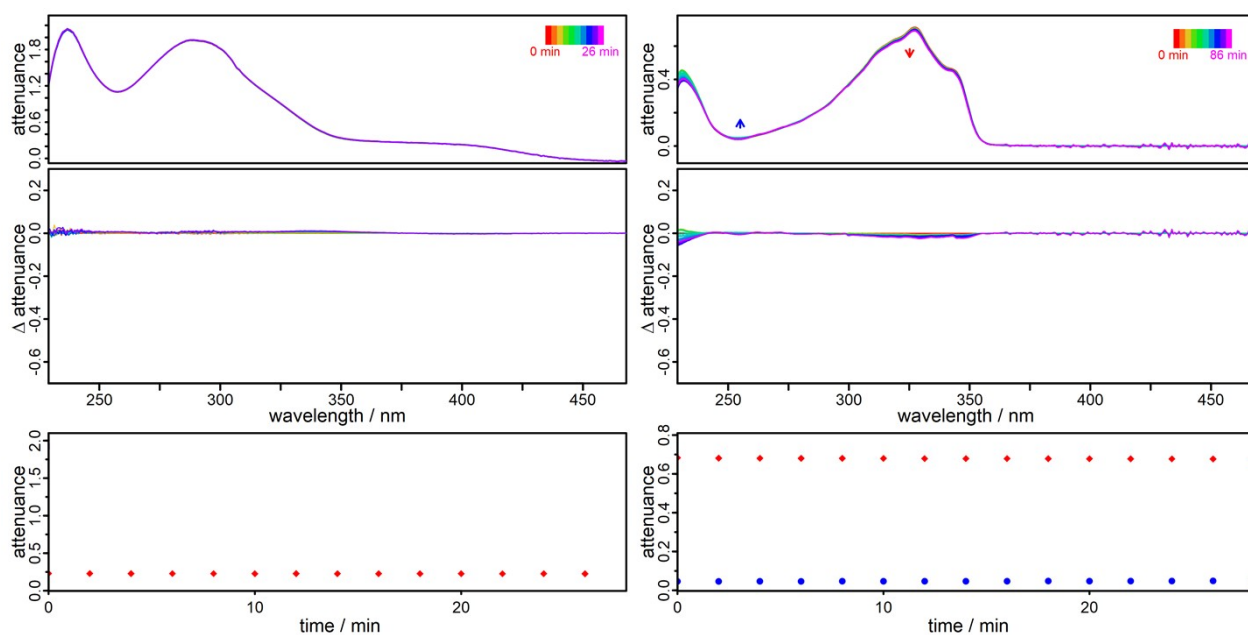


Figure S11.16. Top: Photostability experiment of the complex **CuOMe** (left) and **DPF** (right) ($c = 2 \cdot 10^{-5}$ M) in aerated dichloromethane. **Center:** Difference spectra of the recorded spectra shown above. **Bottom:** Kinetic traces of the selected wavelength (**CuOMe**, $\lambda = 400$ nm; **DPF** $\lambda = 324$ (red) and 255 nm (blue)).

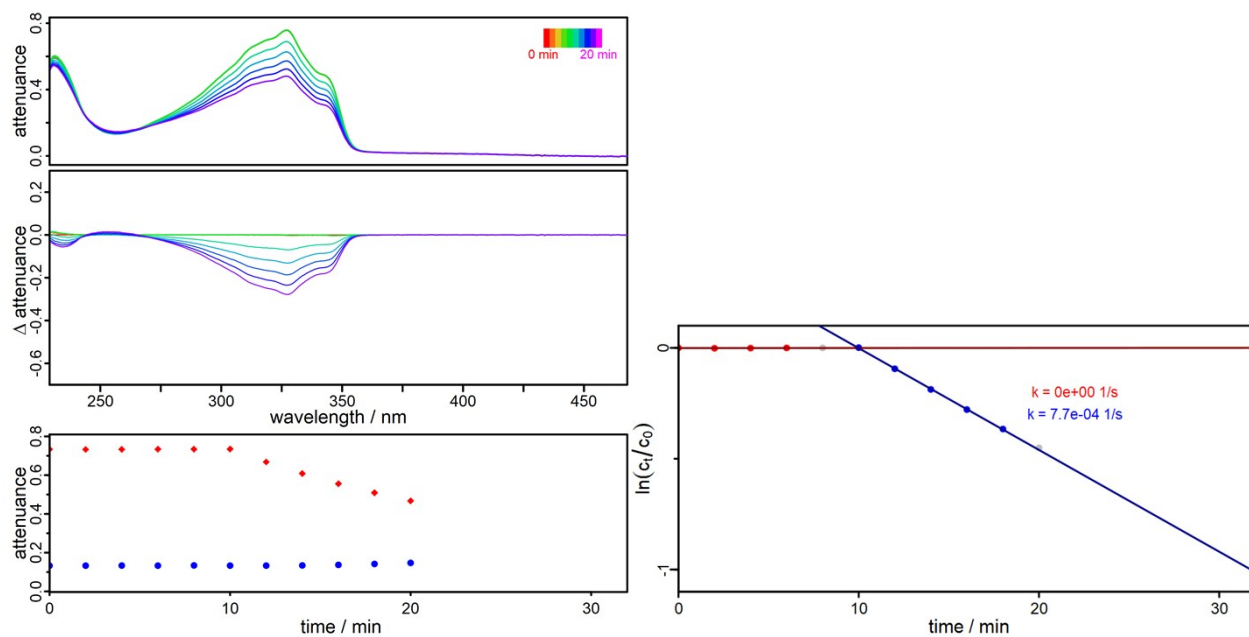


Figure S11.17. **Left, top:** Blank experiment of the reaction of DPF ($c = 2 \cdot 10^{-5}$ M) with singlet oxygen sensitized by **CuOMe** (DPF:CuOMe = 10:1) in aerated dichloromethane. The light source was switched on after 10 minutes. **Left, center:** Difference spectra of the recorded spectra shown above. **Left, bottom:** Kinetic traces of the two selected wavelengths 324 nm (absorption maximum DPF, red arrow top and dots bottom) and 255 nm (absorption maximum DBE, blue arrow top and dots bottom). **Right:** Logarithmic plot of the kinetic trace of the consumption of DPF ($\lambda = 324$ nm) using **CuOMe**. Light switched on at 10 minutes.

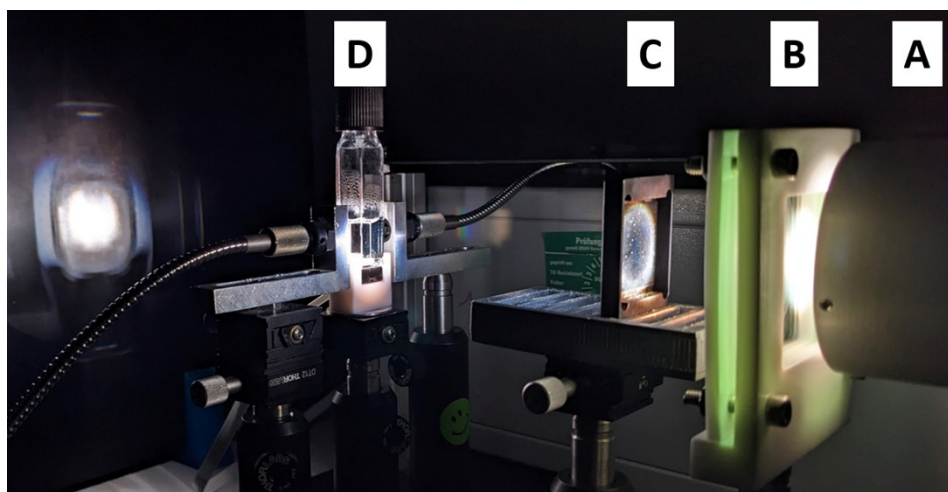


Figure S11.18. Catalytic setup used to probe the catalytic oxygenation of DPF to DBE. **A:** Xenon light source (130 W) with sharp focused on the cuvette. **B:** 400 nm long-pass filter. **C:** Optical density filter OD = 0.5. **D:** Cuvette containing the reaction mixture including a magnetic stirrer (the solution is probed every 2 minutes by a UV/vis spectrometer). The setup was cooled using a fan. After all reactions, the measured temperatures of the solutions did not exceed 27 °C.

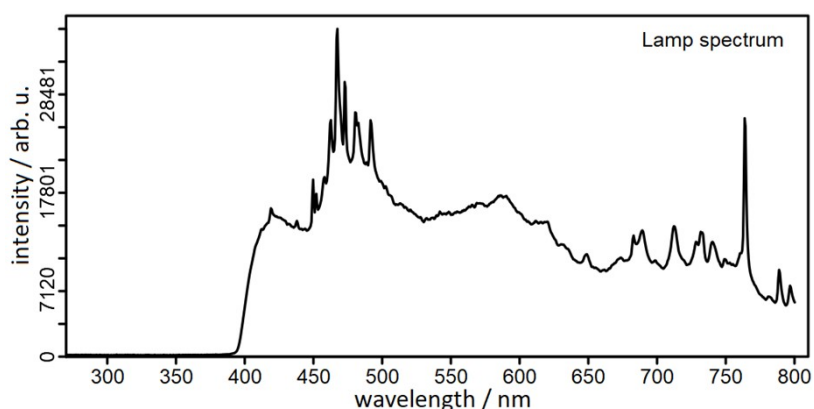


Figure S11.19. Light spectrum used for the catalytic reaction with DPF (recorded directly at the cuvette holder). The spectrum was generated from a Xenon light source, which was passed through a 400 nm long-pass filter and an optical density filter (OD = 0.5).

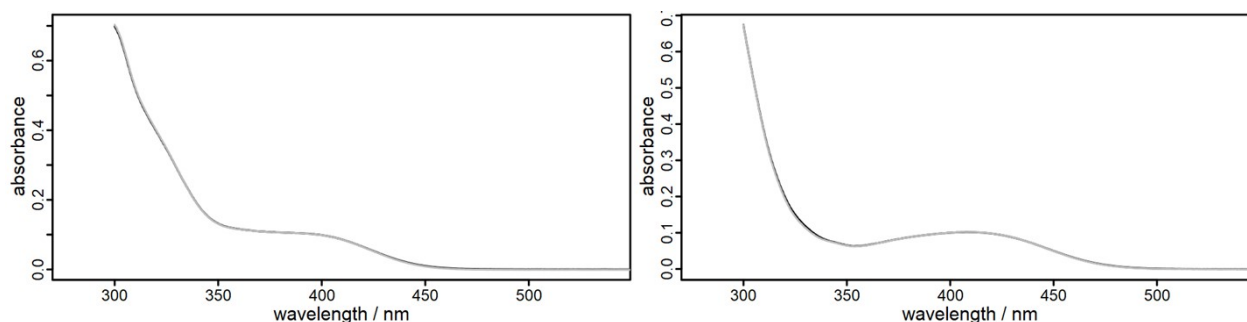


Figure S11.20. UV/vis absorption spectra of **CuOMe** (left) and **Cu(CF₃)₂** (right) before (grey) and after (black) singlet oxygen generation in ambient dichloromethane solution.

12 Photocatalytic Dehalogenation

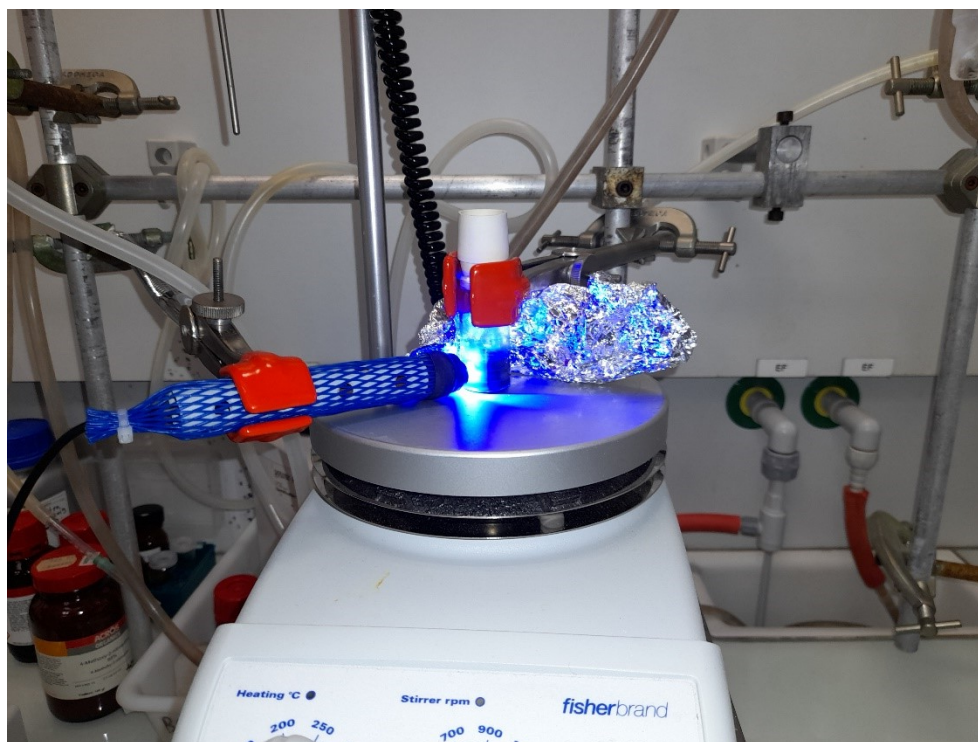


Figure S12.1. Picture of the photochemical setup.

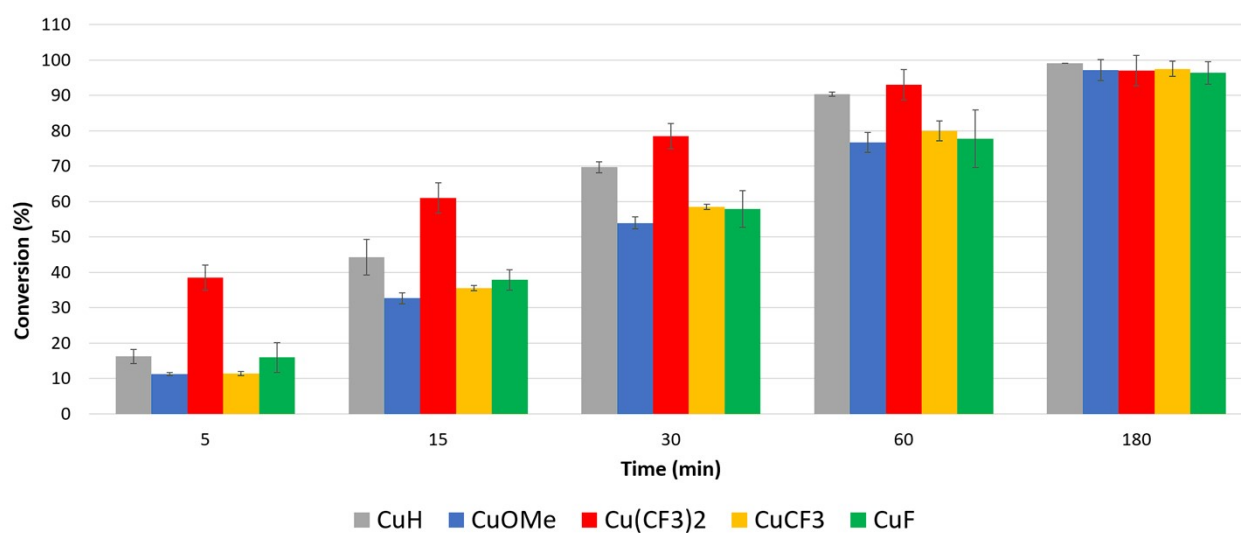


Figure S12.2. Evolution of the quantity of 1-H with time, upon light irradiation (from 0 to 3 hours).

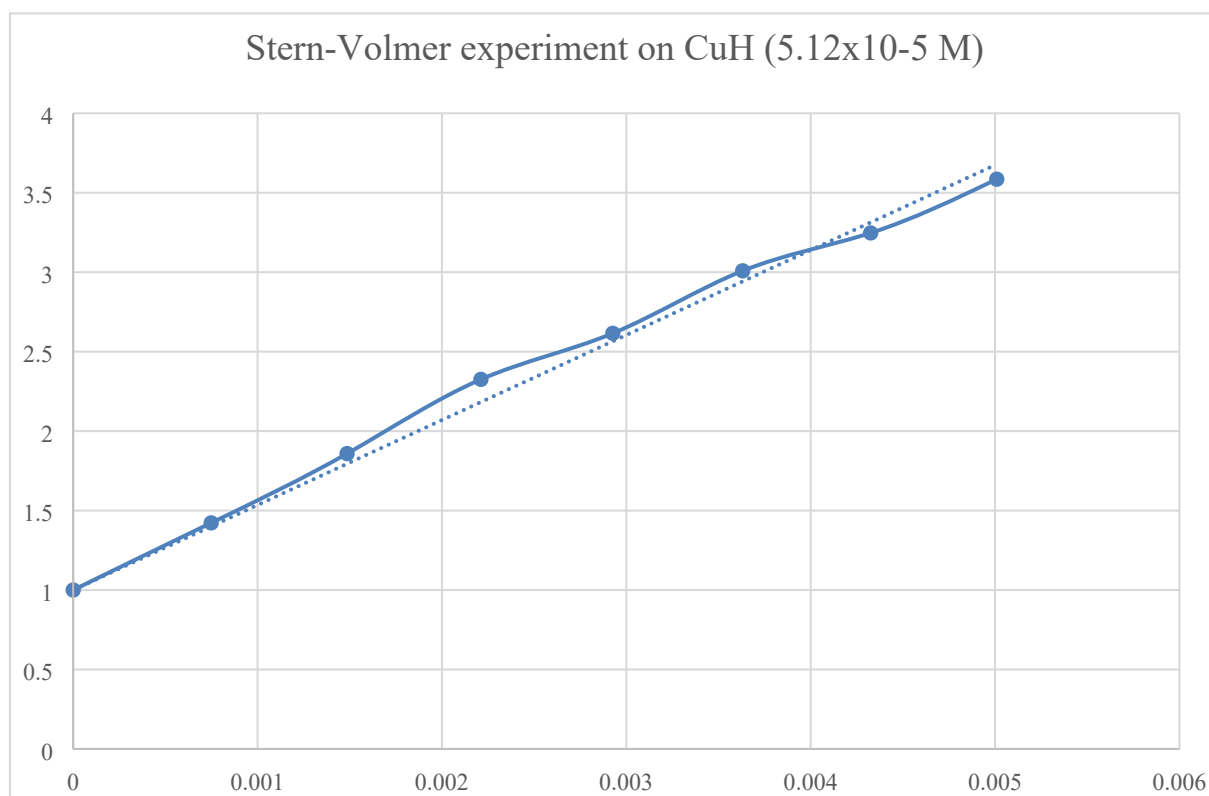


Figure S12.3a. Stern-Volmer experiment for **CuH**: plot of τ_0/τ (where τ and τ_0 are the lifetimes in presence and in absence of BI₁H, respectively) vs. [BI₁H]. Experiments performed in acetonitrile.

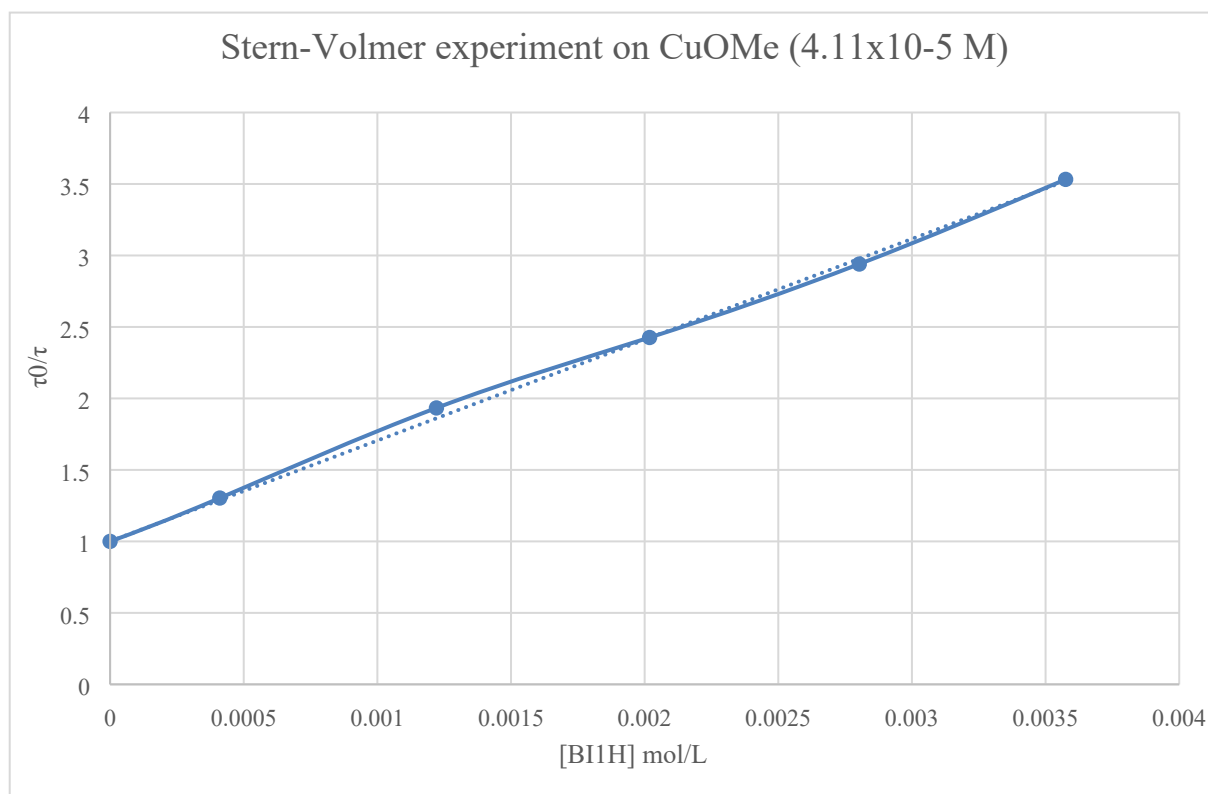


Figure S12.3b. Stern-Volmer experiment for **CuOMe**: plot of τ_0/τ (where τ and τ_0 are the lifetimes in presence and in absence of BI₁H, respectively) vs. [BI₁H]. Experiments performed in acetonitrile.

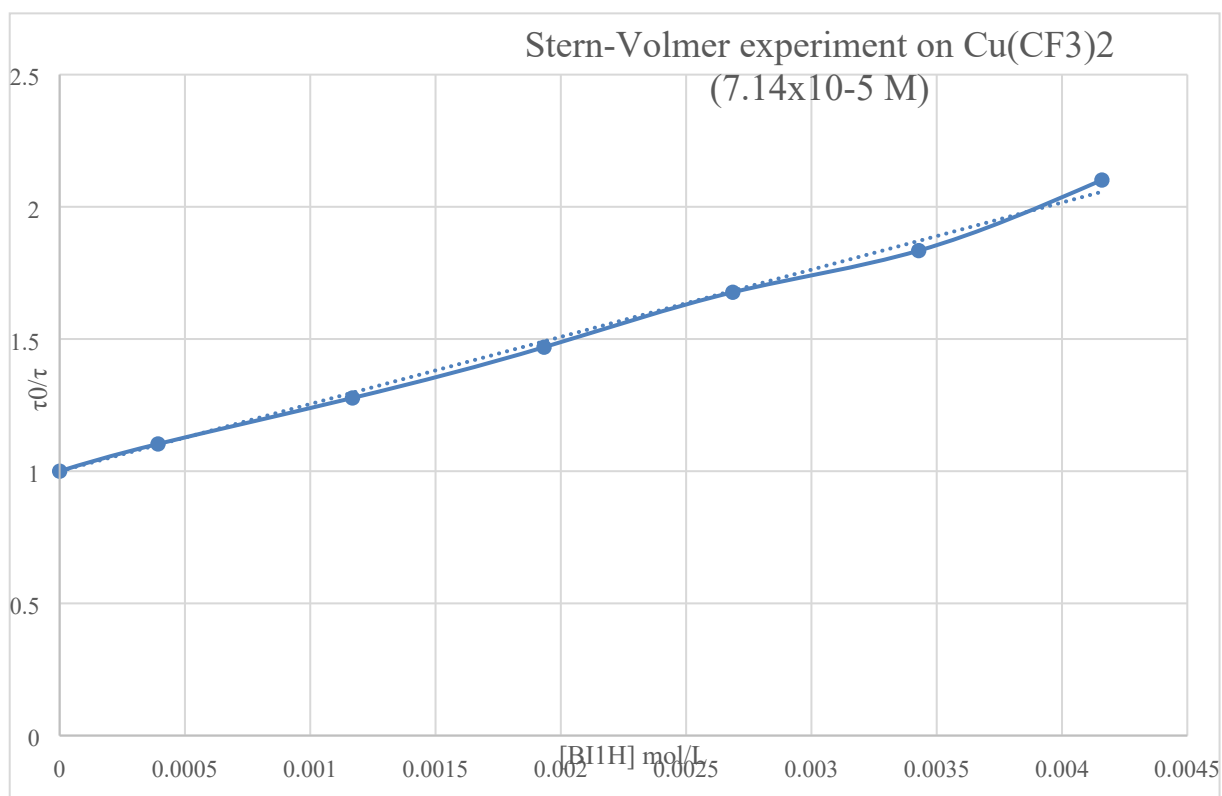


Figure S12.3c. Stern-Volmer experiment for $\text{Cu}(\text{CF}_3)_2$: plot of τ_0/τ (where τ and τ_0 are the lifetimes in presence and in absence of BI_1H , respectively) vs. $[\text{BI}_1\text{H}]$. Experiments performed in acetonitrile.

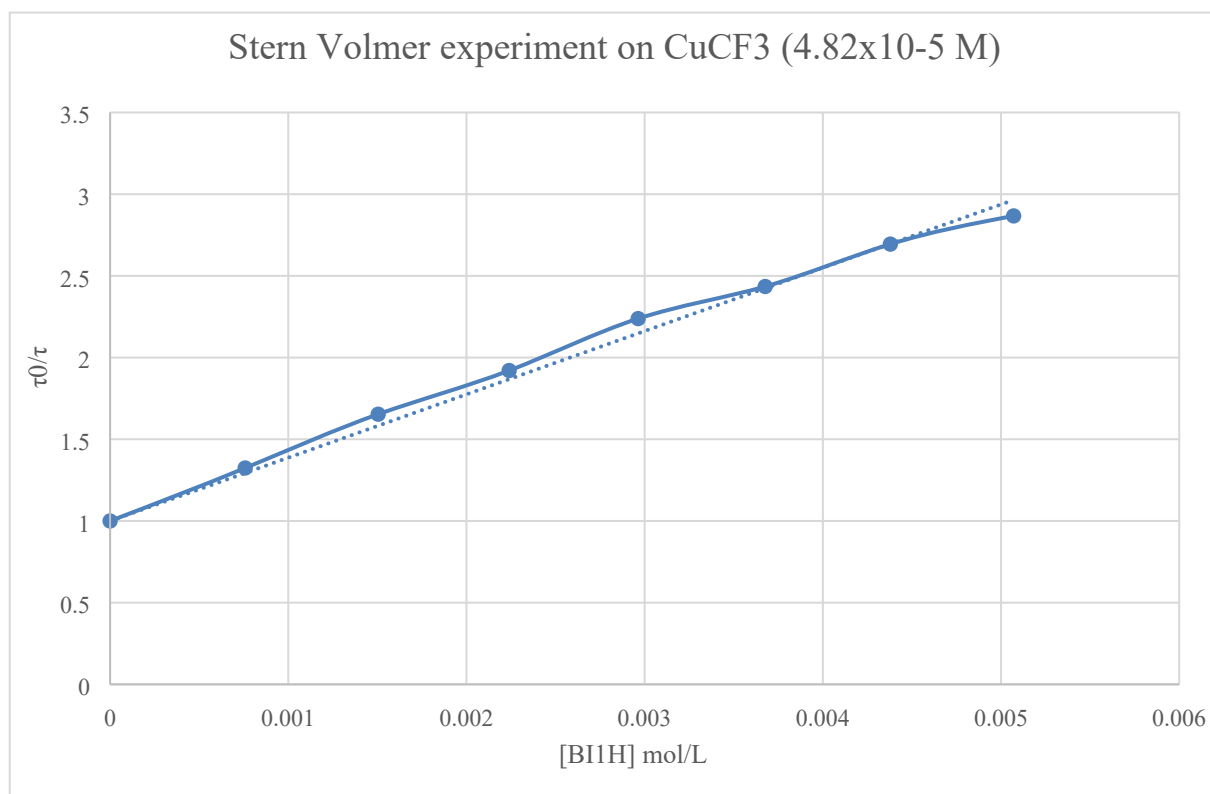


Figure S12.3d. Stern-Volmer experiment for CuCF_3 : plot of τ_0/τ (where τ and τ_0 are the lifetimes in presence and in absence of BI_1H , respectively) vs. $[\text{BI}_1\text{H}]$. Experiments performed in acetonitrile.

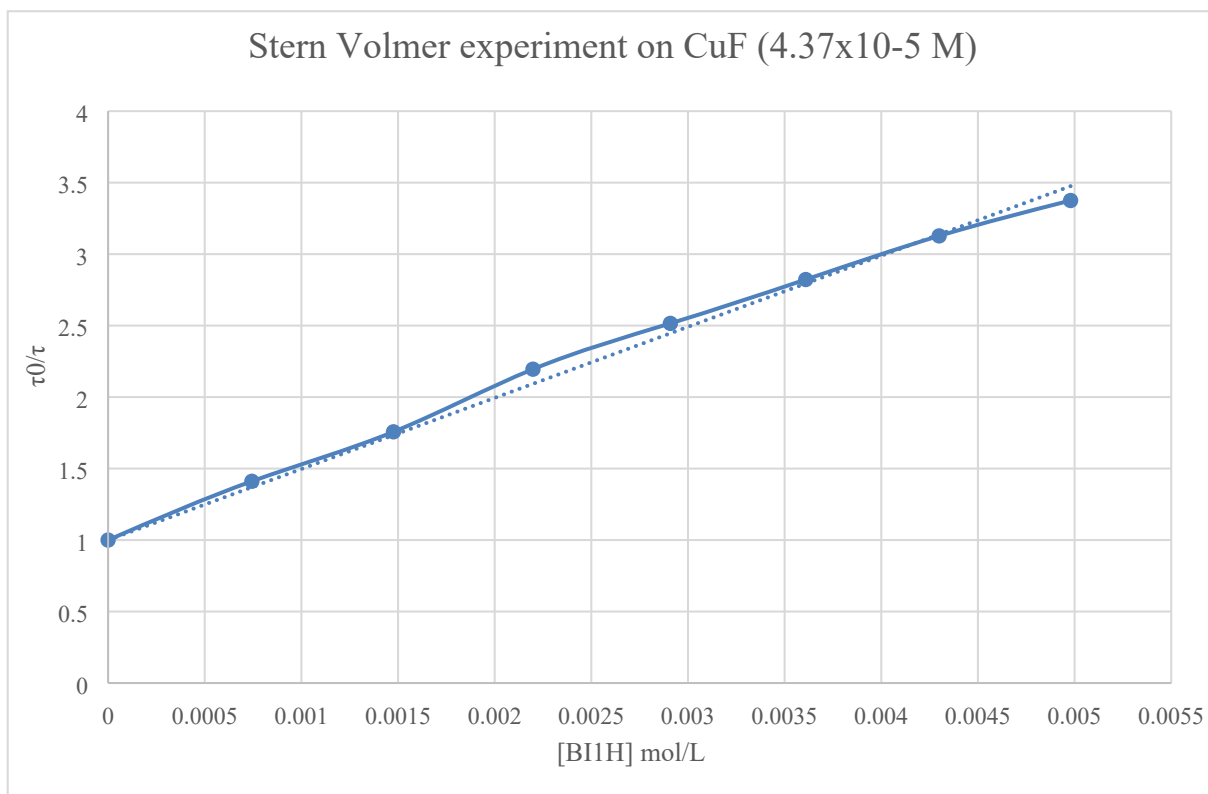


Figure S12.3e. Stern-Volmer experiment for **CuF**: plot of τ_0/τ (where τ and τ_0 are the lifetimes in presence and in absence of BI₁H, respectively) vs. [BI₁H]. Experiments performed in acetonitrile.

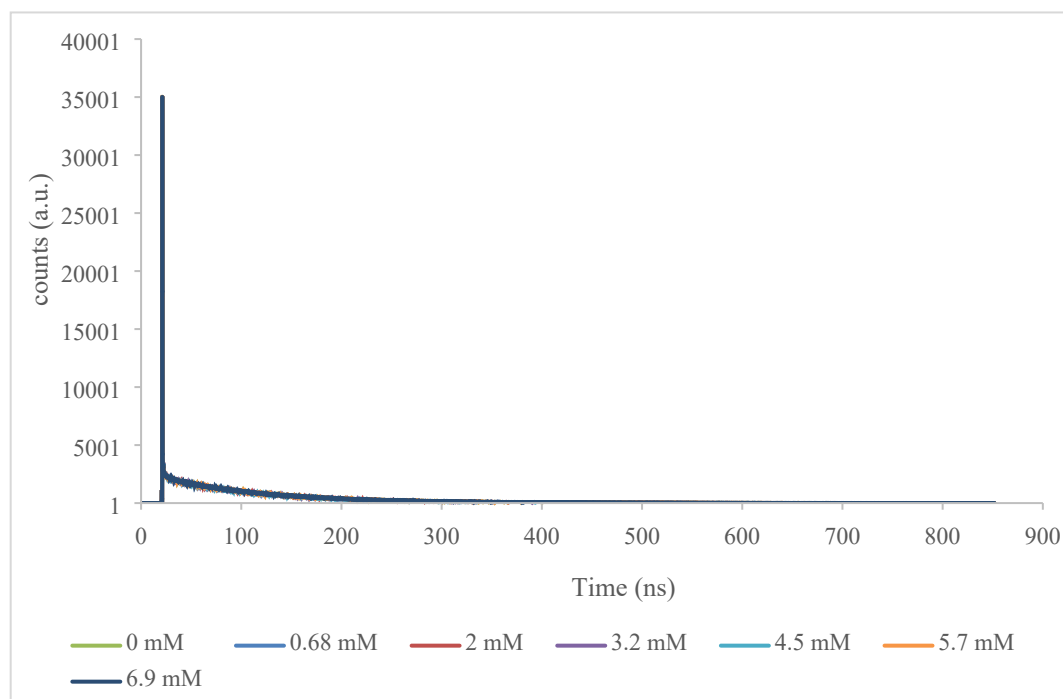


Figure S12.4. Evolution of the emission decay of complex **CuOMe** ($[\text{CuOMe}] = 3.10^{-5}$ M) upon addition of **1-Br**. The concentrations of **1-Br** are given in the caption. Experiments performed in acetonitrile.

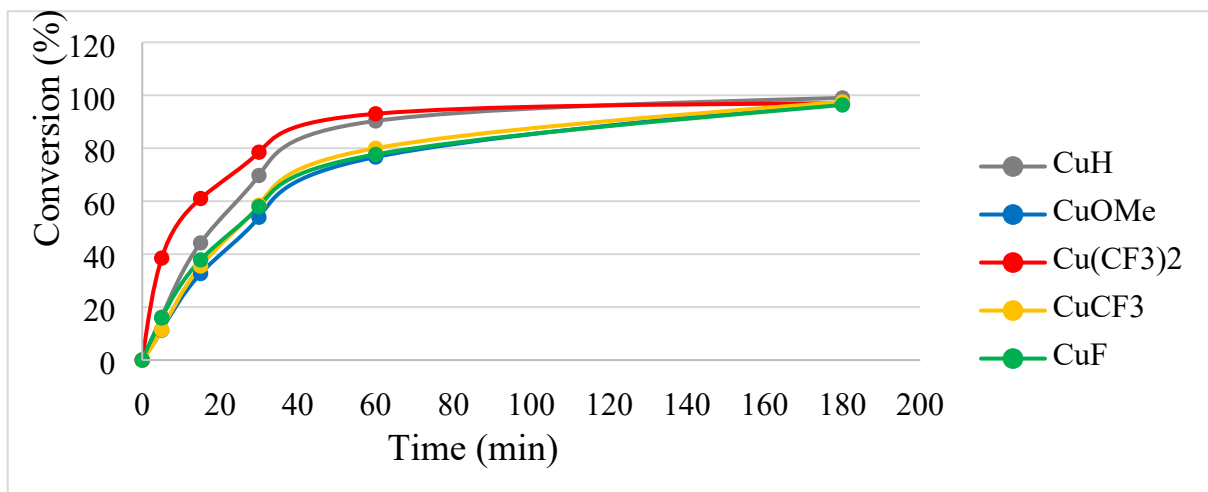


Figure S12.5. Evolution of the quantity of **1-H** with time, upon light irradiation (from 0 to 100 min).

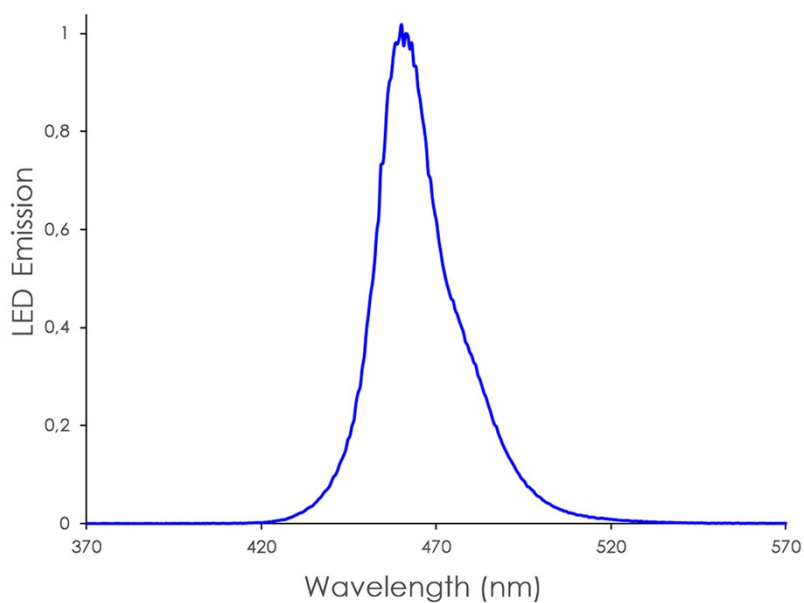


Figure S12.6. Emission spectrum of the light source (blue LED) used.

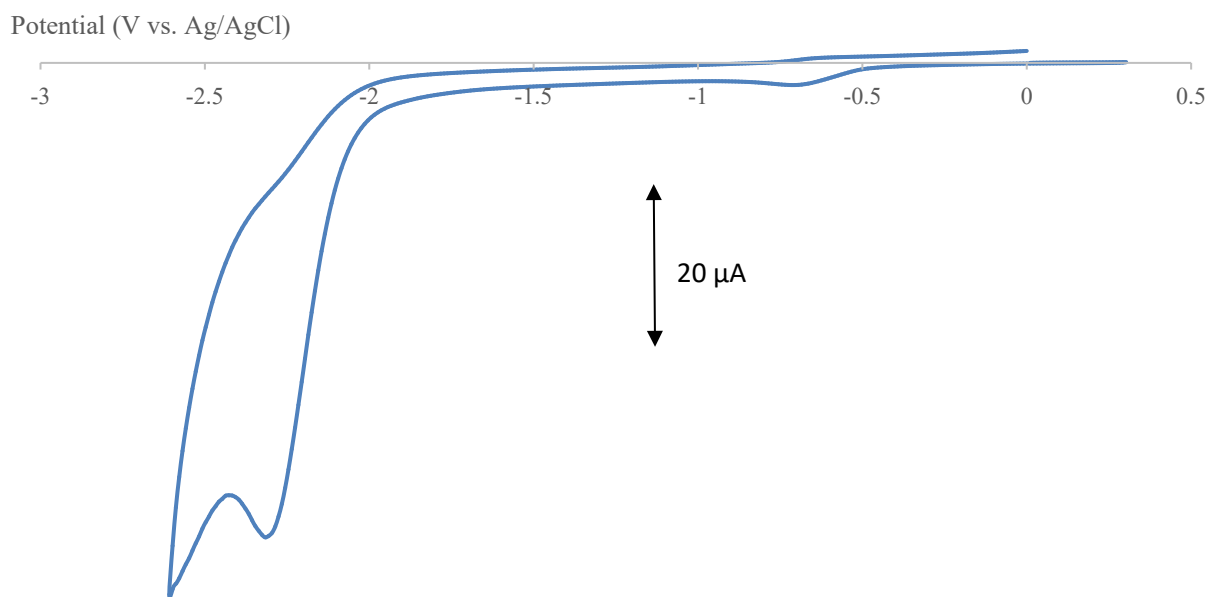


Figure S12.7. Cyclic voltammetry of **1-Br** in acetonitrile, in presence of tetrabutylammonium hexafluorophosphate (0.1 M). Working electrode: platinum disk. Reference: Ag/AgCl in ethanol/LiCl 2M (Metrohm). $E(\text{Fc}^+/\text{Fc}) = 0.51$ V vs. Ag/AgCl. Auxiliary: platinum gauze. Additional comment: measuring the reduction potential for irreversible processes is challenging and the data must be carefully considered. Thus, we estimated a value of $E_{\text{red}} = -2.65$ V vs. Fc^+/Fc meaning that all electron transfer steps from the reduced copper(I) complexes to **1-Br** are endergonic. However, it has been already often reported in the literature that endergonic processes, as predicted by electrochemistry, appear to be very efficient when the photochemical experiment is performed.^{23,24,25}

Table S12.1. Kinetic constants for the reductive quenching of the excited copper(I) complexes with BI_1H , as extracted from the slope of the Stern-Volmer plots.

	$\text{Cu}(\text{CF}_3)_2$	CuCF_3	CuF	CuH	CuOMe
$k_{\text{RQ}} (\text{M}^{-1}\text{s}^{-1})$	$7.64 \cdot 10^9$	$6.67 \cdot 10^9$	$6.15 \cdot 10^9$	$6.23 \cdot 10^9$	$7.07 \cdot 10^9$
$K_{\text{SV}} (\text{M}^{-1})$	254	388	498	536	707

References

- ¹ CrysAlisPro, Rigaku Oxford Diffraction, 2018.
- ² a) G. M. Sheldrick, *Acta Cryst.*, 2015, **A71**, 3–8; b) G. M. Sheldrick, *Acta Cryst.* 2015, **C71**, 3–8.
- ³ a) C. F. Macrae, I. Sovago, S. J. Cottrell, P. T. A. Galek, P. McCabe, E. Pidcock, M. Platings, G. P. Shields, J. S. Stevens, M. Towler, P. A. Wood, *J. Appl. Cryst.* 2020, **53**, 226–235; b) A. L. Spek, *Acta Cryst.* 2009, **D65**, 148–155; c) O. V. Dolomanov, L. J. Bourhis, R. J. Gildea, J. A. K. Howard, H. Puschmann, *J. Appl. Crystallogr.* 2009, **42**, 339–341.
- ⁴ T. Gallavardin, C. Armagnat, *et al.*, *Chem. Commun.* 2012, **48**, 1689–1691.
- ⁵ N. Epelde-Elezcano, V. Martínez-Martínez, E. Peña-Cabrera, C. Gómez-Durán, I. Arbeloaa, S. Lacombe, *RSC Adv.* 2016, **6**, 41991-41998.
- ⁶ M.-A. Schmid, J. Brückmann, J. Bösking, D. Nauroozi, M. Karnahl, S. Rau, S. Tschierlei, *Chem. Eur. J.* 2022, **28**, e202103609.
- ⁷ F. Neese, F. Wennmohs, U. Becker, C. Riplinger, *J. Chem. Phys.* 2020, **152**, 224108.
- ⁸ K. Eichkorn, O. Treutler, H. Öhm, M. Häser and R. Ahlrichs, *Chem. Phys. Lett.* 1995, **242**, 652-660.
- ⁹ O. Treutler, R. Ahlrichs, *J. Chem. Phys.* 1995, **102**, 346-354.
- ¹⁰ a) S. Grimme, J. Antony, S. Ehrlich, H. Krieg, *J. Chem. Phys.* 2010, **132**, 154104. b) S. Grimme, S. Ehrlich, L. Goerigk, *J. Comput. Chem.* 2011, **32**, 1456-1465.
- ¹¹ F. Weigend, R. Ahlrichs, *Phys. Chem. Chem. Phys.* 2005, **7**, 3297-3305.
- ¹² V. Barone, M. Cossi, *J. Phys. Chem. A*, 1998, **102**, 1995.
- ¹³ chemcraftprog.com
- ¹⁴ L. A. Wilfred and L. L. C. Christina, *Purification of Laboratory Chemicals (Sixth Edition)*, Butterworth-Heinemann, Oxford, 2009.
- ¹⁵ D. F. Shiver and M. A. Drezdson, *The Manipulation of Air-Sensitive Compounds (Second Edition)*, John Wiley & Sons. Inc, 1986.
- ¹⁶ a) M. Heberle, S. Tschierlei, N. Rockstroh, M. Ringenberg, W. Frey, H. Junge, M. Beller, S. Lochbrunner, M. Karnahl, *Chem. Eur. J.* 2017, **23**, 312-319. b) M. Rentschler, M.-A. Schmid, W. Frey, S. Tschierlei, M. Karnahl, *Inorg. Chem.* 2020, **59**, 14762-14771. c) F. Doettinger, Y. Yang, M.-A. Schmid, W. Frey, M. Karnahl, S. Tschierlei, *Inorg. Chem.* 2021, **60**, 7, 5391-5401.
- ¹⁷ A. L. Spek, *Acta Cryst.* 2009, **D65**, 148–155.
- ¹⁸ E. M. Kober, J. V. Caspar, R. S. Lumpkin, T. J. Meyer, *J. Phys. Chem.* 1986, **90**, 3722-3732.
- ¹⁹ J. R. Lakowicz, *Principles of Fluorescence Spectroscopy*, 3rd edition, Springer New York, NY, 2006.
doi.org/10.1007/978-0-387-46312-4
- ²⁰ D. Rehm, A. Weller, Kinetics of Fluorescence Quenching by Electron and H-Atom Transfer. *Isr. J. Chem.* 1970, **8**, 259-271. doi.org/10.1002/ijch.197000029
- ²¹ L. P. Kuhn, R. E. Lutz, C. R. Bauer, *J. Am. Chem. Soc.* 1950, **72**, 11.
- ²² R. E. Lutz, S. M. King, *J. Org. Chem.* 1952, **17**, 11, 1519–1528.
- ²³ C.-J. Wallentin, J. D. Nguyen, P. Finkbeiner, C. R. J. Stephenson, *J. Am. Chem. Soc.* 2012, **134**, 21, 8875–8884.
- ²⁴ B. Michelet, C. Deldaele, S. Kajouj, C. Moucheron, G. Evano, *Org. Lett.* 2017, **19**, 13, 3576–3579.
- ²⁵ M. Reckenthäler, A. G. Griesbeck, *Adv. Synth. Catal.* 2013, **355**, 2727–2744.